University of New Orleans
ScholarWorks@UNO

University of New Orleans Theses and Dissertations | Dissertations and Theses

8-7-2008

Application of the Method of Least Squares to a Solution of the Matched Field Localization Problem with a Single Hydrophone

Sean R. Chapin
University of New Orleans

Follow this and additional works at: https://scholarworks.uno.edu/td

Recommended Citation

Chapin, Sean R., "Application of the Method of Least Squares to a Solution of the Matched Field Localization Problem with a Single Hydrophone" (2008). *University of New Orleans Theses and Dissertations*. 854.
https://scholarworks.uno.edu/td/854

This Dissertation is protected by copyright and/or related rights. It has been brought to you by ScholarWorks@UNO with permission from the rights-holder(s). You are free to use this Dissertation in any way that is permitted by the copyright and related rights legislation that applies to your use. For other uses you need to obtain permission from the rights-holder(s) directly, unless additional rights are indicated by a Creative Commons license in the record and/or on the work itself.

This Dissertation has been accepted for inclusion in University of New Orleans Theses and Dissertations by an authorized administrator of ScholarWorks@UNO. For more information, please contact scholarworks@uno.edu.

Application of the Method of Least Squares to a Solution of the Matched Field Localization Problem with a Single Hydrophone

A Dissertation

Submitted to the Graduate Faculty of the
University of New Orleans
in partial fulfillment of the
requirements for the degree of

Doctor of Philosophy
in
Engineering and Applied Science

by

Sean R. Chapin

B.S. Western Michigan University, 1998
M.S. University of New Orleans, 2001

August, 2008

Acknowledgements

A special thanks to the co-chairs of my dissertation committee, Dr. George Ioup and Dr. Juliette Ioup of the Department of Physics at the University of New Orleans. They always had their door open to provide help and support through this journey, and they were (and are) outstanding teachers. I'd also like to thank Dr. George Smith of the Naval Research Laboratory for taking the time to provide guidance on my research. Thank you to the other members of my dissertation committee for their feedback: Dr. Jinke Tang, Dr. Edit Bourgeois, and Dr. Ken Holladay.

Infinite thanks to Aisling for putting up with the long hours and for cheering me up when the going got tough. Thank you to my supervisor Anne for making the completion of this dissertation possible. Thank you to my co-workers in the RAWG team for giving me the space I needed to get my research done. Thank you to the U.S. Navy for providing the time and the funds to complete this project. Finally, thank you to my friends and family for always providing encouragement.

Table of Contents

List of Figures

`

List of Tables

Abstract

The single hydrophone localization problem is considered. Single hydrophone localization is a special case of matched field localization where measurements from only one hydrophone are available. The time series of the pressure at the hydrophone is compared with predicted times series calculated using an ocean acoustic propagation model for many different source locations. The source location that gives the best match between the predicted time series and the measurement is assumed to be the correct source location. Single hydrophone localization algorithms from the literature are reviewed and a new algorithm is introduced. The new algorithm does not require knowledge of the source signal and does not assume the use of a particular ocean acoustic model, unlike some algorithms in the literature.

Source location estimates calculated from the new algorithm are compared with ground truth using simulated ocean acoustic measurements and experimental measurements. Source location estimates calculated using other algorithms from the literature are shown for comparison. The simulated measurements use three source signals with bandwidths of 10 Hz, 100 Hz, and 200 Hz and the ocean is modeled as a Pekeris waveguide. The new algorithm estimates the source location accurately for all three source signals when several of the localization algorithms from the literature give inaccurate estimates. Gaussian white noise signals are added to the measured signals to test the impact of signal-to-noise ratio (SNR) on the algorithm. Four signal-to-noise ratios of 60 dB, 40 dB, 20 dB, and 0 dB are used. The new algorithm gives accurate source location estimates down to an SNR of 20 dB for two of the source signal bandwidths. Source location estimates using other algorithms from the literature break down at either 20 dB or 0 dB.

Source location estimates are calculated using two hydrophone measurements taken at different depths in an experiment conducted near the Bahamas. The new algorithm accurately estimates the source location in both cases. In one case, only two other localization algorithms from the literature locate the source accurately. In the other case, only one other localization algorithm succeeds.

Keywords: single hydrophone localization, matched field localization, matched field processing.

Chapter 1. Introduction

1.1 Matched Field Processing

Matched field processing in underwater acoustics refers to methods of using spatial measurements of the underwater pressure to detect and locate an acoustic source, or to infer environmental parameters of an ocean waveguide. The large collection of techniques developed over the last few decades can be traced to Hinich (1973) and Bucker (1976), who developed algorithms based on comparing spatial measurements of pressure on an array of hydrophones with the measurements predicted by an ocean acoustic propagation model. The spatial pressure distribution of the acoustic field is determined by the location of the source and the environmental parameters such as the sound speed profile of the water and the sound speed in the ocean bottom. If the environmental parameters are known for a given experiment, they can be entered into an acoustic propagation model and the pressure distribution can be predicted for various trial locations of the source. The pressure patterns measured at the hydrophones are then matched to the patterns estimated by the acoustic model. The basic idea is that the source is located, or localized, when the predicted acoustic field using the correct source location matches the measurements of the field at the receivers.

Similar techniques exist for estimating the ocean acoustic environmental parameters such as the sound speed. In this case the source location is known but the environmental parameters are unknown. The acoustic propagation model is run for different combinations of environmental parameters and the resulting pressure patterns are predicted at the hydrophones. Analogous to the localization problem discussed above, we can infer the correct environmental

parameters by looking for the best match between the predicted pressures and the measured pressures. A large body of literature exists on matched field processing and two reviews, with extensive references, are given by Baggeroer *et al*. (1993) and Tolstoy (1993).

1.2 Single Hydrophone Localization

In this dissertation we examine a special case of matched field processing where pressure measurements from only one hydrophone are available to locate a source. The problem is different from the matched field processing problem described above because we have no information on the spatial distribution of the acoustic field in our measurements. We assume we have one time series of the pressure measured at a single point in space where the hydrophone is located. The location of the source producing the disturbance is unknown, and we assume the source produces a broadband signal at the hydrophone. The assumption of a broadband source is necessary because a continuous wave source of a single frequency provides no useful information on the source location without accompanying spatial measurements. In other words, a continuous wave source would produce a sine wave of constant amplitude at the receiver, giving us no insight into the propagation paths of the acoustic energy. If we know the environmental parameters of the ocean waveguide, we can use ocean acoustic propagation models to predict the measurement at the hydrophone for different source locations. We call these replica signals. The location that gives the best match between the replica signal and the measured time series at the hydrophone is assumed to be the correct location of the source. This is conceptually similar to matched field processing techniques using arrays of hydrophones.

Single hydrophone localization techniques are important not only for their intrinsic interest, but also for their computational and experimental simplicity. Using a single hydrophone simplifies the equipment, reduces the cost, and lowers the burden on the computers processing

the measurements. This gives researchers on tight budgets flexibility to put their resources into other parts of the experiment if they can do the job with one hydrophone.

In the following sections we define the terminology and notation used throughout the dissertation. This is followed by a review of the literature on single hydrophone localization techniques discussing their assumptions and implementations.

1.3 Preliminary Considerations

1.3.1 Equations of Ocean Acoustics

The propagation of sound in the ocean is governed, to a good approximation, by the following linear inhomogeneous partial differential equation (Jensen, et al. 1994):

$$\nabla^2 p - \frac{1}{c^2(z)} \frac{\partial^2 p}{\partial t^2} = s(X,t), \tag{1.1}$$

where p is the pressure, $c(z)$ is the sound speed at depth z, t is time, and $s(X,t)$ is a function describing the source producing the disturbance at some location X. Ocean acoustic modeling concerns itself with analytical and numerical techniques of solving equation (1.1) under different boundary conditions. The solution to the equation will give the time dependent pressure at some point in the water (e.g., the location of a hydrophone).

The ocean is generally a time varying medium because environmental factors affecting the ocean are constantly changing. For example, weather conditions, time of day, and the season all affect the sound speed profile in the ocean. Equation (1.1) shows that the pressure measured at a point explicitly depends on the sound speed profile. The reason is that the sound will refract in the ocean as it travels through layers with different sounds speeds. This is analogous to how light will refract as it travels from one medium to another with a different index of refraction. If the sound speed profile is temporally stable in a region where an acoustic experiment is

performed, the ocean can be regarded as a time invariant system. The response of any linear time invariant (LTI) system to a given input can be expressed by a convolution relation (Bracewell 2000)

$$p(t) = \int_{-\infty}^{\infty} s(u)g(t-u)\,du, \tag{1.2}$$

where *t* is the time, *s(t)* is the source signal (i.e., the input), *g(t)* is called the Green's function or impulse response of the system, and *p(t)* is the pressure measured at the hydrophone (i.e., the output or response of the system). We have suppressed the spatial dependence of the terms in the equation for clarity; *p(t)* is the pressure measured at a location *Y*, *s(t)* is the source signal located at *X*, and *g(t)* is a function of both *X* and *Y*. Equation (1.2) is the solution of equation (1.1) expressed as an integral equation. The Green's function *g(t)* is defined to be the solution of equation (1.1) when the source function *s(X,t)* is a delta function. In other words it is the response of the ocean at *Y* to a point source located at *X* emitting a very short duration pulse. The Green's function depends on the location of the source and the receiver and will generally change with different source and receiver locations, with one exception. The principle of reciprocity (Jensen, et al. 1994) states that if the source and receiver locations are interchanged, the Green's function will not change. This is a key fact that makes localization in ocean acoustics possible. In solving the localization problem, we can treat the location of our receiver as the source location in equation (1.1). The source we are trying to locate in our experiment becomes the receiver in the model. Matched field processing takes advantage of this by repeatedly solving equation (1.1) for different receiver locations and compares each solution to our hydrophone measurement. The location that gives the closest match is the location of the source.

Equation (1.2) provides us the means to model a hydrophone measurement at any location we choose in an ocean environment. We use ocean acoustic models to solve equation (1.1) for an impulsive point source and obtain the Green's functions for different source and receiver locations. The next section will describe two acoustic models we will use in this dissertation.

1.3.2 Acoustic Propagation Models

There is a wide variety of acoustic propagation models available today to calculate the Green's functions in an ocean environment. Many of them are based in the frequency domain where the source function is assumed to be radiating at a single frequency. To form the time dependent Green's function from these models, the model must be run repeatedly at all frequencies forming a Green's function in the frequency domain. This function is then inverse Fourier transformed to the time domain yielding the time dependent Green's function. Other models solve equation (1.1) directly in the time domain giving the Green's function immediately.

The acoustic models we will use in this dissertation are BELLHOP and SPARC. The BELLHOP model is a Gaussian beam tracing model (Porter and Bucker 1987) that implements the ray tracing approximation of acoustics by associating a narrow Gaussian beam with each ray. The ray approximation models the sound as narrow beams of acoustic energy traveling through the ocean, similar to the geometric rays used in optics. The advantage of Gaussian beams over standard ray tracing is that it eliminates unrealistic features such as perfect shadows and caustics in the acoustic field. BELLHOP is a frequency domain model that assumes a point source radiating at a single frequency. The radiating point source is approximated by propagating beams over a range of angles from the source location. Those beams arriving at the receiver location are called arrivals and are characterized by their amplitude and time of arrival. The

arrival time is a function of the sound speed and the amplitude is a function of both geometrical spreading and losses of energy from bottom bounces. Two of the single hydrophone localization techniques in the literature that we will discuss explicitly incorporate the ray approximation into their algorithms and use BELLHOP for calculations.

In the time domain, the ray approximation gives the received signal as scaled and delayed replicas of the source signal (Jesus, Porter, et al. 2000; Jensen, et al. 1994). The Green's function is written as

$$g(t) = \sum_{m=1}^{M} a_m \delta(t - \tau_m), \tag{1.3}$$

where m is a ray arrival at the receiver, a_m is the amplitude of arrival m, and τ_m is the time at which arrival m reaches the receiver. The ray model outputs are the arrival times of the rays and their amplitudes. Once the Green's function is constructed using equation (1.3), it is convolved with the source function to model the signal at the hydrophone.

The other model we will use is SPARC (SACLANT Pulse Acoustic Research Code), a time domain acoustic propagation model (Porter 1990, 2008). SPARC is ideally suited for calculating time dependent Green's functions because the model works in the time domain solving equation (1.1) directly. A short duration pulse can be input at any location in the model and allowed to propagate through the ocean. The time dependent Green's function at any desired location can be extracted to use in localization algorithms. Frequency domain acoustic models are more cumbersome to deal with because they need to be repeatedly run at the frequencies in the band of interest and then transformed to the time domain.

1.3.3 Discrete Time Signal Model

Digital signal processing on experimental data is done with discrete time signals of finite length. The approximation of equation (1.2) for these signals is (Brigham 1988)

$$p(m) = \sum_{n=1}^{N} s(n)g(m-n), \tag{1.4}$$

where *m* and *n* are integer indices labeling the values of *s* and *g* at discrete times *m* and *n*. Equation (1.4) will serve as our fundamental model of the pressure measurement at a hydrophone throughout this dissertation. A convenient shorthand for equations (1.2) and (1.4) is (Bracewell 2000)

$$p = s * g, \tag{1.5}$$

where the asterisk represents the convolution operation.

Another way to express convolution is in matrix notation (Bracewell 2000)

$$\begin{bmatrix} g_1 & 0 & 0 & \dots & 0 \\ g_2 & g_1 & 0 & \dots & 0 \\ g_3 & g_2 & g_1 & \dots & 0 \\ \vdots & \vdots & \vdots & & \vdots \\ g_N & \vdots & \vdots & \ddots & \vdots \\ 0 & g_N & g_{N-1} & & \vdots \\ 0 & 0 & g_N & \ddots & \vdots \\ \vdots & \vdots & \vdots & & 0 \\ 0 & 0 & 0 & \dots & g_1 \end{bmatrix} \begin{bmatrix} s_1 \\ \vdots \\ s_M \end{bmatrix} = \begin{bmatrix} p_1 \\ \vdots \\ p_{M+N-1} \end{bmatrix}, \tag{1.6}$$

or $\boldsymbol{p} = \boldsymbol{G}\boldsymbol{s}$ for short. The source signal vector $\boldsymbol{s}$ is of length M, the Green's function vector $\boldsymbol{g}$ is of length N, and $\boldsymbol{G}$ is an M+N-1 by M matrix formed from the elements of $\boldsymbol{g}$. The convolution matrix is of full column rank (Tong, Xu and Kailath 1993).

1.3.4 Other Definitions and Notation

The cross correlation of signal s with signal g is defined as

$$p(m) = \sum_{n=1}^{N} s(n)g(n-m), \tag{1.7}$$

or in pentagram notation (Bracewell 2000)

$$p = g \bigstar s. \tag{1.8}$$

The cross correlation is useful for comparing two signals. If the two signals are very similar at lag *m* as signal *g* is displaced over signal *s*, a peak will appear in the cross correlation. This is a useful tool in matched field processing when comparing a replica signal with a measured signal.

We will use the following definition for calculating the Discrete Fourier Transform F_r of a discrete time function f_k:

$$F_r = \sum_{k=0}^{N-1} f_k e^{-i2\pi kr/N}. \tag{1.9}$$

Many software packages are equipped with Fast Fourier Transform (FFT) algorithms to calculate equation (1.9) very efficiently.

An analytic signal is the complex valued signal $\hat{f}(t)$ associated with the real valued signal *f(t)* defined by the following Fourier transform pair (Bracewell 2000)

$$\hat{f}(t) \leftrightarrow 2H(f)F(f), \tag{1.10}$$

where *f* is the frequency, *H(f)* is the unit step function, and *F(f)* is the Fourier transform of *f(t).* The negative frequency portion of the frequency spectrum of *f(t)* is suppressed by the step function and the result is inverse Fourier transformed to the time domain. The magnitude of the

analytic signal $\hat{f}(t)$ is called the envelope of *f(t)*. Intuitively the envelope is the function that touches the peaks of *f(t)* showing how the general shape of its amplitude varies with time.

The following two facts about matrix algebra will be used in this dissertation:

1). Given an $m \times n$ matrix $\boldsymbol{A}$, the shortest least squares solution to the linear system $\boldsymbol{Ax} = \boldsymbol{b}$ is

$$\boldsymbol{x} = \boldsymbol{A}^{+}\boldsymbol{b}, \tag{1.11}$$

where $\boldsymbol{A}^{+}$ is the pseudoinverse of the matrix $\boldsymbol{A}$ (Strang 1993).

2). If the rank of the matrix $\boldsymbol{A}$ is *n* ($\boldsymbol{A}$ is full column rank), then $\boldsymbol{A}^{+}\boldsymbol{A}=\boldsymbol{I_n}$ where $\boldsymbol{I_n}$ is the $n \times n$ identity matrix (Lutkepohl 1996).

The p-norm of a vector $\boldsymbol{f}$ is defined as

$$\|\boldsymbol{f}\|_p \equiv \left(\sum_n |f(n)|^p\right)^{1/p}. \tag{1.12}$$

One exception to this notation is for the square of the 2-norm, i.e., the sum of the squares of the elements of a vector. We will omit the subscript in those cases because it is easier to read and it is consistent with notation used in the literature,

$$\|\boldsymbol{f}\|^2 \equiv \sum_n |f(n)|^2. \tag{1.13}$$

The ∞-norm of the vector $\boldsymbol{f}$ is

$$\|\boldsymbol{f}\|_\infty \equiv \max_n |f(n)|. \tag{1.14}$$

1.4 Literature Review of Single Hydrophone Localization

1.4.1 Li and Clay (1987)

In 1987 Li and Clay (Clay 1987, Li and Clay 1987) proposed a localizer using the cross correlation function. They construct replica signals by convolving the Green's functions for different source locations with the source signal. Then they cross-correlate the replica signals with the measured signal over a grid of trial source locations. The cross-correlation peaks at the true source location because the replica signal closely matches the measured signal. The equation describing this in our notation is

$$L = \max_X \left[\max_t \frac{h(X,t) \bigstar d(t)}{\|h(X,t)\|_2 \|d(t)\|_2} \right], \tag{1.15}$$

where *t* is the time, *X* is a trial source location, *h(X,t)* is the replica signal for location *X*, and *d(t)* is the measured signal. The function in the brackets is calculated for all trial source locations and the location *X* corresponding to the maximum value of the bracketed function is the estimate of the source location.

1.4.2 Frazer and Pecholcs (1990)

The Frazer and Pecholcs technique (Frazer and Pecholcs 1990) is distinct from the others because it does not rely on a measurement or estimate of the source signal. The information required is the measured signal at the hydrophone and the predicted Green's functions for each trial source location. Frazer and Pecholcs (1990) proposed a family of localizers listed below. The notation is as follows: *h(X)* is the replica signal for trial source location *X*, *d* is the measured signal, *D* is the FFT of the measured signal, $g(X)$ is the Green's function for source location *X*, and *G(X)* is the FFT of the Green's function for source location *X*. A discussion of the localizers follows the list.

$$\chi_2^{\infty} = \frac{\|h(X) \bigstar d\|_{\infty}}{\|h(X)\|_2 \|d\|_2}. \tag{1.16}$$

$$\chi_1^{\infty} = \frac{\|h(X) \bigstar d\|_{\infty}}{\|h(X)\|_1 \|d\|_1}. \tag{1.17}$$

$$\mu_1^{\infty} = \frac{\|h(X) \bigstar d\|_{\infty}}{\|h(X) \bigstar d\|_1}. \tag{1.18}$$

$$\varphi_{\infty}^1 = \frac{{\|D\|_1}/{\|G(X)\|_1}}{\left\|{D}/{G(X)}\right\|_{\infty}}. \tag{1.19}$$

$$\theta_{\infty}^1 = \frac{\left\|{D}/{G(X)}\right\|_1}{\left\|{D}/{G(X)}\right\|_{\infty}}. \tag{1.20}$$

$$\beta_1^{\infty} = \frac{\|d * g(X)^{-1}\|_{\infty}}{\|d * g(X)^{-1}\|_1}, \tag{1.21}$$

where $d * g(X)^{-1}$ is the inverse FFT of D/G(X).

$$\nu_1^1 = \frac{\left\| d_\omega^2 \left| D \right| \right\|_1 \Big/ \left\| d_\omega^2 \left| G(X) \right| \right\|_1}{\left\| d_\omega^2 \left| D/G(X) \right| \right\|_1}, \tag{1.22}$$

where $d_\omega^2 \equiv d/d\omega^2$.

The first thing we want to point out is that the χ_2^∞ localizer is the same as the one developed by Li and Clay described in the previous section. The χ_1^∞ and μ_1^∞ localizers are variations of this with different normalization factors in the denominator. The β_1^∞ norm works in the time domain on the inverse FFT of the Fourier deconvolution. The φ_∞^1, θ_∞^1, and ν_1^1 localizers all work in the frequency domain on the Fourier deconvolution of *D* and *G(X)*. The idea is that the Fourier deconvolution *D/G(X)* will give an estimate of the source signal spectrum, assumed to be smooth compared to *G(X)*. *G(X)* typically has many nulls in it for underwater acoustic problems. If the correct *G(X)* is put in, the resulting Fourier division will be relatively smooth. When the incorrect *G(X)* is put in, the division will result in a spiky spectrum because of the nulls of *G(X)* in the denominator. This drives the value of the norm of the division higher when *G(X)* is not correct. If the norm of the division is put in the denominator of the localizer function, then the localizer will reach a peak value at the true source location.

To gain a better understanding of how the Frazer and Pecholcs localizers work, we will go through a numerical example comparing the values of the localizers when the trial source location is correct with when it is incorrect. Figure 1.1 shows the source signal, Green's function, and measured signal we will use for this example. The source signal is a linear frequency modulated (LFM) chirp with frequency sweep of 25 Hz to 225 Hz. Its amplitude is

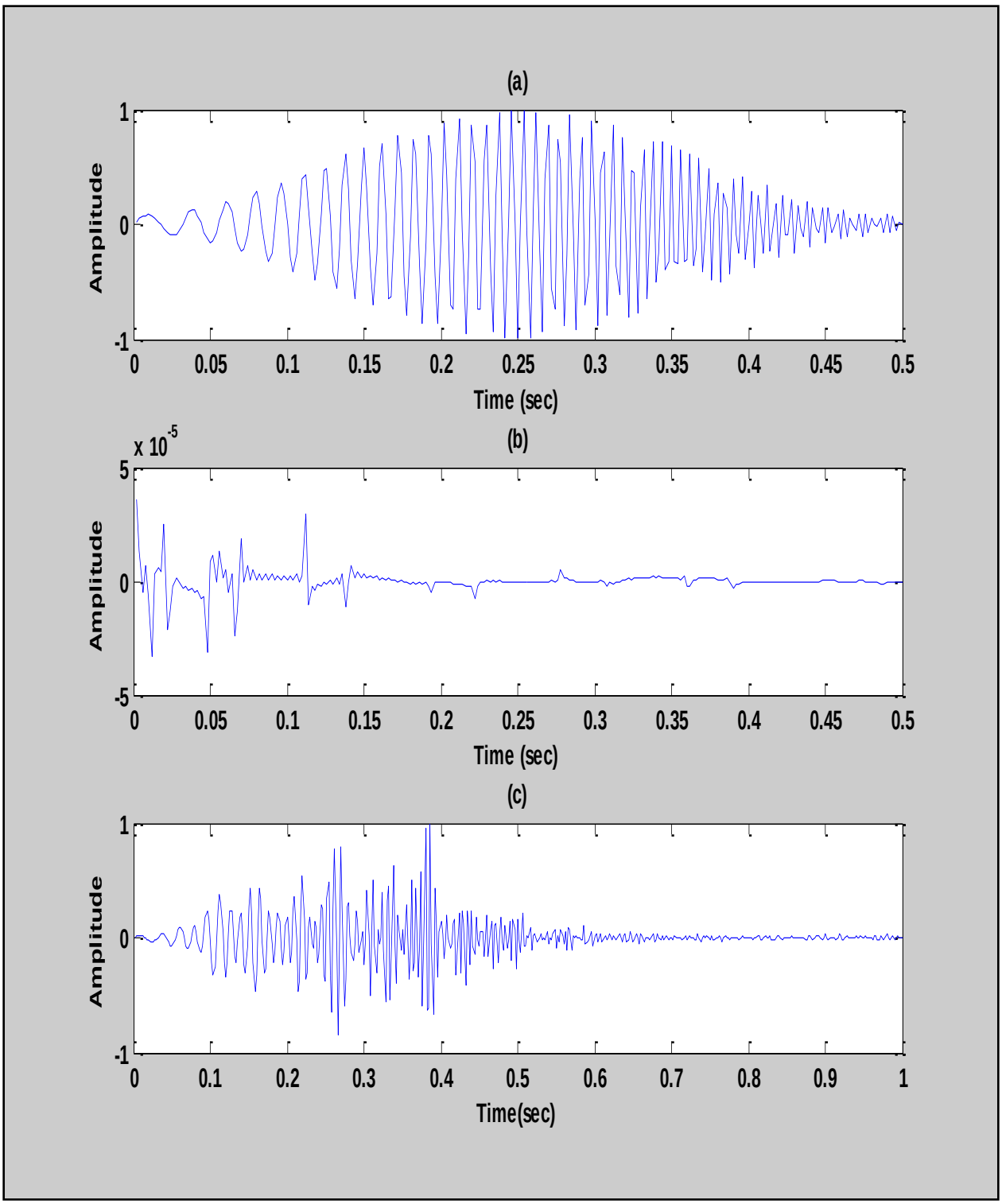

Figure 1.1 (a) The source signal. (b) Green's function. (c) Measured signal.

modulated with a Hamming window and the duration of the signal is 0.5 seconds. The sampling interval is 0.002 seconds, giving a cutoff frequency of 250 Hz. The Green's function is representative of what would be found in a shallow underwater acoustic environment. Notice that there are several arrivals representing reflections of the source signal energy from the ocean surface and the bottom. The measured signal was calculated by convolving the source signal with the Green's function. In this case the Green's function significantly distorts the source signal on its way to the receiver. Figure 1.2 shows the energy spectra of the source signal, Green's function, and measured signal in the frequency domain. The source signal spectrum is very smooth and centered at 125 Hz. The Green's function spectrum is irregular in shape and features a number of nulls. By the convolution theorem (Bracewell 2000), the spectrum of the measured signal is the product of the source spectrum and the Green's function spectrum. The irregular shape and the nulls of the Green's function show in the frequency band where the source signal is most prominent.

The next task is to calculate the Frazer and Pecholcs localizer functions when the correct Green's function from Figure 1.1 is used, and for an incorrect Green's function corresponding to a different source location. Figure 1.3 shows the result of $D/G(X)$ for each case where D is the measured signal spectrum and $G(X)$ is the Green's function. When the correct Green's function is used, the smooth spectrum of the source signal is deconvolved out. If the incorrect Green's function is used, a spectrum with a number of large peaks results. These peaks are there because the nulls in the spectrum of the Green's function cause large values in the division operation where there are not corresponding nulls in the measured signal's spectrum. This is the essential feature for understanding Frazer and Pecholc's frequency domain based localizers. The Fourier division is sensitive to these nulls and only the correct Green's function with nulls in the same

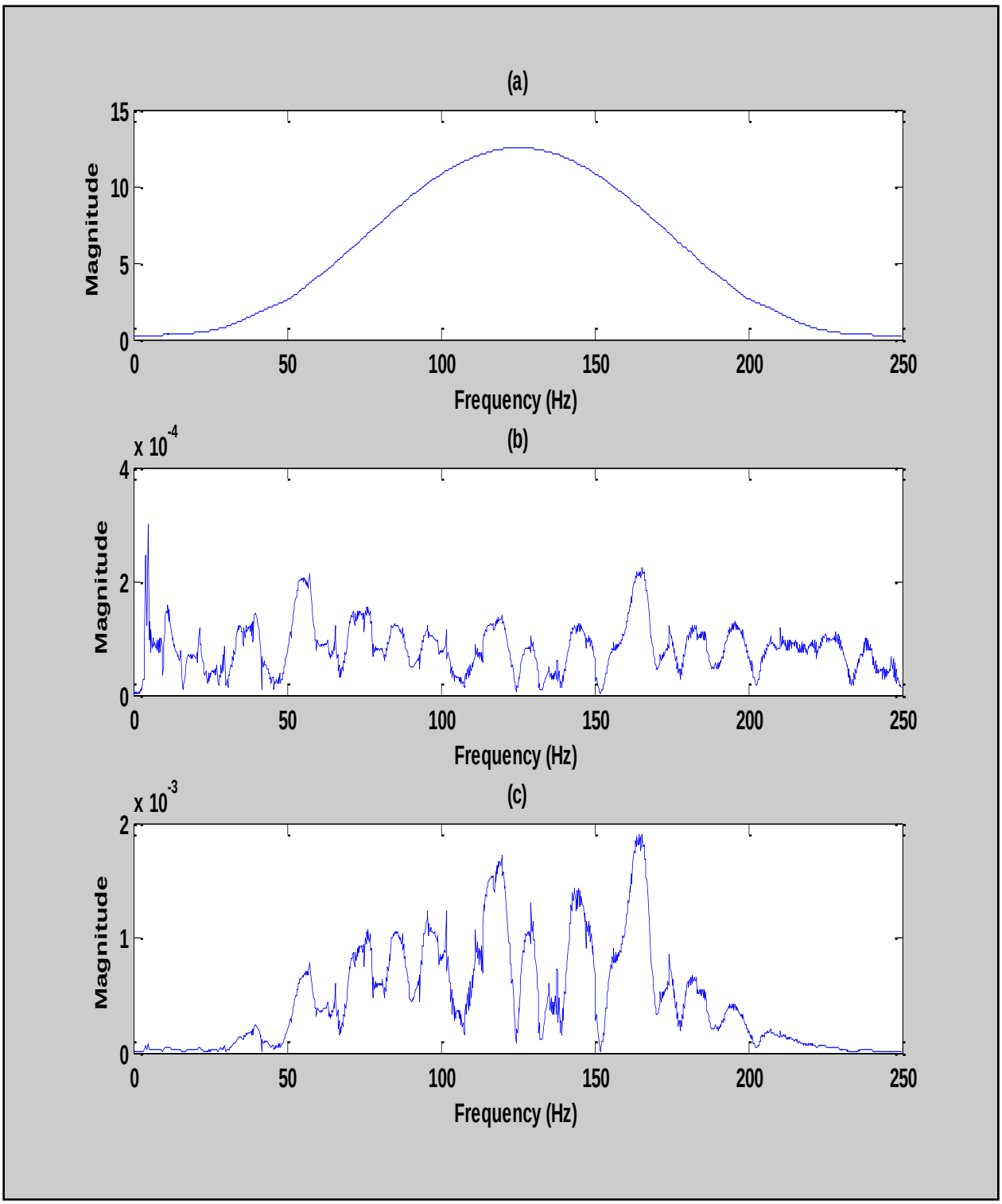

Figure 1.2. (a) The source signal spectrum. (b) Spectrum of Green's function, (c) Spectrum of measured signal.

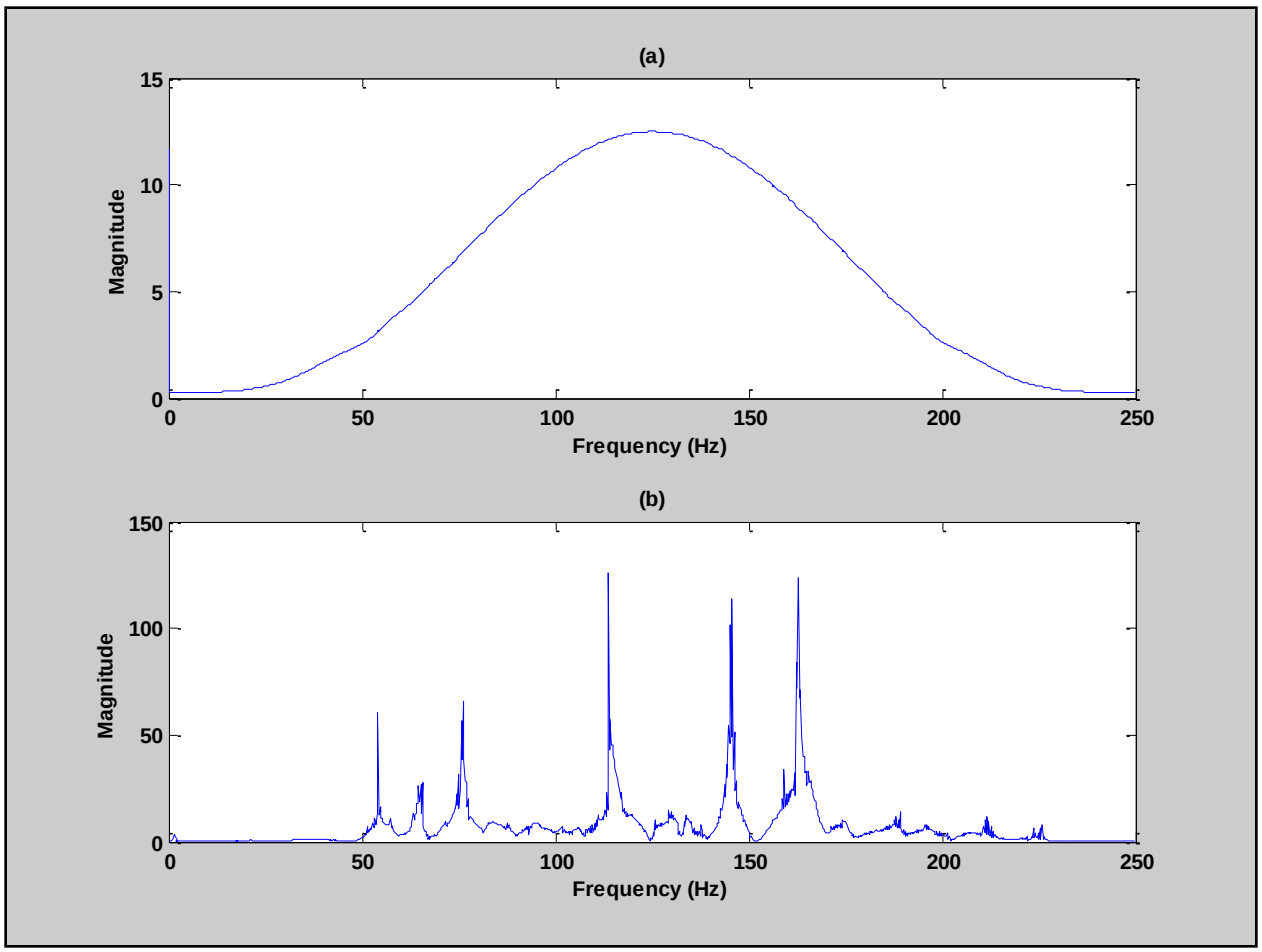

Figure 1.3. (a) Magnitude of D/G(X) for the correct source location; (b) magnitude of D/G(X) for the incorrect source location

locations as those in the measured signal's spectrum can prevent these large peaks from appearing.

To understand the time domain localizer β_1^{∞} we need to look at the inverse FFT of these Fourier deconvolutions to see what happens in the time domain. Figure 1.4 (a) shows the result when the correct Green's function is used. The Hamming windowed LFM pulse is retrieved just as the frequency domain picture in Figure 1.3 (a) suggested. Figure 1.4 (b) shows the recovered signal with the incorrect Green's function. An irregular function results bearing little resemblance to the original source signal. The β_1^{∞} localizer works on a different principle than

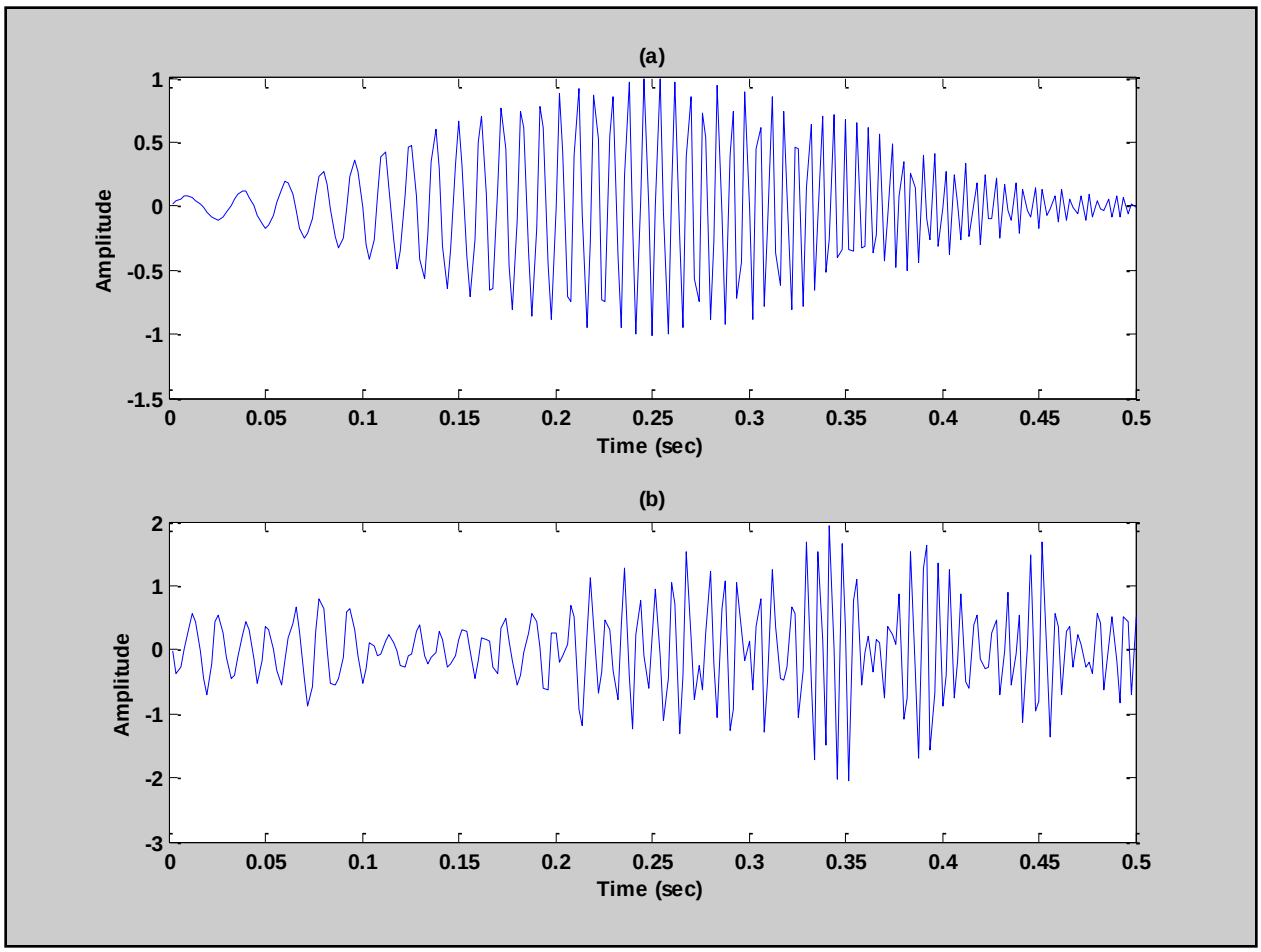

Figure 1.4. (a) The inverse FFT of D/G(X) for the correct source location; (b) the inverse FFT of D/G(X) for the incorrect source location shown in Figure 1.3(b).

the frequency domain localizers. It is sensitive to the duration of the signal in the time domain. Shorter duration source signals tend to give lower values in the denominator of this localizer. If the original source signal is sufficiently compressed in the time domain, this localizer will have higher values when the deconvolution is correct. As Figure 1.4 (b) shows, the incorrect result gives a ragged and spread out signal estimate that tends to decrease the value of the localizer.

We are now left to discuss the χ and μ localizers. These localizers work with the cross correlation of the replica signal with the measured signal. They are the only localizers in the

family that rely on knowledge of the source signal for their calculation. The χ_2^∞ localizer is idential to the Clay localizer; χ_1^∞ and μ_1^∞ are similar but with different normalizations. Figure 1.5 shows the cross correlation with the incorrect Green's function; Figure 1.6 shows the cross correlation with the correct Green's function. Qualitatively both waveforms look similar suggesting these localizers are less sensitive to the different Green's functions. The peak value of the cross correlation and the 1-norms are similar too. The similarity of the localizers suggests that a calculation of the localizers over all source locations could result in many false peaks.

The results in Table 1.1 summarize the values of the Frazer and Pecholc's localizer functions for our sample case. All of the localizers in this example showed higher values at the correct location except the μ_1^∞ localizer. Both the χ and μ localizers are based on the cross correlation of the replica signal with the measured signal but have different normalization factors. The failure of the μ localizer but not the χ localizers suggests that the normalizations used in these localizers are very important. Notice the strong differences between the θ and φ localizers. Those are sensitive to the smoothness of the source signal spectrum estimate from the Fourier division. The assumption that the source signal spectrum be smooth compared to *G(X)* is important for these localizers.

1.4.3 Lee (1998)

The next localizer we will look at is by Lee (1998) and is another one based on cross correlation. The source signal is assumed to be known and the Green's function is measured directly by calculating the cross correlation of the measured signal and the source signal, as in equation (1.7). The result of this calculation is equivalent to the received signal resulting from the transmission of the autocorrelation of the source signal through the ocean environment. Provided the autocorrelation of the source signal is a narrow pulse, the resulting cross correlation

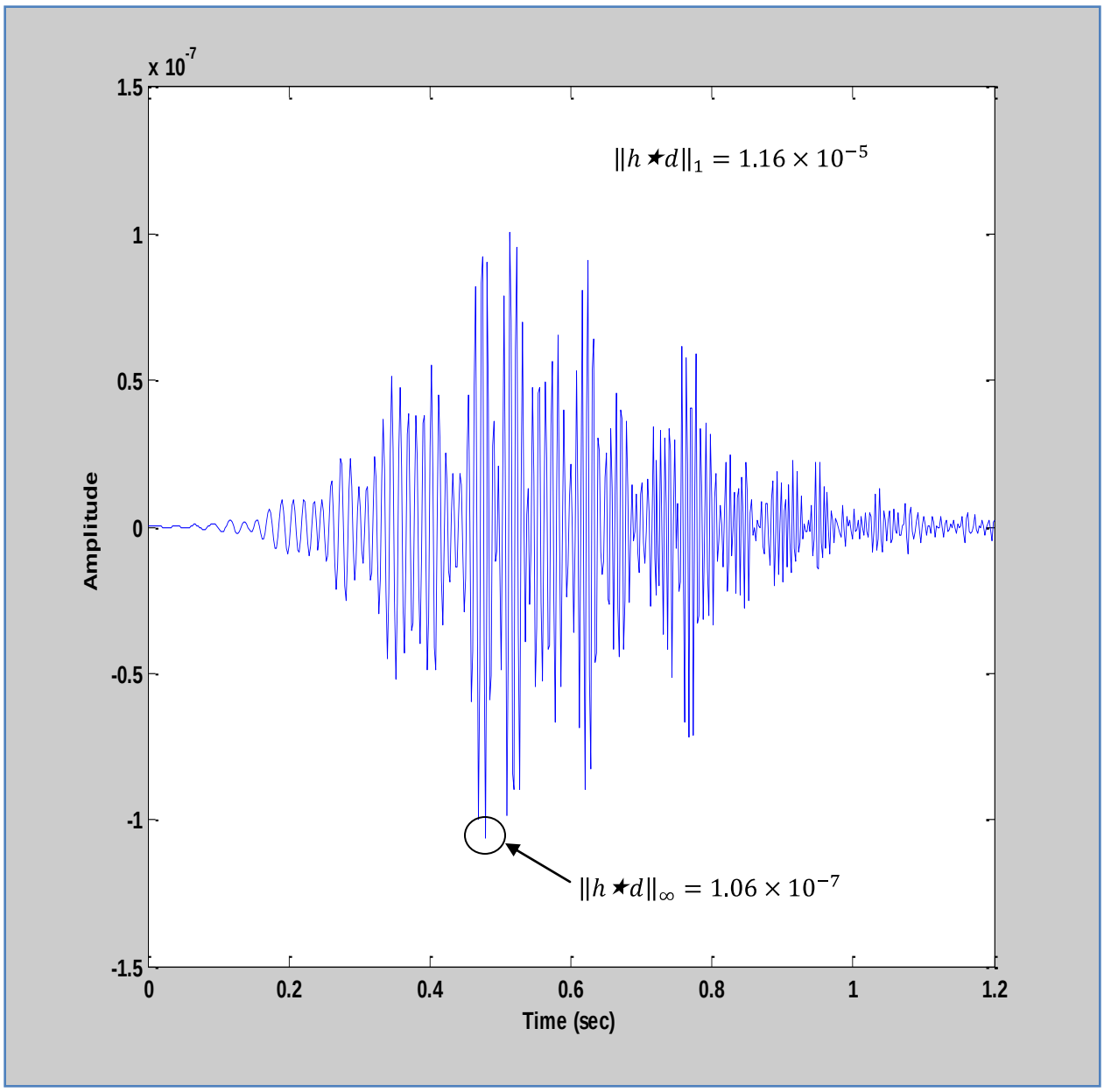

Figure 1.5. The cross correlation of the replica signal with the measured signal for the incorrect source location.

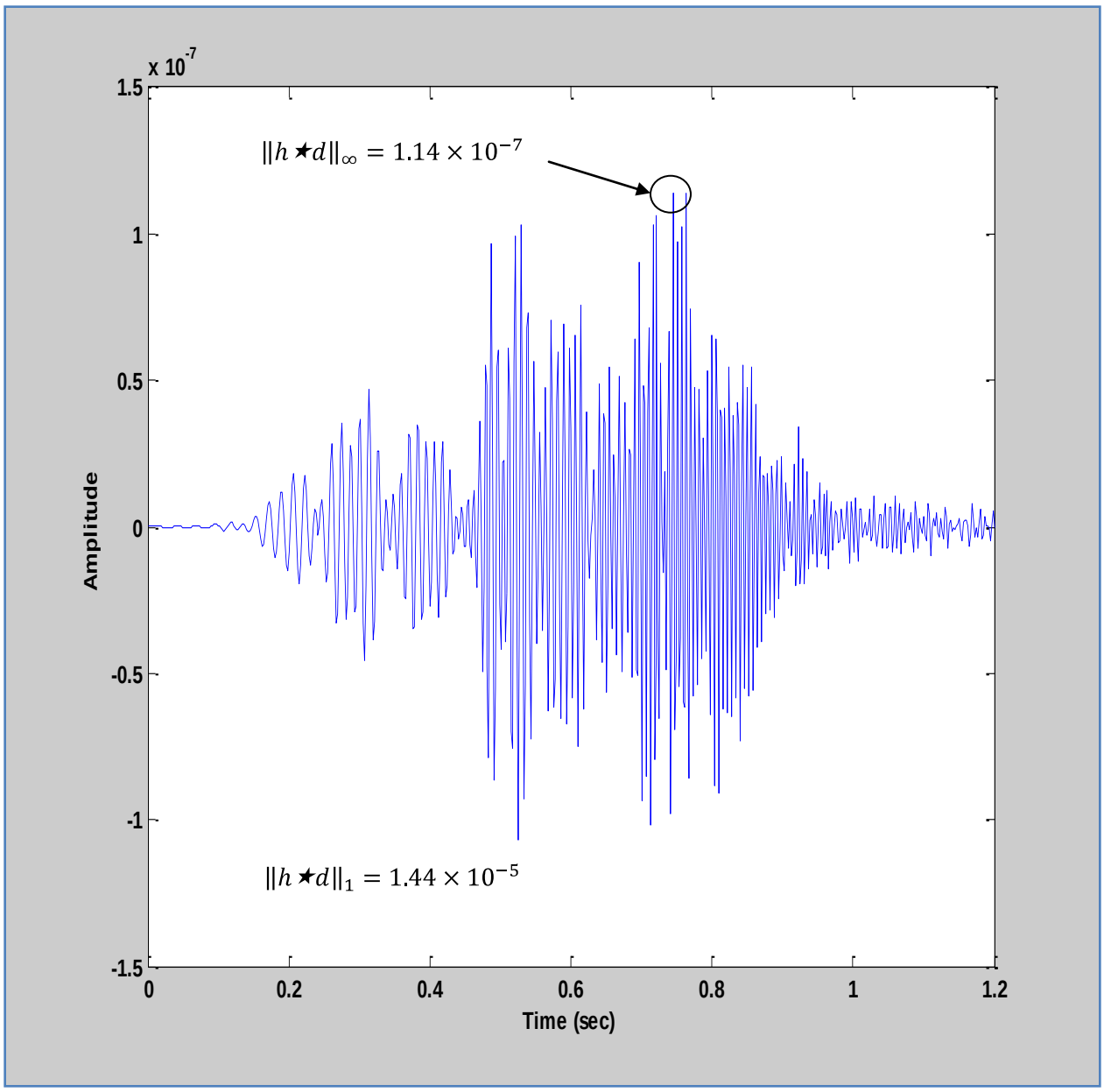

Figure 1.6. The cross correlation of the replica signal with the measured signal for the correct source location.

Localizer	Incorrect Source Location	Correct Source Location
χ_2^∞	**0.2267**	**0.2784**
χ_1^∞	**0.0011**	**0.0014**
μ_1^∞	**0.0091**	**0.0079**
φ_∞^1	**0.0404**	**0.4409**
θ_∞^1	**113.4**	**889.0**
β_1^∞	**0.0051**	**0.0118**
ν_1^1	**0.0003**	**0.0004**

Table 1.1. Frazer & Pecholcs localizer values for the correct and incorrect source locations.

should give a good approximation of the Green's function. The Green's function estimate can then be directly compared to the Green's functions calculated from an acoustic propagation model using the cross correlation again. The localizer will reach a peak value when the estimated Green's function most resembles the Green's function from the model corresponding to the correct source location. This localizer is very similar to the Clay localizer except that the cross correlation is calculated between the Green's functions, rather than between a replica signal and the measured signal. Here is the Lee localizer in our mathematical notation:

$$L = \max_X \|\hat{g} \bigstar g(X)\|_\infty, \tag{1.23}$$

where $\hat{g}$ is the Green's function estimate from cross correlating the measurement with the source signal, and $g(X)$ is the Green's function calculated from the acoustic propagation model for location X.

1.4.4 Porter *et al.* (1998)

Porter *et al.* (1998) developed another localizer based on the cross correlation of the measured signal with a replica signal with one important difference from the previous localizers we've looked at: they cross correlate the logarithm ($\log_{10}$) of the envelopes of the replica signal and measured signal rather than the signals themselves. The principle behind this is that in many environments only the first few arrivals at the receiver dominate the measured signal energy. The later arrivals are attenuated more from multiple bottom interactions on their journey to the receiver. The localizers by Porter *et al*. use the envelope of the signals to put less emphasis on the fine details of the signal. They use the logarithm to emphasize the larger energy portions of the signal. The hypothesis is that the localizer will be more robust. The equation is as follows

$$L = \max_{X} \| r_{le} \bigstar g_{le}(X) \|_{\infty}, \tag{1.24}$$

where r_{le} is the logarithm of the envelope of the measured signal and $g_{le}(X)$ is the logarithm of the envelope of the replica signal for location X. Again we calculate the replica signal over all trial source locations X and look for where the localizer peaks.

1.4.5 Jesus *et al.* (2000)

The localizers developed by Jesus *et al.* (Jesus, Porter, et al. 1998, 2000) are the first we've discussed that explicitly assume that the acoustic propagation model used is a ray tracing model (they used BELLHOP). This is often desirable because ray models run very quickly and the output is simple to interpret.

First we define some notation:

X: the source location.

$\boldsymbol{y}$: measurement signal vector at the hydrophone.

$\boldsymbol{S}[\boldsymbol{\tau}(X)]$: matrix of source signal replicas; each column contains one replica of the source signal delayed by an amount defined by $\boldsymbol{\tau}(X)$.

$\boldsymbol{\tau}(X)$: vector defining arrival times from a ray based acoustic propagation model for source location X.

$\boldsymbol{a}(X)$: amplitude vector defining amplitudes of arrivals from ray based acoustic propagation model for source location X.

$\boldsymbol{\varepsilon}$: random noise vector (representing measurement noise).

The signal model is

$$\boldsymbol{y} = \boldsymbol{S}[\boldsymbol{\tau}(X)]\boldsymbol{a}(X) + \boldsymbol{\varepsilon}. \tag{1.25}$$

The received signal model is composed of scaled and delayed replicas of the source signal as predicted by acoustic ray theory. The localizer calculates the product of the measurement signal vector **y** with the matrix $\boldsymbol{S}$. The resulting vector's elements are squared and summed for all trial source locations. In other words, they calculate the inner product of the measurement vector with scaled and delayed replicas of the source signal. The idea is that the localizer will peak when the $\boldsymbol{\tau}(X)$ time delay vector has the correct arrival times in it corresponding to the true source location. The localizer equation is written

$$L = \max_{X} \|\boldsymbol{y}^{H}\boldsymbol{S}(\boldsymbol{\tau})\|_2, \tag{1.26}$$

where X is the source location and ^{H} is the Hermitian transpose (complex valued signals are admissible). Jesus *et al.* generalize their localizers to the case of N snapshots of the measured signal. For example, the source could repeat itself several times giving multiple measurements

to use in the algorithm. We will not be looking at this case, however, and will focus on the case where only a single measurement is available.

1.4.6 Tiemann *et al.* (2006)

A recent paper by Tiemann *et al*. (2006) looked at marine mammal localization with a single hydrophone. Ray theory was explicitly assumed for this technique by assuming source signal arrivals in the measurement can be clearly identified. Localization is done by matching arrival times estimated from the measured signal to arrival times calculated from a ray tracing model. The sperm whale clicks they measured were broadband and of very short duration. The ray model of propagation is ideal for signals like this and arrivals at the receiver can be easily identified. Their method was to match the arrivals at the receiver to the arrivals calculated by a ray propagation model (they used BELLHOP). To do the matching, they created bins with a width of 15 milliseconds across the length of the measurement and the arrival time vector from the ray model. They considered any arrivals in a particular bin that are present in both the measured signal and the calculated arrivals to be overlapping. This process is continued across the entire measurement tabulating the overlaps. If there are arrivals that do not overlap in a bin, they are considered nonoverlapping and those are tabulated. A net overlap score is calculated by summing the overlaps and then subtracting the sum of the nonoverlapping arrivals. The score is calculated for each trial source location. The location with the highest net overlap score is the location of the source.

This technique is similar to other techniques where ray arrival times in the measurement are compared to those calculated by a model. Instead of calculating a cross correlation as in many of the methods described above, or through matrix algebra, Tiemann *et al.* (2006) use a binning and counting technique to match up the arrivals.

1.4.7 Other Localization Techniques

There are other papers in the literature that use geometric ray tracing techniques to calculate the ray arrival times at a hydrophone for different source locations (Hassab 1976; Cato 1998; Aubauer, Lammers and Whitlow 2000). This would be a useful technique for broadband source signals in environments that can be approximated by a constant sound speed profile. A paper by Unpingco *et al.* (1999) describes a synthetic aperture technique for tracking moving sources under certain assumptions. Kuperman and D'Spain (2001) describe a technique for localizing in range only for broadband sources in deep water. We will not examine these techniques further because of their more restrictive assumptions.

Chapter 2 A New Technique for Single Hydrophone Localization

2.1 Description

Although we described several approaches to single hydrophone localization from the literature, the amount of work done on single sensor localization is small when compared to the voluminous literature on matched field processing with multiple receivers. Most of the methods we described from the literature are variations on the basic idea of comparing replica signals generated using the source signal and an acoustic model, with the measurement at the receiver. A maximum or a minimum in the resulting metric is used to quantify the correlation and determine the true source location. All of the above methods, except the algorithm by Frazer and Pecholcs (1990), rely on knowledge of the source signal that is transmitted, and this might be a limitation in some situations where this information may not be available or easily obtained.

We propose a new single hydrophone localization algorithm using the method of least squares. Least squares is well established and can be implemented efficiently using matrix algebra packages. This algorithm does not require knowledge of the source signal. The Green's function estimate can be calculated from any acoustic propagation model. There is no assumption built into the new algorithm requiring that a particular model be used (e.g., a ray model). This frees up researchers to use any model that is appropriate for their experiment and it gives them options to balance their resources. This can be important because some propagation models are computationally intense.

2.2 Algorithm

First we will establish some notation and then lay out the steps of the algorithm. Recall equation (1.6) describing a discrete time LTI system for underwater acoustics

$$\boldsymbol{m} = \boldsymbol{G}\boldsymbol{s}, \tag{2.1}$$

where $\boldsymbol{G}$ is the convolution matrix of the Green's function for a source and receiver in the environment of the experiment, $\boldsymbol{s}$ is the discrete time source signal vector, and $\boldsymbol{m}$ is the measurement vector at the receiver. Generally there will be some interfering noise that we will model as a random vector $\boldsymbol{n}$ added to the measurement vector

$$\boldsymbol{m} = \boldsymbol{G}\boldsymbol{s} + \boldsymbol{n}. \tag{2.2}$$

We know the location of our receiver but do not know the location of the source. Using the environmental information our propagation model requires, such as the sound speed profile of the water, we can calculate a set of trial Green's functions over a grid of possible source locations. Each trial Green's function represents the propagation characteristics for a particular source and receiver geometry. For example, in a two dimensional problem where the coordinates are range and depth, we can calculate the Green's functions over a rectangular grid of ranges and depths where the source might be located. If the grid is sufficiently large to include the source, our algorithm should identify the range and depth of its location. The source signal is assumed to be unknown. The question is how can we find the location without knowing either the signal or the Green's function? The answer is that we will simultaneously estimate the source signal and test each Green's function. Here is the model of our system:

$$\boldsymbol{m} = \widehat{\boldsymbol{G}}\hat{\boldsymbol{s}} + \boldsymbol{n}. \tag{2.3}$$

$\hat{G}$ is a trial Green's function from our search grid and $\hat{\boldsymbol{s}}$ is our estimate of the source signal that we obtain by solving the equation:

$$\hat{\boldsymbol{s}} = \widehat{\boldsymbol{G}}^{+}\boldsymbol{m}. \tag{2.4}$$

$\widehat{\boldsymbol{G}}^{+}$ is the pseudo-inverse of $\widehat{\boldsymbol{G}}$. The pseudo-inverse creates the shortest least squares solution to the problem, as we pointed out in equation (1.11). Now that we have our source signal estimate $\hat{\boldsymbol{s}}$, we can use it to calculate a replica signal $\widehat{\boldsymbol{m}}$, assuming that $\widehat{\boldsymbol{G}}$ is the correct Green's function:

$$\widehat{\boldsymbol{m}} = \widehat{\boldsymbol{G}}\hat{\boldsymbol{s}}. \tag{2.5}$$

To summarize the last few steps, we create a replica signal by temporarily assuming that our trial Green's function $\widehat{\boldsymbol{G}}$ is the correct one. Then we estimate the source signal using the least squares solution to equation (2.3). The resulting least squares estimate of the source signal is then convolved with the trial Green's function in equation (2.5) to give us a replica signal $\widehat{\boldsymbol{m}}$. The final step is to compare our replica signal with the measured signal and calculate the squared difference between them:

$$\|\boldsymbol{e}\|^{2} = \|\boldsymbol{m} - \widehat{\boldsymbol{m}}\|^{2}. \tag{2.6}$$

The process in equations (2.4) through (2.6) is repeated for every trial source location *X*. The localizer function is denoted

$$L = \min_{X} \|\boldsymbol{e}\|^{2}. \tag{2.7}$$

The localizer will achieve a minimum value when the Green's function corresponding to the correct source location *X* is input into the algorithm. The next section will show why this is true.

2.3 Analysis of Algorithm

There are two possibilities when a trial Green's function $\widehat{\boldsymbol{G}}$ is input into the algorithm: either it is the correct Green's function describing the system or it is not.

Case 1: $\widehat{\boldsymbol{G}} = \boldsymbol{G}$ (the Green's function for the correct source location is used). Substituting $\widehat{\boldsymbol{G}} = \boldsymbol{G}$ into equation (2.4) gives

$$\hat{\boldsymbol{s}} = \widehat{\boldsymbol{G}}^{+}\boldsymbol{m} = \boldsymbol{G}^{+}\boldsymbol{m}. \tag{2.8}$$

Recall from equation (2.2) that $\boldsymbol{m} = \boldsymbol{G}\boldsymbol{s} + \boldsymbol{n}$ and substitute it into equation (2.8):

$$\hat{\boldsymbol{s}} = \boldsymbol{G}^{+}\boldsymbol{G}\boldsymbol{s} + \boldsymbol{G}^{+}\boldsymbol{n}. \tag{2.9}$$

Assuming that the signal to noise ratio is high enough to render the contribution of the second term to be negligible, we have

$$\hat{\boldsymbol{s}} = \boldsymbol{G}^{+}\boldsymbol{G}\boldsymbol{s}. \tag{2.10}$$

Using the fact that $\boldsymbol{G}^{+}\boldsymbol{G} = \boldsymbol{I}$ if and only if G is full column rank (Lutkepohl 1996), eq. (2.10) becomes

$$\hat{\boldsymbol{s}} = \boldsymbol{s}. \tag{2.11}$$

Finally we have for the replica signal vector

$$\widehat{\boldsymbol{m}} = \widehat{\boldsymbol{G}}\hat{\boldsymbol{s}} = \boldsymbol{G}\boldsymbol{s} = \boldsymbol{m}, \tag{2.12}$$

and the difference between the replica signal and the measured signal is

$$\|\boldsymbol{e}\|^2 = \|\boldsymbol{m} - \widehat{\boldsymbol{m}}\|^2 = \mathbf{0}. \tag{2.13}$$

Case 2: $\widehat{\boldsymbol{G}} \neq \boldsymbol{G}$ (a Green's function for an incorrect source location is used). Substituting equation (2.2) into equation (2.4) gives

$$\hat{\boldsymbol{s}} = \widehat{\boldsymbol{G}}^{+}\boldsymbol{m} = \widehat{\boldsymbol{G}}^{+}\boldsymbol{G}\boldsymbol{s}, \tag{2.14}$$

where we assume again that the noise term $\boldsymbol{n}$ is negligible and neglect that term.

The replica signal vector becomes,

$$\widehat{\boldsymbol{m}} = \widehat{\boldsymbol{G}}\hat{\boldsymbol{s}} = \widehat{\boldsymbol{G}}\widehat{\boldsymbol{G}}^{+}\boldsymbol{G}\boldsymbol{s}. \tag{2.15}$$

The matrix product $\widehat{\boldsymbol{G}}\widehat{\boldsymbol{G}}^{+} \neq \boldsymbol{I}$ for a full column rank matrix (Lutkepohl 1996). The product is equal to the identity matrix only when the system is full row rank (Lutkepohl 1996). Calculating the difference between the measured signal and the replica signal gives

$$\boldsymbol{e} = \boldsymbol{m} - \widehat{\boldsymbol{m}} = \boldsymbol{G}\boldsymbol{s} - \widehat{\boldsymbol{G}}\widehat{\boldsymbol{G}}^{+}\boldsymbol{G}\boldsymbol{s}. \tag{2.16}$$

We simplify equation (2.16) into a more convenient form:

$$\boldsymbol{e} = \left(\boldsymbol{I} - \widehat{\boldsymbol{G}}\widehat{\boldsymbol{G}}^{+}\right)\boldsymbol{G}\boldsymbol{s}. \tag{2.17}$$

Therefore $\|\boldsymbol{e}\|^2 > 0$ in Case 2 showing that our localizer should achieve a minimum only when the Green's function for the correct source location is put into the algorithm. The assumptions we made in equations (2.10) and (2.14) that the noise vector $\boldsymbol{n}$ is small is important and we will look at the impact of a larger $\boldsymbol{n}$ in Chapter 3.

Another notable case is when the Green's function has very few arrivals close together in time. For example, there could be one direct arrival followed very closely by a reflected arrival.

When this happens the Green's function resembles a delta function and therefore the convolution matrix will resemble an identity matrix. In other words, there is not much distortion of the source signal on its way to the receiver. Inspection of equation (2.3) shows that the source signal estimate will be very close to the measured signal. This will propagate through the algorithm and give a replica signal that is very close to the measured signal. The localizer output will take on very small values in these cases and give unreliable location estimates. Cases like this could pose a problem for any single hydrophone localization algorithm because they all generally rely on multiple interactions of the source signal energy with the surface and the bottom. To function properly, these algorithms require unique Green's functions for different source and receiver geometries. Researchers must be aware of this in their experimental planning and should try to put the hydrophone in an advantageous position. It is also important to keep this case in mind when interpreting the localization data.

2.4 Discussion

The algorithm we've described is based on solving the least squares problem, giving it the benefit of the fast algorithms that have been developed over the years. The Levinson-Durbin recursion (Levinson 1947; Durbin 1960) is a very popular algorithm used to solve equation (2.3) in a computationally efficient and stable manner. Another benefit is that the least squares formulation naturally accommodates the presence of some random noise in the measured signal. Least squares finds a solution to minimize $\boldsymbol{m - Gs}$ and therefore will minimize the effects of the noise vector $\boldsymbol{n}$ (Strang 1993).

Our algorithm makes no assumptions about the nature of the source signal. Only four of the seven single hydrophone localization algorithms developed by Frazer and Pecholcs (1990)

require no knowledge of the source signal. However Frazer and Pecholcs do make assumptions on the smoothness of the source signal spectrum and on its duration in the time domain for one of their localizers. This potentially limits the application of their localizer if the source signal does not meet their assumptions. Although Tiemann *et al.* (2006) and other localizers based on ray arrival times do not explicitly rely on knowledge of the source signal, they do make the assumption that the source signal is of a wide enough bandwidth that distinct arrivals are measured at the hydrophone. We propose our localizer as the only one among the ones we've reviewed in this dissertation that is both model independent and source signal independent.

As with any matched field processing algorithm, our algorithm shares the same potential sensitivity to inaccuracies in the acoustic modeling. This could be caused by the inaccuracies in the model itself or by coarse environmental information fed into the model. Researchers should also experiment with the search grid of trial source locations to determine the appropriate grid spacing. There may be a balance of the fineness of the grid required for localization and the computational resources available to run the algorithm over the whole grid.

2.5 Analysis Plan

In the next chapter we present results from simulation data to explore the capability and sensitivity of our new algorithm. First we look at an initial case with simulated data to demonstrate the algorithm in a simple environment and compare it with the other localizers described in Chapter 1. Sensitivities we explore parametrically include signal to noise ratio and source signal bandwidth. With that understanding, we test the localization algorithm on some experimental ocean acoustic data to show it can be successfully used in a real ocean environment.

Chapter 3 Simulation Results

3.1 Introduction

In this chapter we test the new method developed in Chapter 2 on some simulated data sets, look at some of its sensitivities, and compare its localization accuracy to the existing techniques described in Chapter 1. To minimize any possible biases from the particular acoustic propagation model selected, we use a closed form analytical solution to the Pekeris waveguide problem (Pekeris 1948; Jensen, et al. 1994) to calculate the Green's functions. We look at the sensitivity of our localization algorithm to source signal bandwidth and signal to noise ratio (SNR).

The source signal is a linear frequency modulated pulse described by the following equation:

$$s(t) = w(t)\sin(2\pi f_1 t + \pi k t^2), \tag{3.1}$$

where t is the time, $w(t)$ is the amplitude, f_1 is the frequency at which the sweep begins and k is a constant that determines the rate of increase of the sweep. The instantaneous frequency f_i at time t is given by $f_i(t) = f_1 + kt$. The frequency of the signal increases linearly as a function of time. The constants f_1 and k can be chosen to get the desired frequency sweep over the period of the signal. We choose a Hamming window (Harris 1978) for the amplitude function w(t),

$$w(t) = 0.54 - 0.46\cos 2\pi t. \tag{3.2}$$

The Hamming window smoothes the sharp rise and fall of the amplitude of the LFM pulse compared to if no amplitude modulation were used (*i.e.* $w(t)$ = constant). It is a convenient

window to use because it is a built in function of Matlab, the software package we used to do most of the calculations in this dissertation.

The ocean environment we simulate is a Pekeris waveguide (Pekeris 1948; Jensen, et al. 1994), a model of a single water layer over an infinitely deep fluid bottom layer. Each layer is characterized by a sound speed and a density. Although the Pekeris waveguide model may be too simple an approximation for some environments, we use it here to simplify the computations and to minimize biases that may creep into the sensitivity analysis from assumptions built into the particular acoustic propagation model used to calculate Green's functions. The Pekeris waveguide model is well understood and has a relatively simple closed form solution. This makes the Green's function calculations simple and fast over a grid of trial source locations.

The Green's function is synthesized from the following frequency dependent solution to the Pekeris waveguide problem (Pekeris 1948; Jensen, et al. 1994):

$$G(r,z,f) = -\frac{i}{2D}\sum_{\mathrm{n}=1}^{\mathrm{M}}\sqrt{\frac{2}{\pi k_{rn} r}}\sin(k_{zn}z_s)\sin(k_{zn}z)e^{-i(k_{rn}r-\frac{\pi}{4})}, \qquad (3.3)$$

where r is the range of the receiver, z is the depth of the receiver, z_s is the source depth, D is the water depth, f is the source frequency, k_{rn} is the radial wave number of mode n, and k_{zn} is the vertical wave number of mode n. To obtain the time dependent Green's function, we calculate Equation (3.2) at every discrete frequency f over the bandwidth defined by the problem and take the inverse FFT of the result. This process is repeated for every trial source location and the Green's functions are stored for input into the localization algorithm. For our experiment, we used the following parameters to characterize the waveguide:

Source depth z_s: 99 meters.

Receiver depth z: 150 meters.

Receiver range: 2100 meters.

Water depth D: 300 meters.

Sound speed in the water: 1500 meters/second.

Sound speed in the bottom: 1650 meters/second.

Density of the water: 1 kg/m^3.

Density of the bottom: 1.9 kg/m^3.

The sound speed and density of the bottom are representative of a sandy bottom and the water depth is shallow enough to allow for many interactions of the sound in the water column with the bottom. The grid over which we calculated the trial Green's functions began at a range of 500 meters from the receiver and went out to 3000 meters, at intervals of 10 meters. The grid extended over the entire 300 meter water column at intervals in depth of 2 meters.

To simulate the signal measurement at the hydrophone, we convolved the Green's function for the true source location using equation (3.2) with the source signal from equation (3.1). We input the result into the localization algorithms as the measured signal. Figure 3.1 shows the three source signals we used, each with different bandwidths. Different bandwidths were achieved by adjusting the constants f_1 and k in equation (3.1). The first bandwidth was a 10 Hz LFM sweep from 120 Hz to 130 Hz. The second bandwidth was a 100 Hz sweep from 75 Hz to 175 Hz. The third bandwidth was a 200 Hz sweep from 25 Hz to 225 Hz. The durations of each of these source signals is 0.5 seconds. The purpose of doing these simulations with three

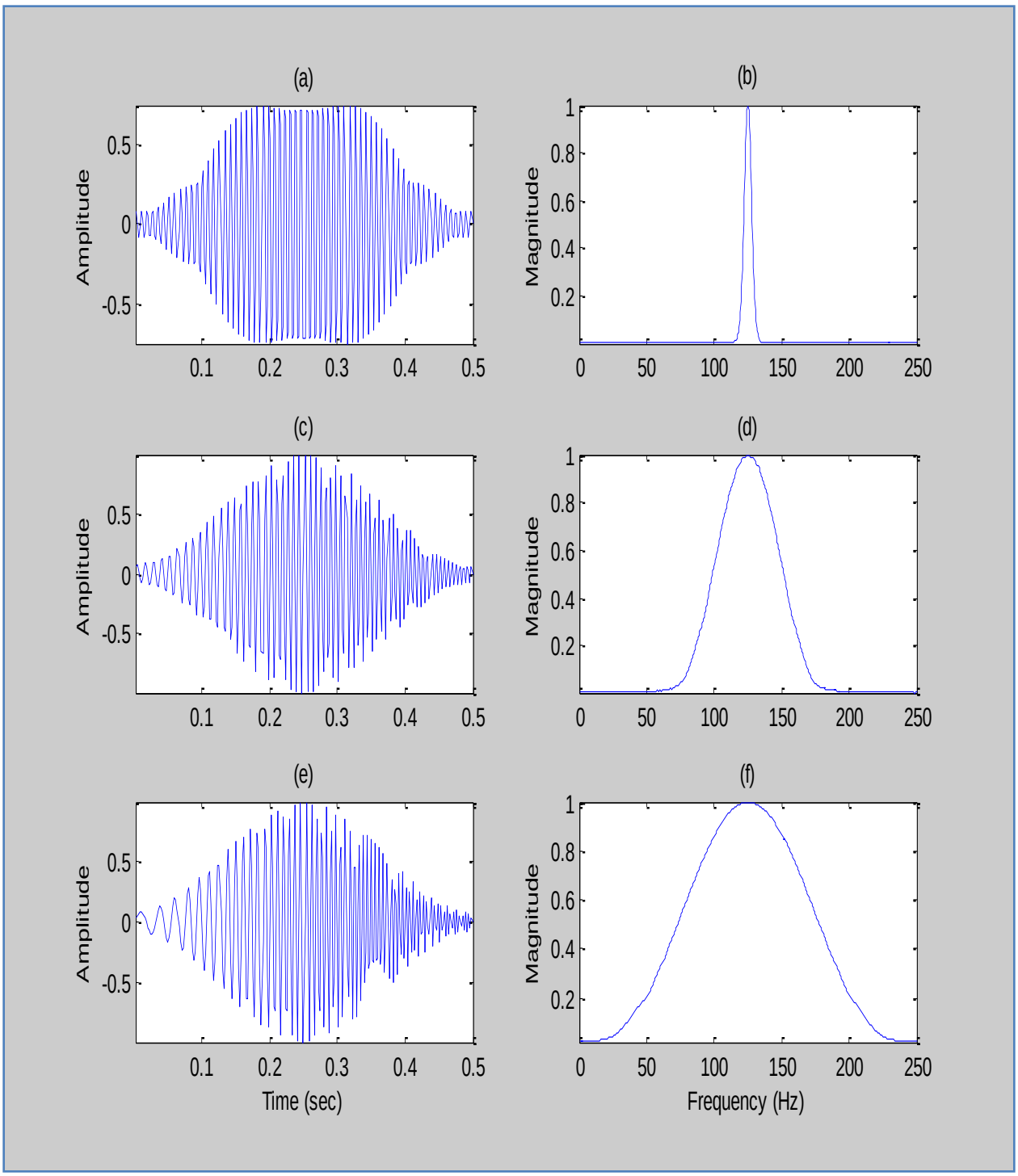

Figure 3.1. The source signals in the time domain and frequency domain. (a) Time domain view of 10 Hz LFM sweep over 0.5 seconds; (b) Frequency domain view of 10 Hz LFM sweep from 120 Hz to 130 Hz; (c) Time domain view of 100 Hz LFM sweep over 0.5 seconds; (d) Frequency domain view of 100 Hz LFM sweep from 75 Hz to 175 Hz; (e) Time domain view of 200 Hz LFM sweep over 0.5 seconds; (f) Frequency domain view of 200 Hz LFM sweep from 25 Hz to 225 Hz. All of the signals are modulated by a Hamming window.

different bandwidths is to test the sensitivity of our new algorithm to the bandwidth of the source signal, and to compare this sensitivity with that of the other localizers we described in Chapter 1. Bandwidth is an essential consideration in the single hydrophone localization problem because we are trying to exploit variability of the Green's function with frequency to locate the source. The more frequencies we have available in our data, the greater the chance we can calculate unambiguous replica signals and locate the source.

Figure 3.1 shows the time domain and the frequency domain representations of the three LFM source signals we use. Figure 3.2 shows the Green's function for the correct source and receiver pair calculated from equation (3.3) in the time domain and the frequency domain. Notice the presence of multiple spikes in the time domain representing reflections of the sound from the surface of the water and the bottom. The frequency domain plot illustrates that the interaction of the sound with the surface and the bottom strongly attenuates some frequencies, but not others. Figure 3.3 shows the convolution of each of the source signals with the Green's function in both the time and the frequency domain. There is significant distortion of the source signal when it travels to the receiver because of the multiple interactions with the surface and the bottom. It is the uniqueness of this distortion for each source and receiver pair that we want to exploit in the localization problem.

3.2 Source Signal Bandwidth Parameterization

3.2.1 10 Hz Source Signal Bandwidth

The first case we look at is the localization results for the 10 Hz LFM sweep from 120 Hz to 130 Hz. Figure 3.4 shows the ambiguity plot for this case using our localization algorithm. The ambiguity plot is a plot of the reciprocal of $\|\mathbf{e}\|^2$ from equation (2.6) as a function of depth

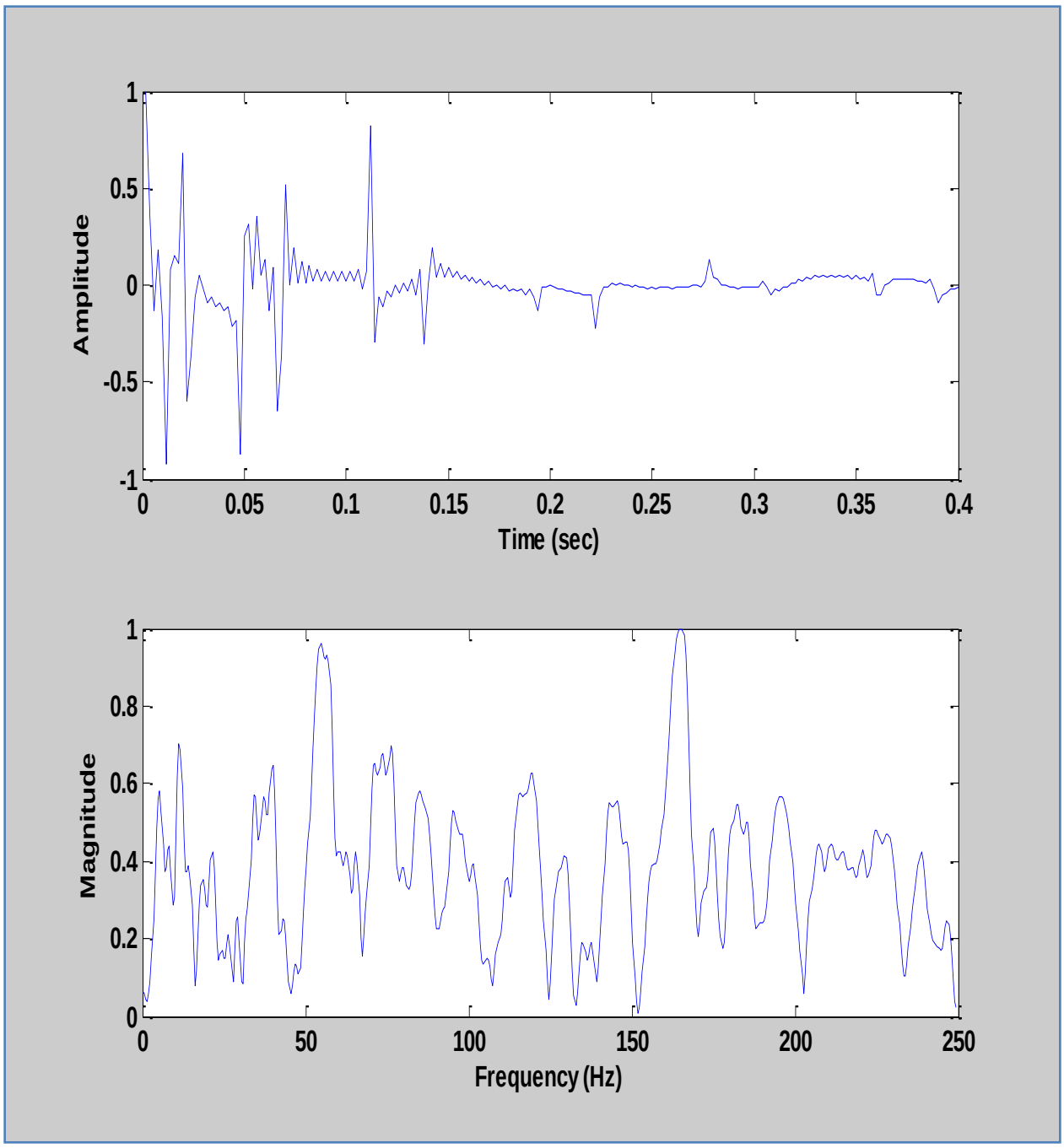

Figure 3.2. (a) Time domain view of the correct Green's function; (b) Frequency domain view of the correct Green's function.

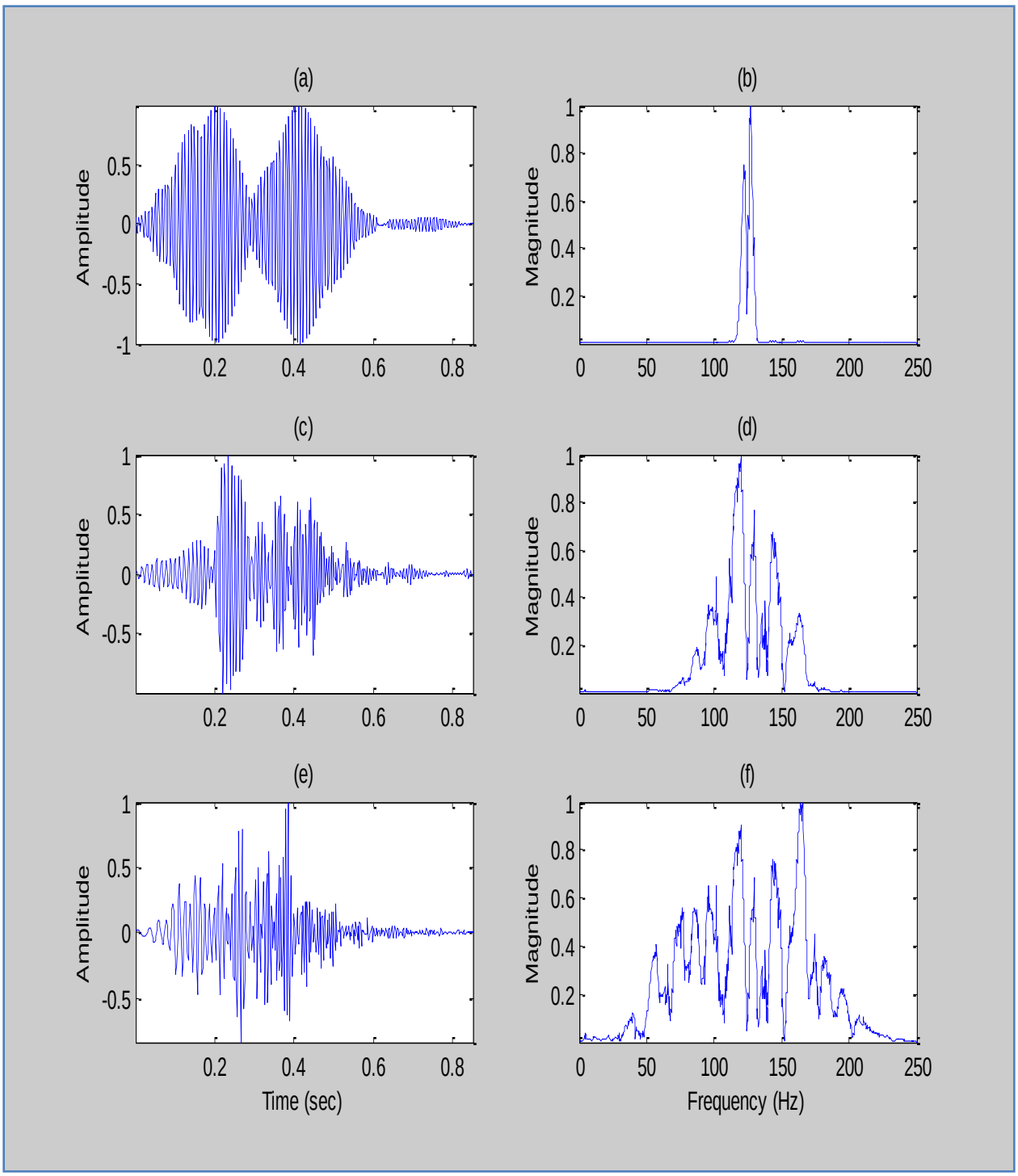

Figure 3.3. The receiver signals calculated by convolving the source signals in Figure 3.1 with the Green's function in Figure 3.2. (a) Time domain measured signal for the 10 Hz LFM sweep; (b) Frequency domain measured signal for 10 Hz LFM sweep; (c) Time domain measured signal for the 100 Hz LFM sweep; (d) Frequency domain measured signal for the 100 Hz LFM sweep; (e) Time domain measured signal for the 200 Hz LFM sweep; (f) Frequency domain measured signal for the 200 Hz LFM sweep.

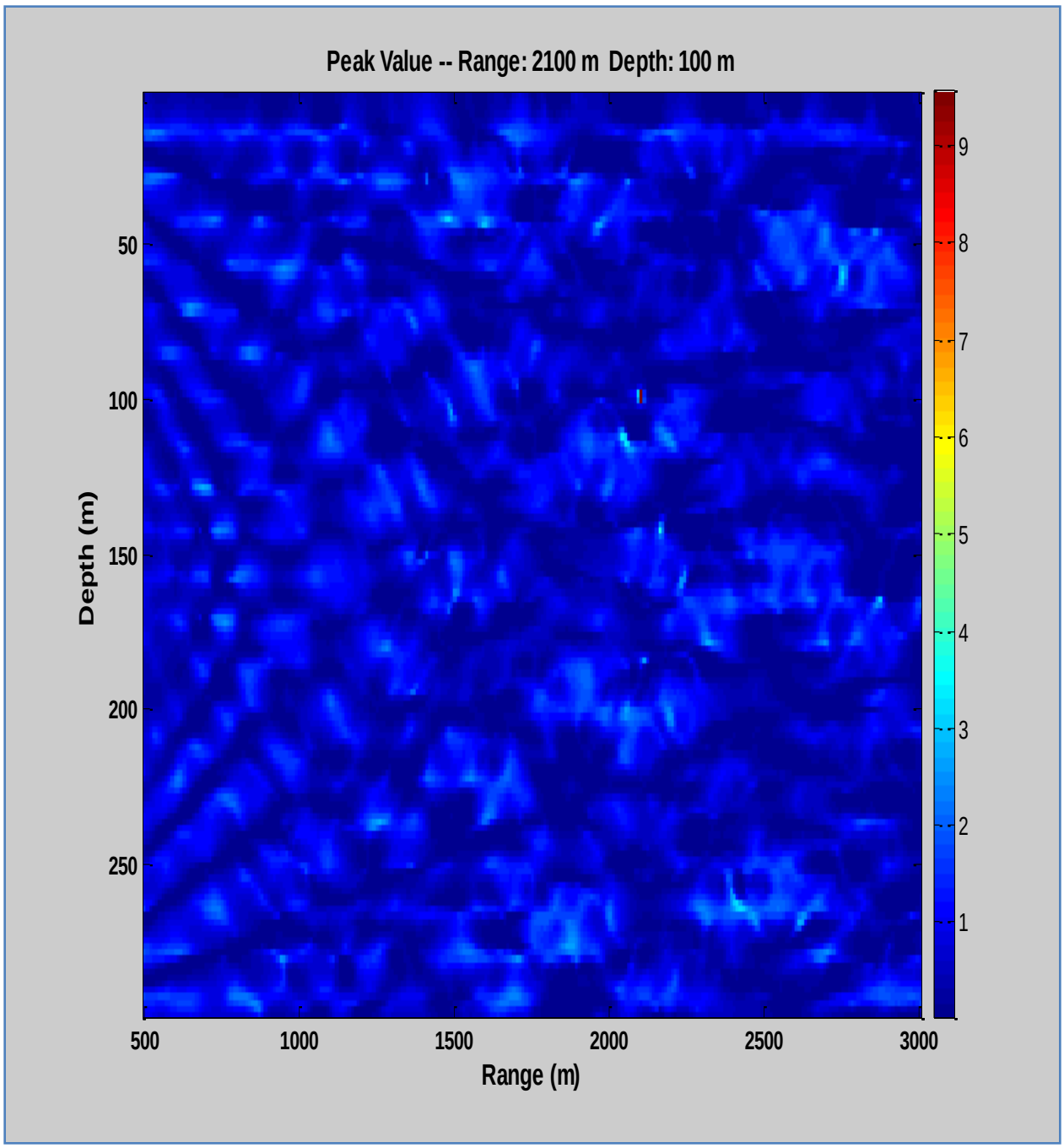

Figure 3.4. Ambiguity plot of our new single hydrophone localization algorithm over a grid of trial source locations for the 10 Hz case. The colors correspond to the reciprocal of the value of the localizer function in each bin. The peak of the localizer function occurs at a range of 2100 meters and a depth of 100 meters. The true location of the source is a range of 2100 meters and a depth of 99 meters.

of the source and range of the source from the receiver. We plotted the reciprocal so that the peak value will represent the source location estimate, to be consistent with the other localizers we discussed in Chapter 1. Our grid spacing was 10 meters in range and 2 meters in depth. There is a clear peak at a range of 2100 meters and a depth of 100 meters. Recall that the true location of the source is at a range of 2100 meters and depth of 99 meters. The localizer successfully located the source within 1 meter despite the source being slightly off of the grid of trial source locations, and having only a 10 Hz signal bandwidth. Note that localization within 1 meter is the best possible because of the discrete grid of locations over which the calculations are done. Figure 3.5 gives a close up view of the localizer peak and shows that the peak quickly tapers off in both range and depth. The peak drops off within about 20 meters in range and 4 meters in depth.

We now consider the performance of the other single hydrophone localizers for comparison. One issue to consider first is that the localizers by Jesus *et al*. (2000) and Tiemann *et al*. (2006) require their Green's functions be calculated using a ray model. We used BELLHOP to do this by modeling the Pekeris waveguide using a constant sound speed profile in the water column and a constant sound speed in the bottom. Figure 3.6 overlays the analytical Green's function for the Pekeris waveguide with the estimated ray arrivals from BELLHOP. There is good agreement between the two models in timing and sign for many of the arrivals. There are two arrivals in the 0.2 to 0.25 second range where BELLHOP's estimate is misaligned in time and opposite in sign to the analytical solution. These disagreements are not surprising because the ray approximation of acoustics is most accurate with broadband, high frequency signals. Although our signals are broadband, we are operating on the low end of the frequency

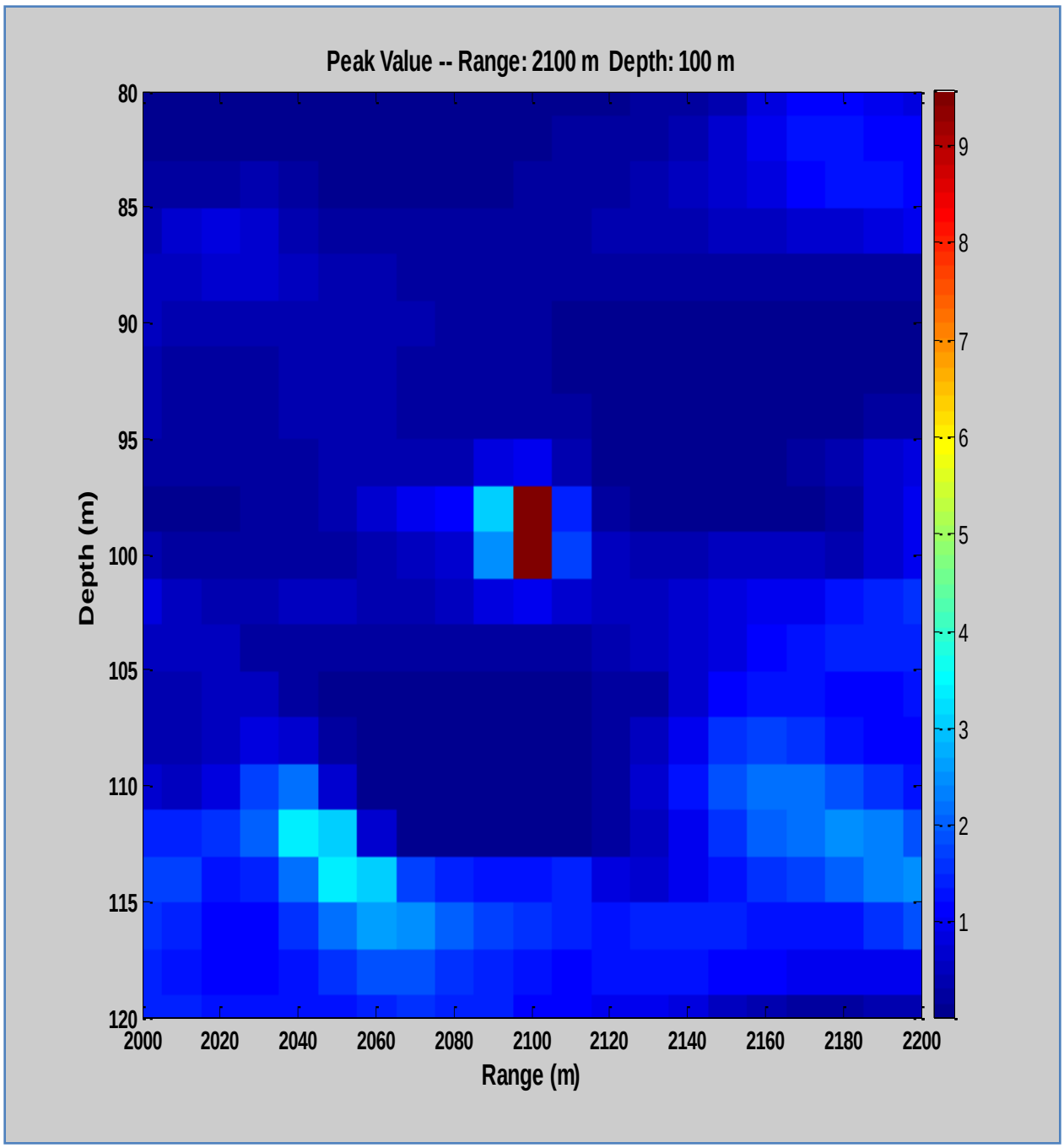

Figure 3.5. Close up view of the localizer function in Figure 3.3 around the source location. The range bin size is 10 meters and the depth bin size is 2 meters. The localizer function tapers off in depth within about 4 meters of the source and tapers off in range within about 20 meters of the source.

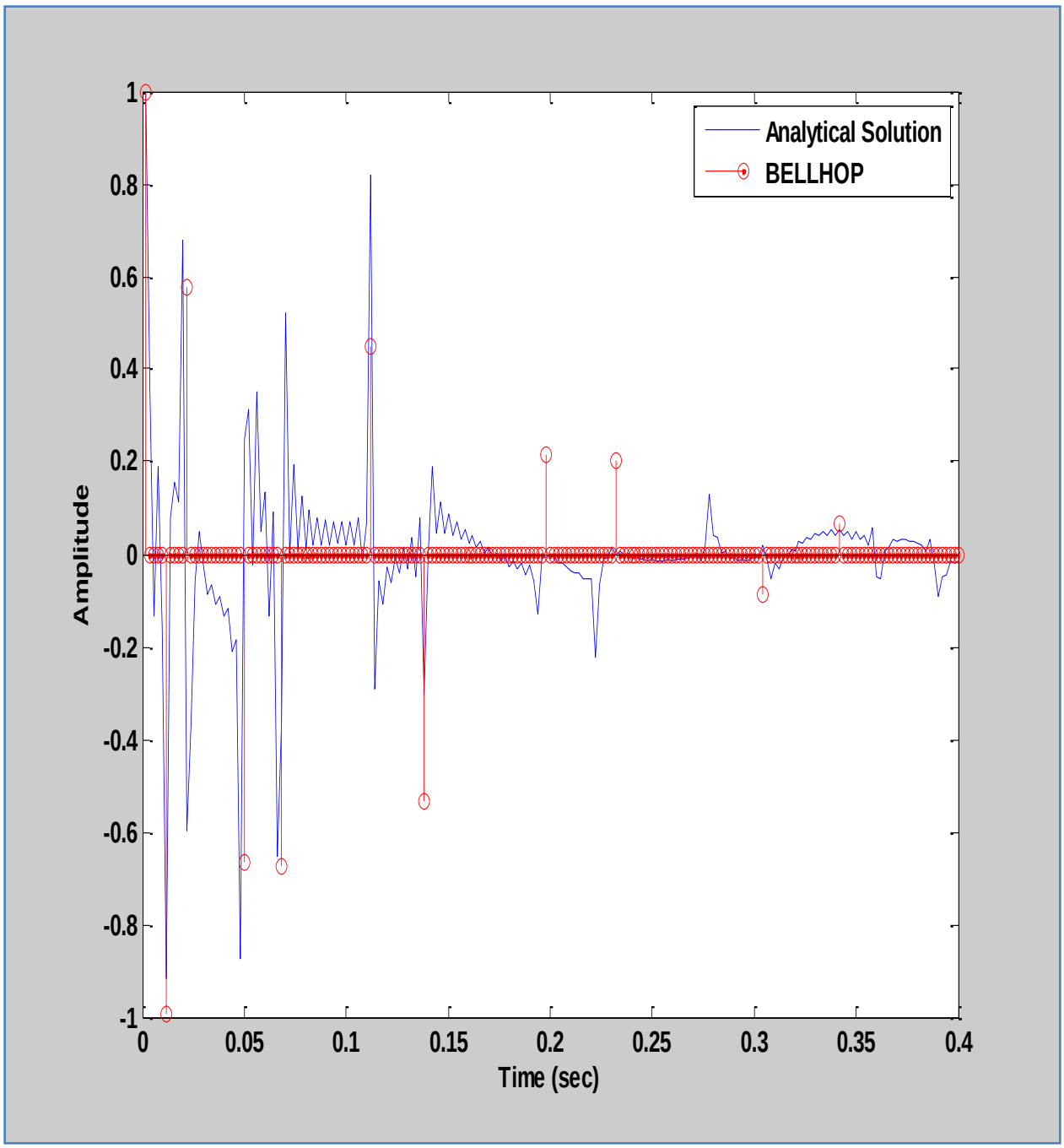

Figure 3.6. Overlay of the analytical solution to the Pekeris waveguide with the ray approximation calculated by the BELLHOP acoustic ray model for our trial case. There is generally good agreement here with the exception of the arrivals in the 0.2 to 0.25 second range where there is an apparent misalignment in time and sign reversal given by BELLHOP.

scale where the ray approximation is the least accurate. However, the literature on the ray based localizers discussed in Chapter 1 shows that the ray approximation can be used successfully at lower frequencies and we saw similar successes in some of our trials.

Figures 3.7 and 3.8 show the ambiguity plots for our new localizer and the localizers discussed in Chapter 1 for comparison. To identify each localizer, the last name of the first author of each localizer is displayed above each plot. For the localizers developed by Frazer *et al*. (1990), we add the phonetic spelling of the Greek letter they used to label each localizer discussed in section 1.4.2. For example, the localizer corresponding to equation (1.17) is labeled Frazer Chi1 in our plot. The number corresponds to the subscript on the Greek letter in equation (1.17) to distinguish it from equation (1.16) which has the same Greek letter with a subscript of 2. Also notice that the localizer shown by equation (1.16) is the same as the one by Li and Clay (1987) given by equation (1.15). We plotted this localizer once with the label of Clay/Frazer Chi2. This nomenclature will be used hereafter to identify the different localizers shown in the ambiguity plots.

The only localizers that are successful in this case are the Clay/Frazer Chi2 localizer and our new localizer (Chapin). The others gave estimates several hundred meters from the source location with many peaks in the ambiguity plots. The Clay/Frazer localizer uses the source signal directly and therefore has an advantage over our localizer function. In fact, the Porter, Lee, Jesus, Tiemann, Frazer Chi1, Frazer/Clay Chi2, and Frazer Mu localizers all require explicit knowledge of the source signal to do the calculations. Only our localizer and the remaining Frazer localizers can be calculated without knowledge of the source signal. The results suggest that a source signal with a relatively narrow bandwidth of 10 Hz could pose a problem for most

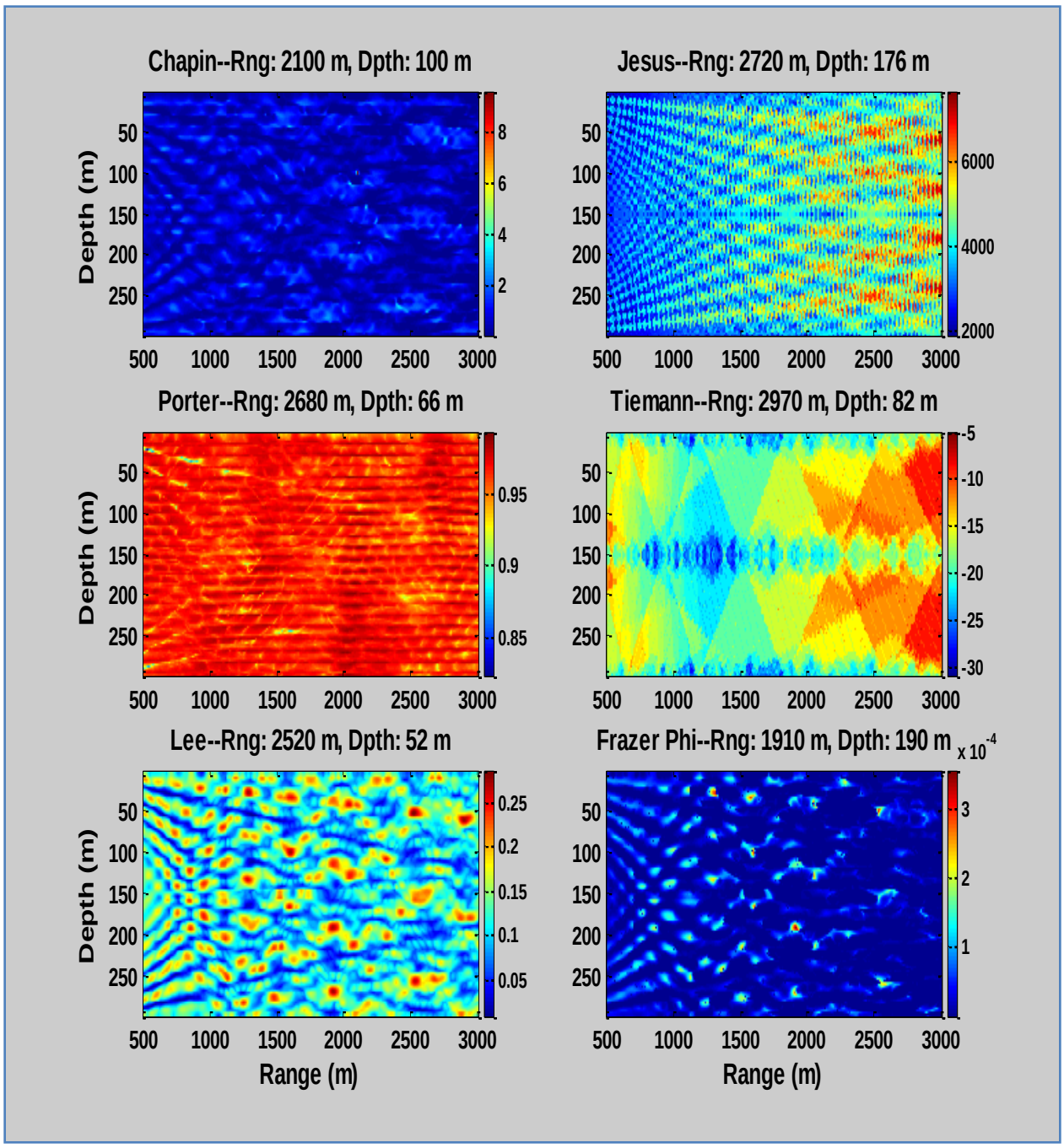

Figure 3.7. Ambiguity plots of several of the localizers for the 10 Hz bandwidth source signal. The plots are labeled by the last name of the first author of the papers discussed in Chapter 1. For the localizers developed by Frazer *et. al.*, the name is followed by a phonetic spelling of the Greek letter that labels their localizers discussed in section 1.4.2. The new localizer we introduced in this dissertation is labeled with the author's last name and it appears in the upper left corner. Each name is followed by the range and the depth of the source location estimate for that localizer. Only the Chapin localizer successfully located the source among those shown in this figure.

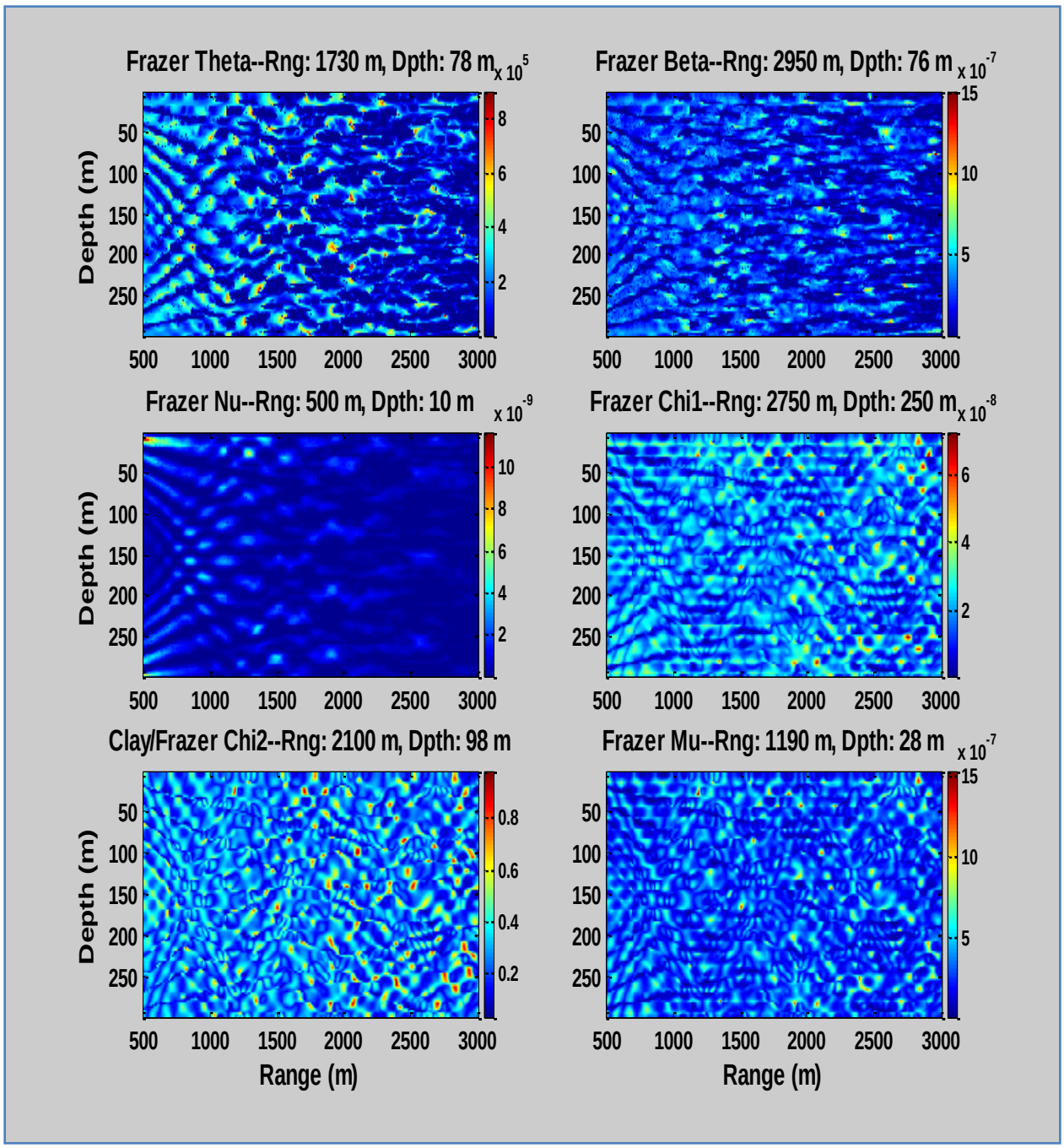

Figure 3.8. Ambiguity plots of several of the localizers for the 10 Hz bandwidth source signal. The plots are labeled by the last name of the first author of the papers discussed in Chapter 1. For the localizers developed by Frazer *et. al.*, the name is followed by a phonetic spelling of the Greek letter that labels their localizers discussed in section 1.4.2. Each name is followed by the range and the depth of the source location estimate for that localizer. Only the Clay/Frazer localizer succeeds in locating the source among those shown in this figure.

of the localizers. Knowledge of the source signal only helped mitigate this with the Clay/Frazer localizer. Our localizer was able to locate the source within 1 meter with no source signal knowledge.

3.2.2 100 Hz Source Signal Bandwidth

We next consider a 0.5 second duration, 100 Hz bandwidth, LFM source signal sweeping from 75 Hz to 175 Hz. Figures 3.9 and 3.10 show the results and more of the localizers were successful in this case. Our localizer and the Porter, Frazer Chi1, Clay/Frazer Chi2, and Frazer Mu localizers were all successful at locating the source within 1 meter of its true location. The Frazer/Clay localizer uses the source signal in its calculation giving it an advantage. The additional 90 Hz of frequency content over the 10 Hz bandwidth case apparently benefited the Frazer Chi1 and Mu localizers because there was more detail in the replica signals to distinguish between different locations. The other Frazer localizers based on frequency domain calculations failed to locate the source, as in the 10 Hz bandwidth case. They do not use source signal information and are sensitive to small variations in the frequency content of the Green's functions from location to location. This suggests that if the Green's function for a location close to the true source location differs only slightly from the true Green's function, the localizer could fail to give an unambiguous peak. The ray-based localizers Tiemann and Jesus also failed to localize here and that was likely because a 100 Hz bandwidth is inadequate for the ray approximation to be valid and because the signals are low frequency.

3.2.3 200 Hz Source Signal Bandwidth

Our final case concerning source signal bandwidth is a 0.5 second duration, 200 Hz LFM signal sweeping from 25 Hz to 225 Hz. The results are shown in Figures 3.11 and 3.12. The

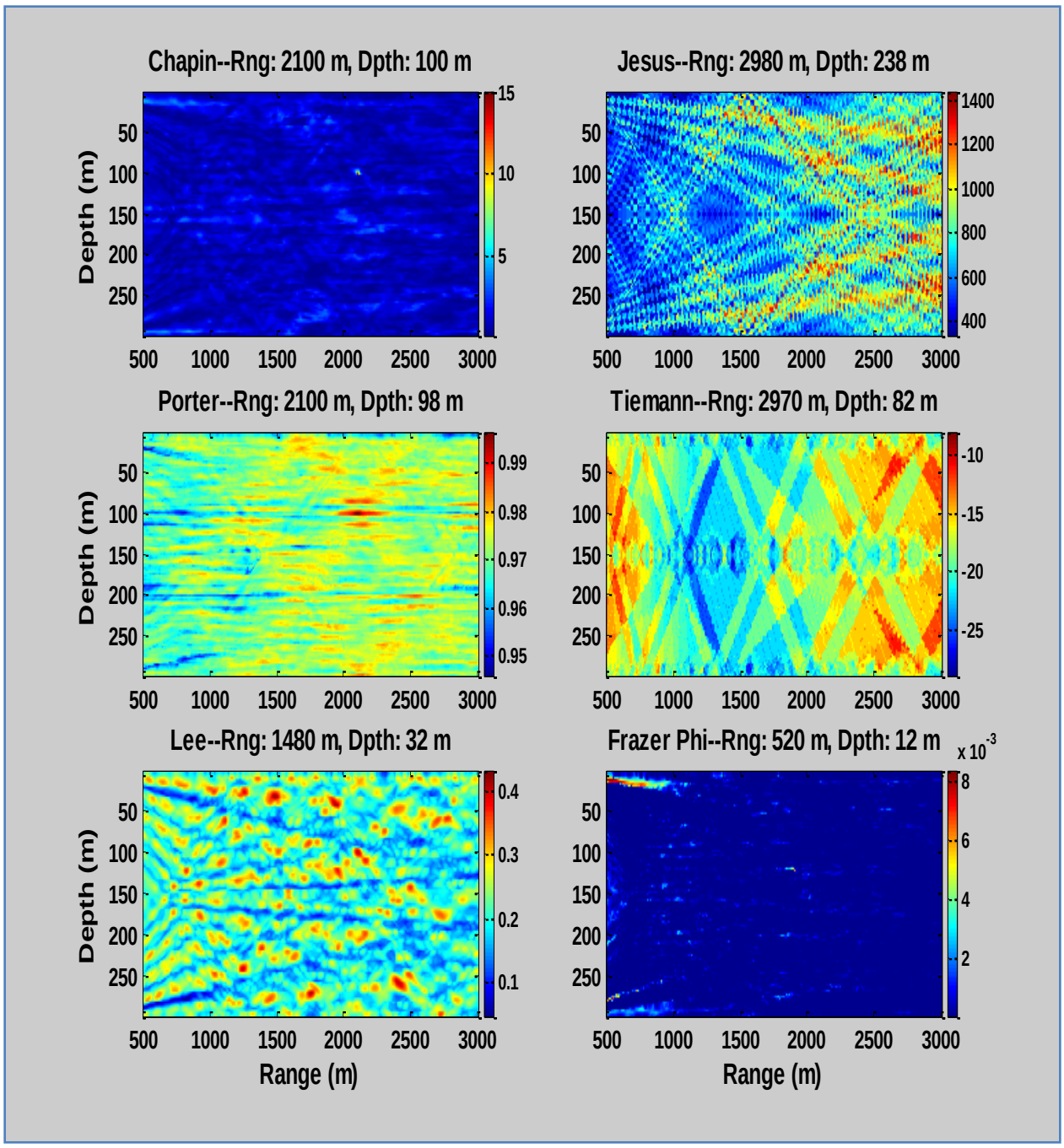

Figure 3.9. Ambiguity plots of several of the localizers for the 100 Hz bandwidth source signal. Our localizer and the Porter localizer are successful here.

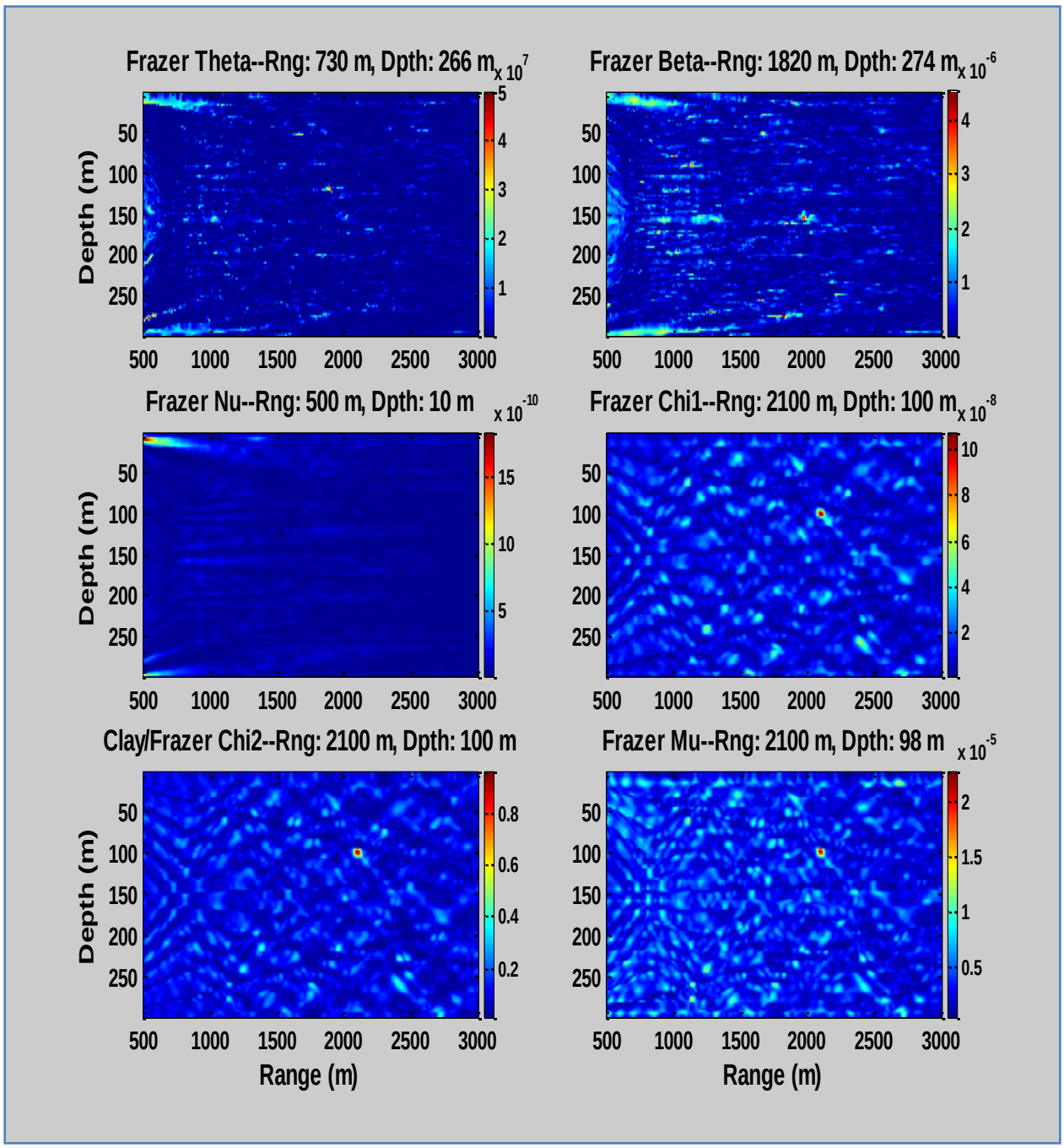

Figure 3.10. Ambiguity plots of several of the localizers for the 100 Hz bandwidth source signal. The Frazer Chi1, Mu, and Clay/Frazer Chi2 localizers are all successful. They require knowledge of the source signal for their calculation.

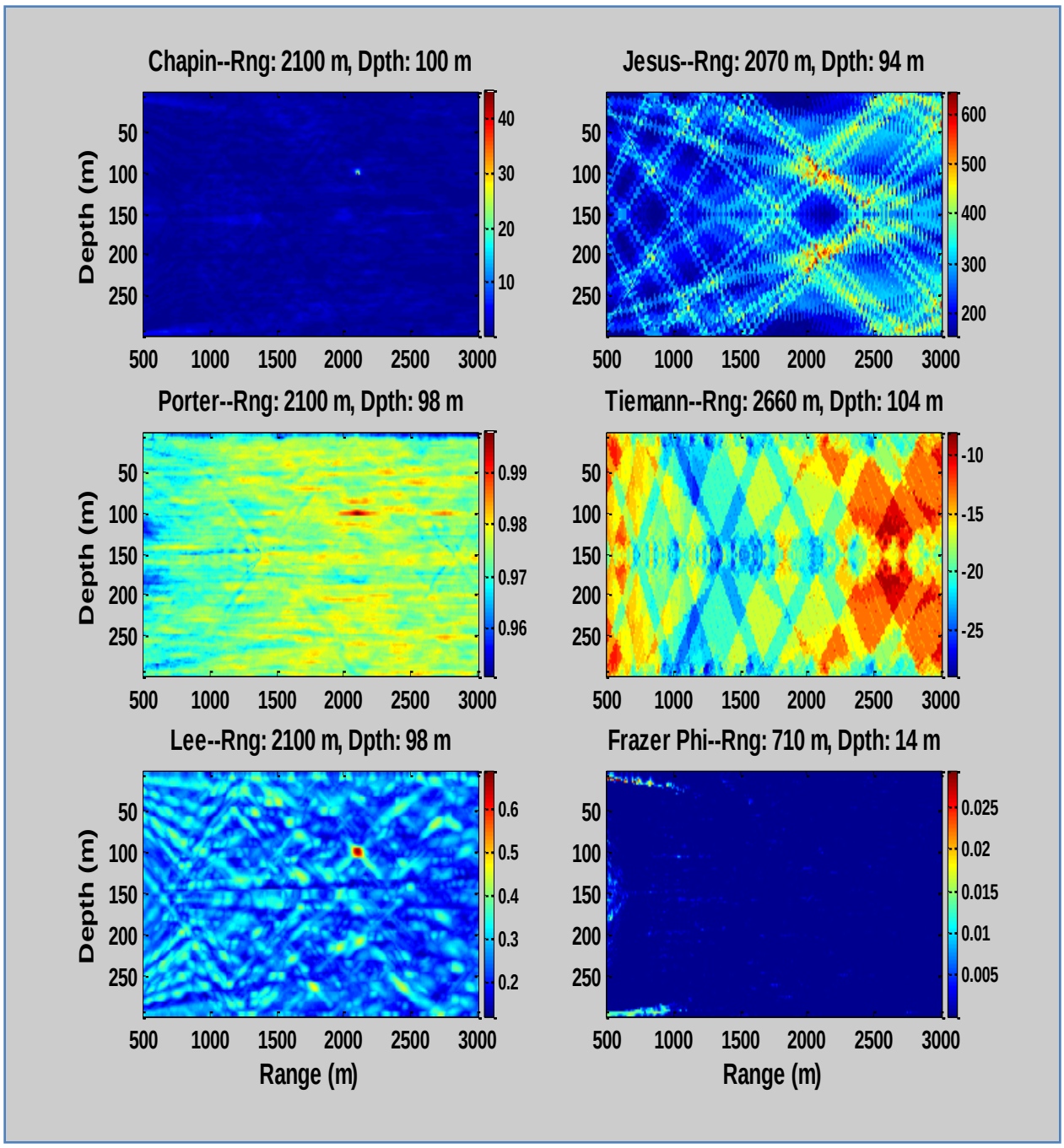

Figure 3.11. Ambiguity plots of several of the localizers for the 200 Hz bandwidth source signal. The Chapin, Porter, Lee and Jesus localizers succeed in this case, although the Jesus localizer is less accurate. The Frazer Phi and Tiemann localizers continue to have difficulty.

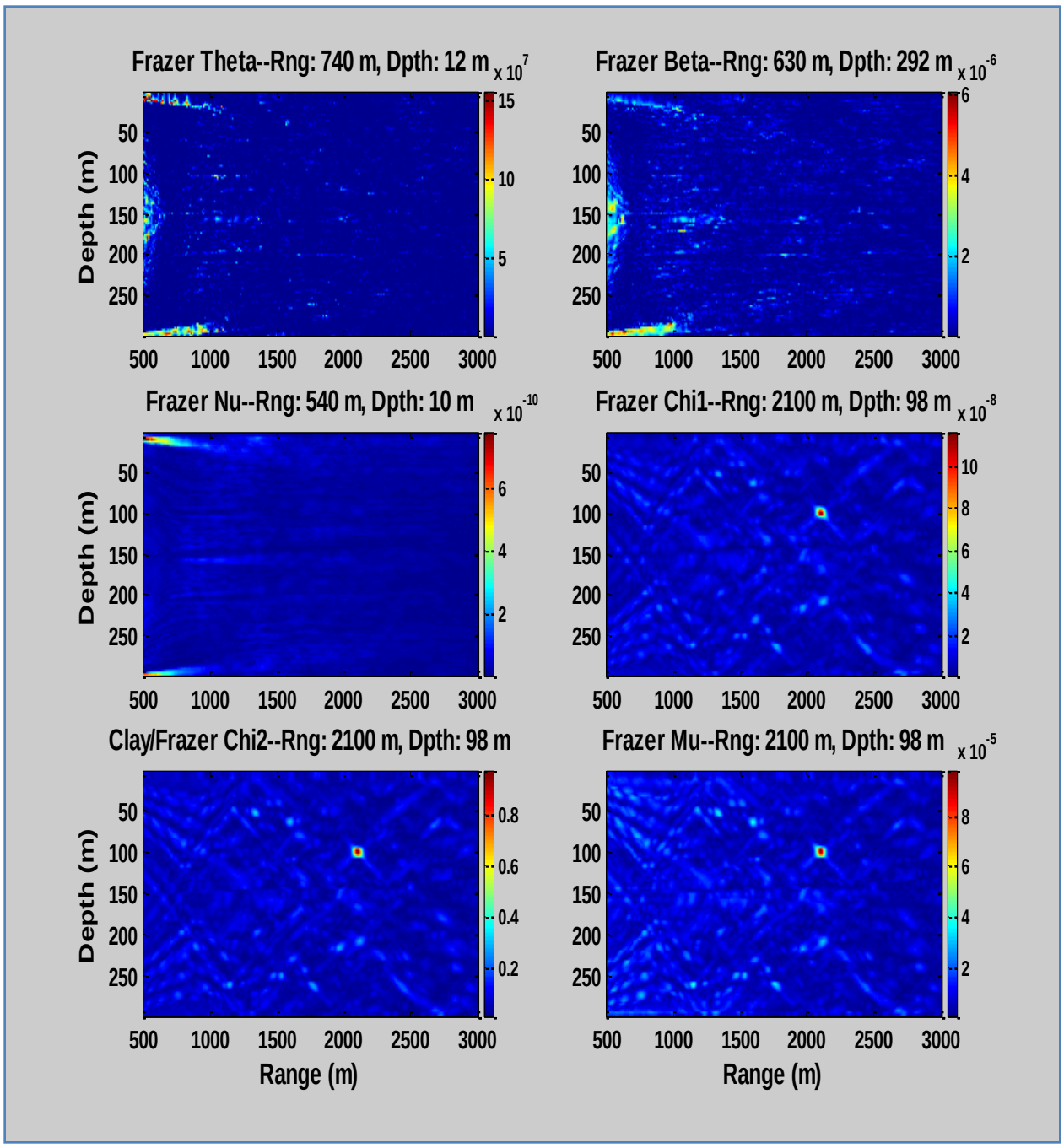

Figure 3.12. Ambiguity plots of several of the localizers for the 200 Hz bandwidth source signal. The Frazer Chi1, Mu, and Clay/Frazer Chi2 localizers are all successful. The other Frazer localizers continue to have difficulty.

results improve upon the 100 Hz case with successful localization by the Chapin, Porter, Lee, Jesus, Frazer Chi1 & Mu, and Clay Frazer Chi 2 localizers. The Lee and Jesus localizers have their first successes here after difficulty with the 10 Hz and 100 Hz bandwidth cases.

The Lee localizer calculates the cross-correlation of the estimated Green's function from the measurement with Green's functions from an acoustic model. The Green's function generally consists of many short duration, high amplitude peaks representing reflections of the sound from the surface of the water and the bottom. It takes a broad range of frequencies to produce short duration spikes in the time domain. The Lee localizer needs 200 Hz of bandwidth in this case to get reasonable approximations to the Green's functions and to successfully locate the source. A similar argument applies to the Jesus localizer which incorporates the ray approximation of acoustics explicitly into the signal model. The Green's functions in the ray approximation consist of spikes separated by zeros. These will also require a broad range of frequencies to approximate adequately for single hydrophone localization. The Tiemann localizer, also based on the acoustic ray approximation, fails again. The time domain measured signals in Figure 3.3 show that there are not clear and distinguishable arrivals in the measurement to compare with the output of a ray acoustic model. Clear and identifiable arrivals in the measurement signal are required for the Tiemann localizer to function properly.

3.2.4 Summary of Source Signal Bandwidth Parameterization

Our parametric study of the impact of source signal bandwidth on single hydrophone localization shows that only our new localizer function and the Clay/Frazer Chi2 localizers are successful with 10 Hz of bandwidth. The Clay/Frazer localizer has the additional advantage of knowledge of the source signal. More of the localizers are successful with 100 Hz and 200 Hz of bandwidth to work with. This is consistent with a common statement made in the literature that

one trades aperture for bandwidth in matched field processing. In other words, we are trading off the lack of spatial measurements of the acoustic field for the availability of broadband information in the measurement signal. Our results suggest that if too much broadband information is lost because of source signal limitations, such as in the 10 Hz and 100 Hz cases, many of the localizer functions we discuss may fail. Our new localizer function demonstrates a unique quality of robustness down to a 10 Hz bandwidth without requiring knowledge of the source signal, something none of the other localizers show.

3.3 Signal-to-Noise Ratio Parameterization

In this section we extend our parameterization from section 3.2 to the impact of noise on our localizer and compare that to the impacts on the others. We look at four signal-to-noise ratios: 60 dB, 40 dB, 20 dB, and 0 dB. The signal-to-noise ratio (SNR) is calculated using the following definition:

$$SNR = 20\log_{10}\frac{\max_t|m(t)|}{\sqrt{E\{(kn(t))^2\}}}, \tag{3.4}$$

where *m(t)* is the measured signal and *n(t)* is a vector of random noise drawn from a Gaussian probability distribution with zero mean and variance of one, *k* is a multiplier used to scale *n(t)* to get the desired SNR, and $E\{\cdot\}$ is the mathematical expectation operator. The denominator is the standard deviation of the noise vector and the numerator is the maximum absolute amplitude of the measurement signal. This is an appropriate definition for use with transient signals with widely varying amplitudes. It is intuitive because the amplitudes of the noise vector can be easily compared with the peak amplitude of the measured signal by inspection. For example, an SNR of 0 dB implies that the standard deviation of the noise vector is the same as the maximum

amplitude of the measured signal, on average. An SNR of 40 dB implies that the maximum amplitude of the signal is 100 times that of the standard deviation of the noise. Using this definition, we add a scaled random vector to our measured signals and repeat the analysis of section 3.2.

Plots of the measurement signals with the 60 dB, 40 dB, 20 dB, and 0 dB signal-to-noise ratios are shown in Figures 3.13, 3.14, 3.15, and 3.16 respectively. The noise level is 10 times greater than the previous SNR as we progress from 60 dB to 0 dB. The noise in the signal is particularly pronounced at the 20 dB and 0 dB levels; most of the original features in the signal are barely perceptible at 0 dB. Our expectation is that the performance of the localizers will degrade significantly at 20 dB and 0 dB SNR.

The results of our SNR analysis are in Tables 3.1, 3.2, and 3.3 and the ambiguity plots are in the Appendix for brevity. To summarize the results, we calculated the distance between the true source location and the estimated source location for each localizer, signal bandwidth, and SNR and placed those distances in the table. The boxes are color coded with red or green to show, at a glance, which localizers performed well. We use an arbitrary distance of 50 meters as the threshold between a successful localization of the source and an unsuccessful localization. If the estimated source location is less than or equal to 50 meters from the true source location, we color the box green. If it is greater than 50 meters, we color it red. We regard the 50 meter threshold as a reasonable number based on a qualitative examination of the ambiguity plots and the distance errors in the table. For example, in the 100 bandwidth case, the Frazer Theta and Frazer Beta localizers go from a distance error of 1392 meters down to 96 meters as we move from 40 dB to 20 dB SNR. This suggests there is an element of chance involved in the apparent improved performance of those localizers as the noise levels increased. Choosing a threshold of

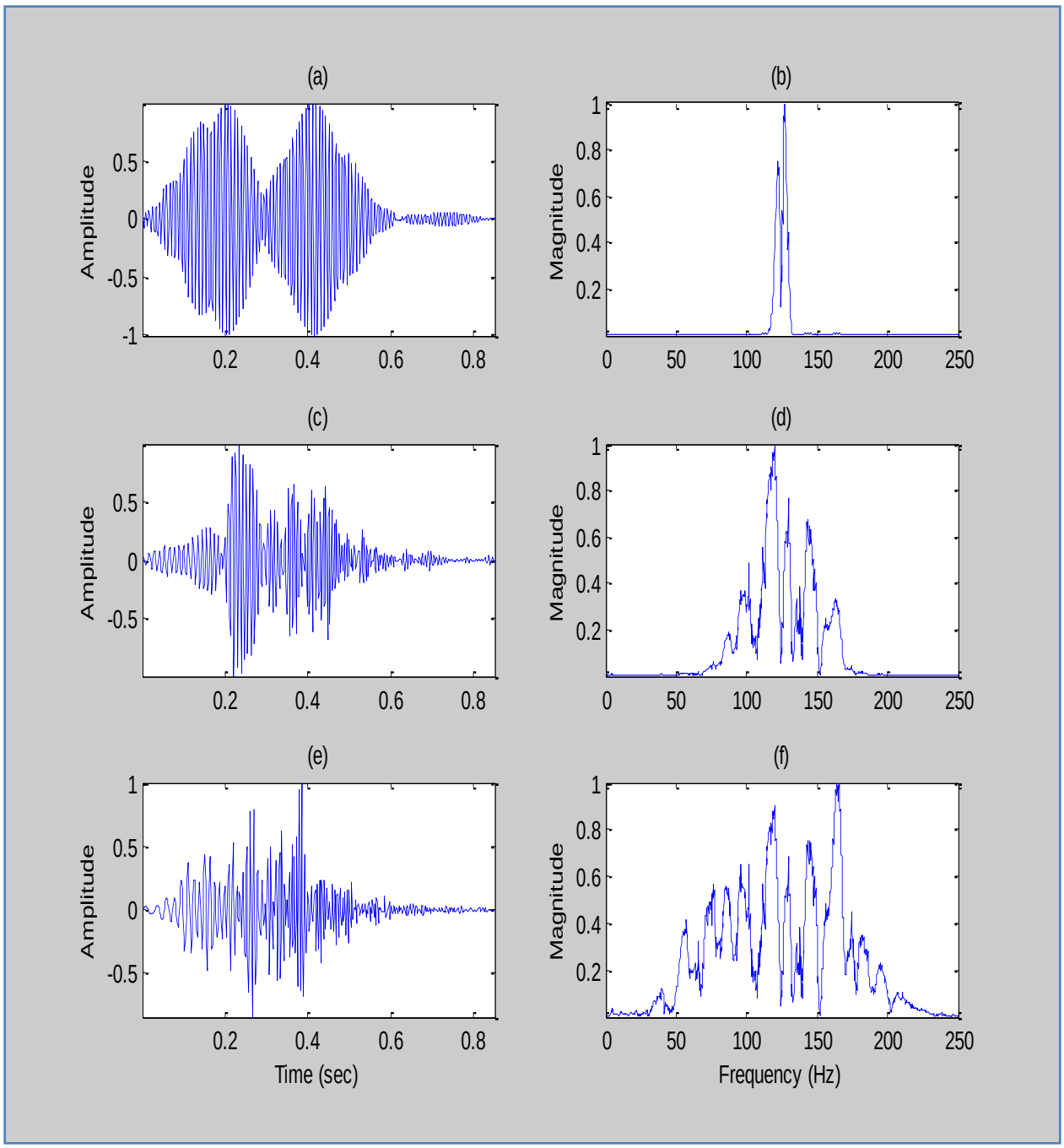

Figure 3.13. Plots of the 60 dB SNR measured signals in the time and frequency domains. (a) Time domain measured signal using the 10 Hz bandwidth LFM sweep. (b) Frequency domain measured signal using the 10 Hz bandwidth LFM sweep. (c) Time domain measured signal using the 100 Hz bandwidth LFM sweep. (d) Frequency domain measured signal using the 100 Hz bandwidth LFM sweep. (e) Time domain measured signal using the 200 Hz bandwidth LFM sweep. (f) Frequency domain measured signal using the 200 Hz bandwidth LFM sweep.

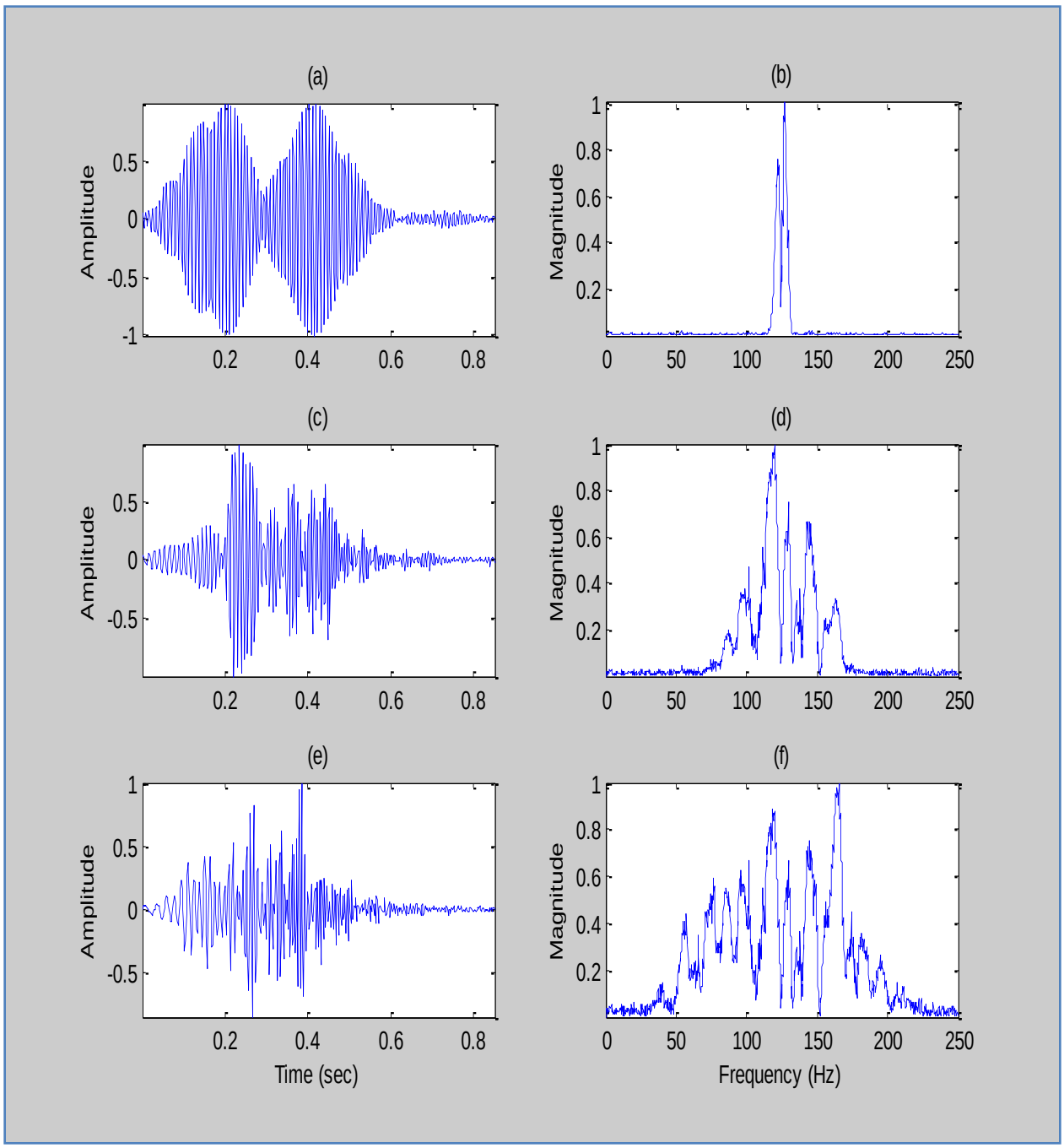

Figure 3.14. Plots of the 40 dB SNR measured signals in the time and frequency domains. (a) Time domain measured signal using the 10 Hz bandwidth LFM sweep. (b) Frequency domain measured signal using the 10 Hz bandwidth LFM sweep. (c) Time domain measured signal using the 100 Hz bandwidth LFM sweep. (d) Frequency domain measured signal using the 100 Hz bandwidth LFM sweep. (e) Time domain measured signal using the 200 Hz bandwidth LFM sweep. (f) Frequency domain measured signal using the 200 Hz bandwidth LFM sweep.

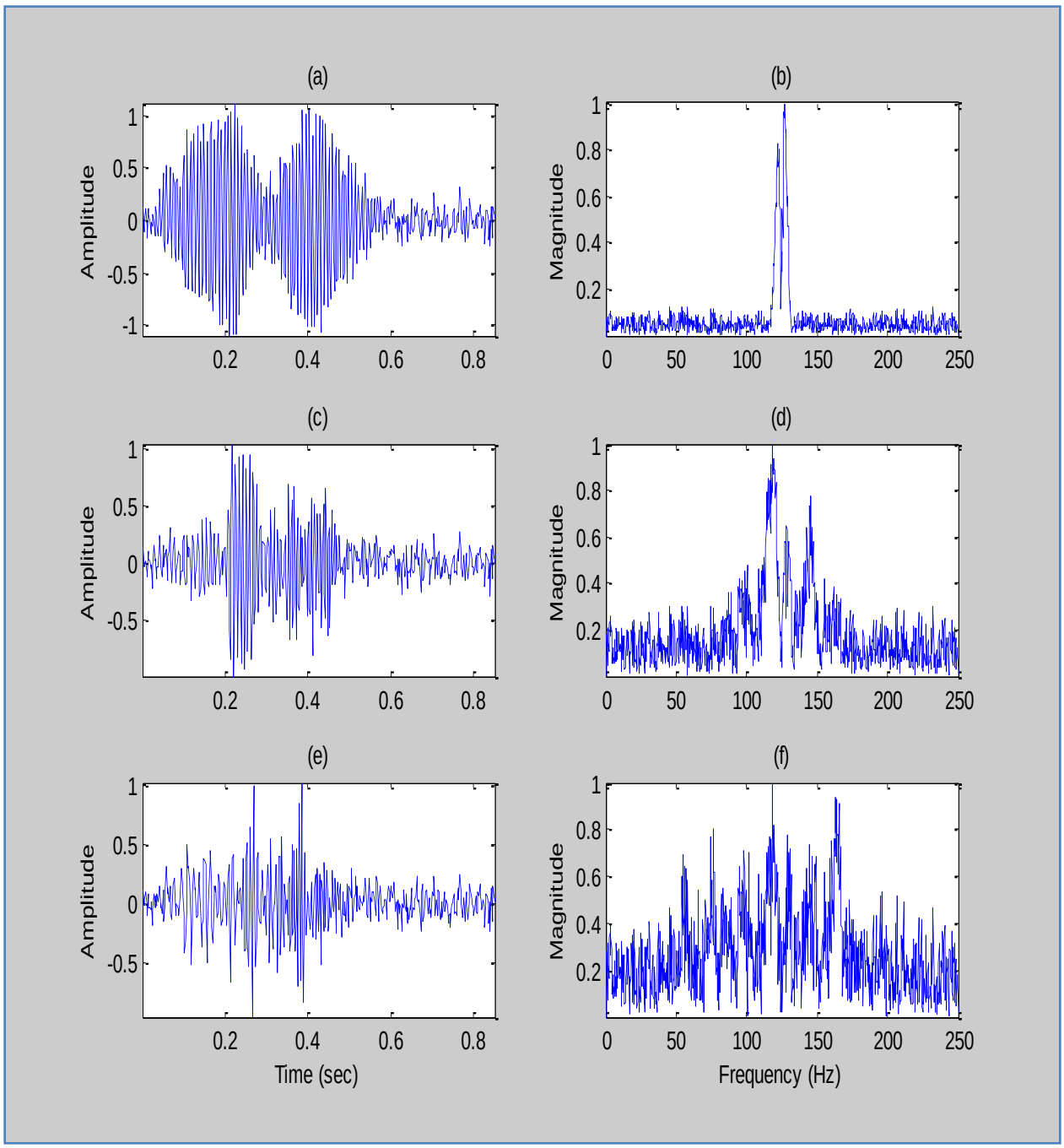

Figure 3.15. Plots of the 20 dB SNR measured signals in the time and frequency domains. (a) Time domain measured signal using the 10 Hz bandwidth LFM sweep. (b) Frequency domain measured signal using the 10 Hz bandwidth LFM sweep. (c) Time domain measured signal using the 100 Hz bandwidth LFM sweep. (d) Frequency domain measured signal using the 100 Hz bandwidth LFM sweep. (e) Time domain measured signal using the 200 Hz bandwidth LFM sweep. (f) Frequency domain measured signal using the 200 Hz bandwidth LFM sweep.

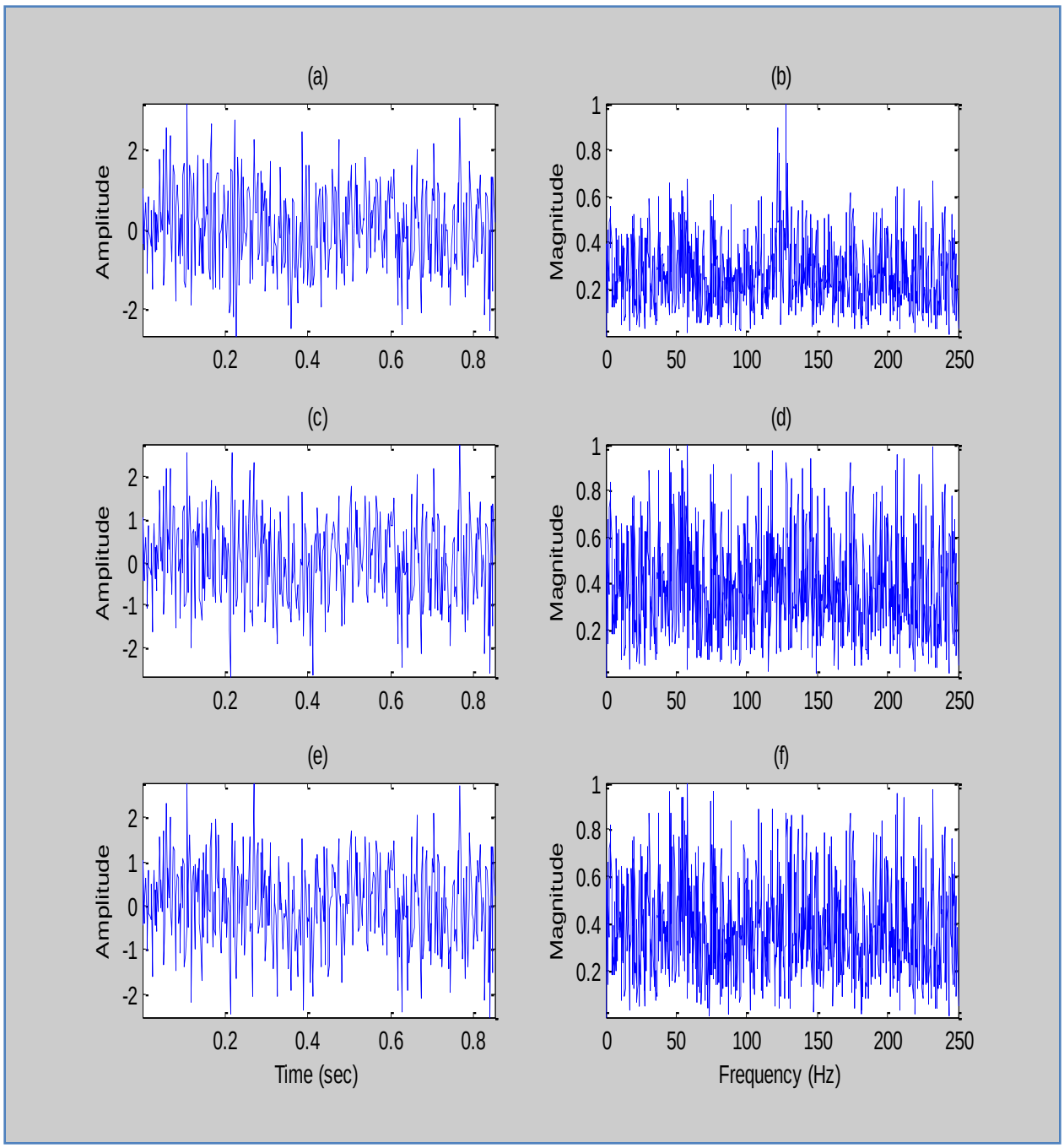

Figure 3.16. Plots of the 0 dB SNR measured signals in the time and frequency domains. (a) Time domain measured signal using the 10 Hz bandwidth LFM sweep. (b) Frequency domain measured signal using the 10 Hz bandwidth LFM sweep. (c) Time domain measured signal using the 100 Hz bandwidth LFM sweep. (d) Frequency domain measured signal using the 100 Hz bandwidth LFM sweep. (e) Time domain measured signal using the 200 Hz bandwidth LFM sweep. (f) Frequency domain measured signal using the 200 Hz bandwidth LFM sweep.

BW=10 Hz	SNR				
	Inf.	60	40	20	0
Chapin	1	1	1	1	843
Porter	581	581	74	765	1592
Lee	423	423	423	423	423
Jesus	625	625	625	625	862
Tiemann	870	870	870	870	851
Frazer Phi	211	1602	1602	1602	1602
Frazer Theta	371	1402	1402	96	96
Frazer Beta	850	790	790	96	96
Frazer Nu	1602	1602	1602	1602	1602
Frazer Chi1	667	667	667	667	183
Clay/Frazer Chi2	1	1	1	1	1
Frazer Mu	913	913	913	913	396

Table 3.1. Localization errors in meters for the 10 Hz bandwidth source signal at all SNRs.

BW=100 Hz	SNR				
	Inf.	60	40	20	0
Chapin	1	1	1	81	856
Porter	1	1	10	1561	677
Lee	624	624	624	624	492
Jesus	891	891	881	741	223
Tiemann	870	870	870	890	851
Frazer Phi	1582	1602	1602	1602	1602
Frazer Theta	1380	1392	1392	96	670
Frazer Beta	330	1392	1392	96	670
Frazer Nu	1602	1602	1602	1602	1602
Frazer Chi1	1	1	1	1	10
Clay/Frazer Chi2	1	1	1	1	10
Frazer Mu	1	1	1	1	491

Table 3.2. Localization errors in meters for the 100 Hz bandwidth source signal at all SNRs.

BW=200 Hz	SNR				
	Inf.	60	40	20	0
Chapin	1	1	1	10	293
Porter	1	1	1	1344	560
Lee	1	1	1	1	90
Jesus	30	30	31	61	467
Tiemann	560	560	560	240	851
Frazer Phi	1393	1602	1602	1602	1602
Frazer Theta	1363	221	221	670	670
Frazer Beta	1483	221	221	670	670
Frazer Nu	1563	1602	1602	1602	1602
Frazer Chi1	1	1	1	1	878
Clay/Frazer Chi2	1	1	1	1	878
Frazer Mu	1	1	1	1	878

Table 3.3. Localization errors in meters for the 200 Hz bandwidth source signal at all SNRs.

100 meters would indicate successful localization in these cases. In our judgment that is not reasonable so we choose a lower threshold to reduce the chance of false positives.

The results show that there is little difference between the 60 dB, 40 dB, and no noise cases for each source signal bandwidth. The differences emerge at 20 dB SNR, with the exception of the 10 Hz bandwidth cases where little changes. In the 100 Hz bandwidth case, our localizer and the Porter localizer fail to localize within 50 meters after success at lower noise levels. The 200 Hz bandwidth case shows our localizer succeeds, but the Porter localizer fails. The Jesus localizer fails by a slim margin relative to our threshold. At the 0 dB level, most of the localizers fail with the exception of the Clay/Frazer Chi2 localizers, and the Frazer Chi1 localizer in the 100 Hz bandwidth case. Recall that these localizers had the benefit of knowledge of the

source signal and that they are based on the cross correlation of the replica signal with the measured signal (see equations (1.16) and (1.17)).

The main lesson of this SNR analysis is that the performance of our localizer and the others degrades around the 20 dB level, although success is still possible. At the 0 dB level, the results suggest that localization is impossible without knowledge of the source signal. To identify the sensitivities of the localizer's performance to noise more precisely would require a Monte Carlo analysis using many noise realizations to collect statistics on the localization error. The sensitivities are not likely to be the same in every ocean environment. The Green's functions are generally complex and variable when modeling different locations and environments. A formal analysis to take these factors into account would be a massive computational effort and is outside the scope of this dissertation.

Chapter 4 Experimental Results

4.1 Introduction

In this chapter we consider the performance of our localizer on experimental data. The cases we looked at in Chapter 3 considered the sensitivity of the localizers under ideal conditions for which we could model the acoustic environment exactly. Controlled conditions are the correct approach to understand the sensitivities of our algorithm. However, scenarios in the real world contain many factors outside of our control and we must resort to approximations in our modeling. An important test of any signal processing algorithm is its ability to provide useful information under experimental conditions for which our knowledge of the environment is imperfect. We demonstrate that our algorithm can localize a source using experimental data and we continue our comparison with other single hydrophone localizers from the literature.

The experiment from which our data were taken is described in Field and Leclere (1993). The acoustic source was a 22 second LFM signal swept from 25 Hz to 150 Hz and was located 96 meters below the surface. The depth of the water was 915 meters and there were 15 element arrays of hydrophones located at various distances from the source. We will consider the data taken from 2 hydrophones located at a range of 1500 meters from the source and at depths of 129 meters and 250 meters. The sound speed profile is shown in Figure 4.1 and the density profile in Figure 4.2. The sound speed in the water is a downward refracting profile and a layer with high speed and density is evident about 200 meters into the ocean bottom. Field and Laclere (1993) state that the sound speed profile in the water was measured during the experiment and the sound speeds and densities in the bottom were extracted from Deep Sea Drilling Profiles in the vicinity

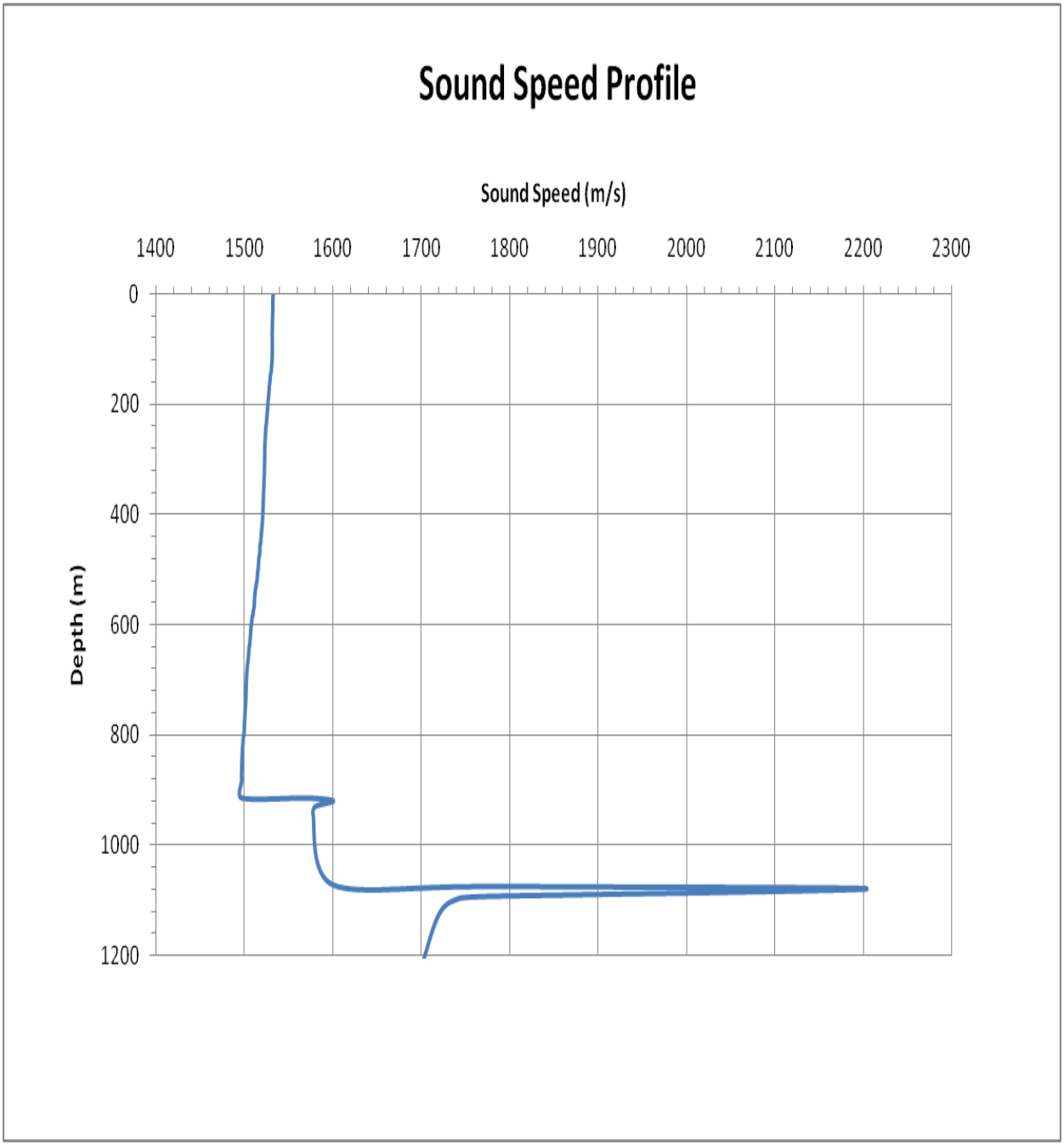

Figure 4.1. The sound speed profile of the water column and the bottom that we use in the acoustic propagation model to calculate the Green's functions. The water depth is 915 meters and there is a downward refracting sound speed profile. A layer of high sound speed and density is evident about 200 meters below the ocean bottom.

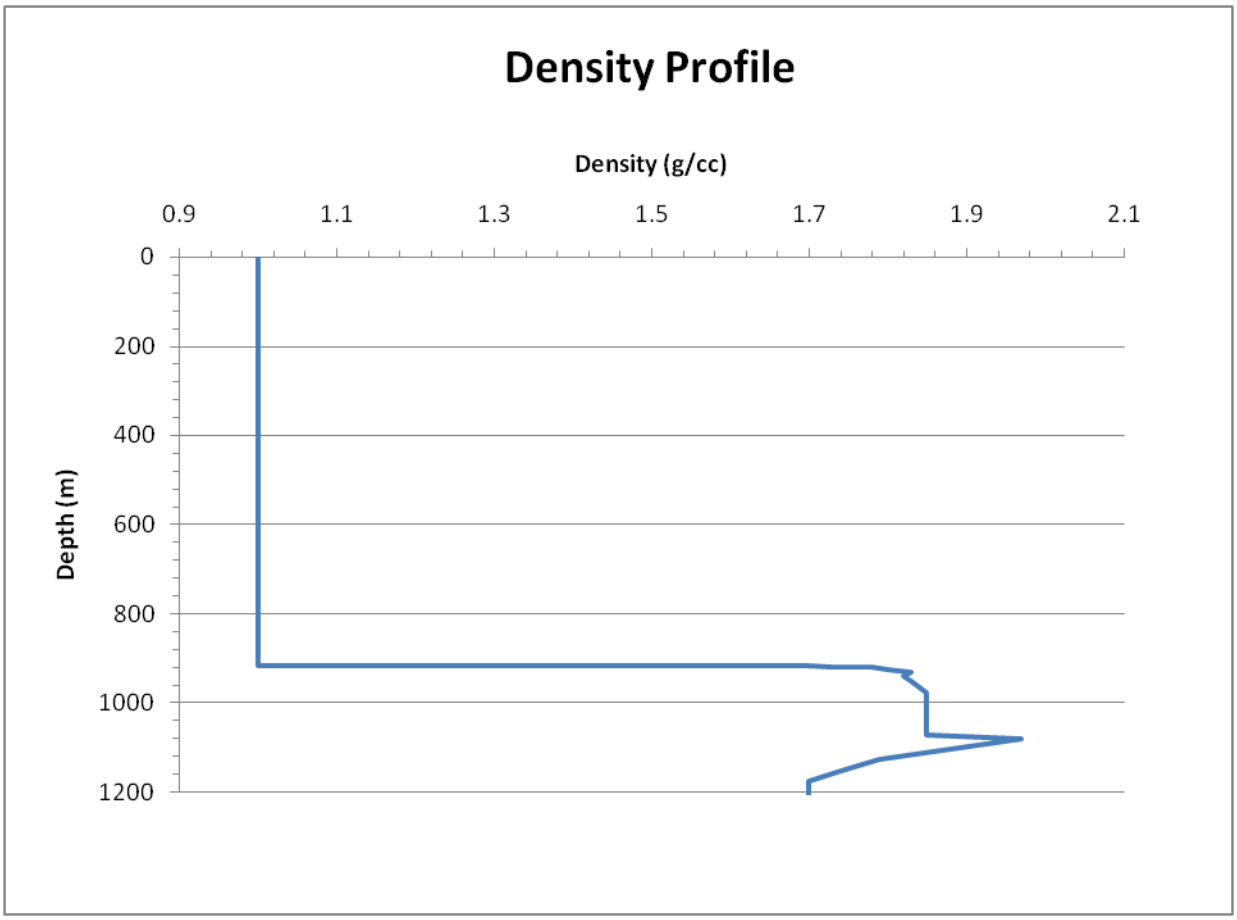

Figure 4.2. The density profile of the water column and the bottom that we use in the acoustic propagation model to calculate the Green's functions. The water is assumed a constant density of 1 g/cc and the bottom density was extracted from Deep Sea Drilling Profiles done in the vicinity of the experiment.

of the experiment. These sound speeds and densities are used in the SPARC acoustic propagation model (see section 1.3.2) to generate the Green's functions over a grid of trial source locations.

Field and Laclere (1993) correlate the measured hydrophone data with the source signal to estimate the Green's function directly from the data. This is possible because the autocorrelation of the source signal is narrow in time. We use that correlated data as our measurement data and the autocorrelation of the source as our source signal for the localizers

that require it. The following derivation from Field and Laclere (1993) shows that the correlated measurement data can be interpreted as the transmission of the autocorrelation of the source through the ocean to the receiver. The data received at the hydrophone is modeled as

$$p(t) = g(t) * s(t) + n(t), \tag{4.1}$$

where *p(t)* is the measured signal, *s(t)* is the source signal, *g(t)* is the Green's function, and *n(t)* is noise. Calculating the cross correlation of *p(t)* with *s(t)* gives

$$\begin{aligned} h(t) &= \left[s(t) \bigstar \left(g(t) * s(t)\right)\right] + \left[s(t) \bigstar n(t)\right] \\ &= \left[g(t) * \left(s(t) \bigstar s(t)\right)\right] + \left[s(t) \bigstar n(t)\right] \\ &= \left[g(t) * a(t)\right] + \left[s(t) \bigstar n(t)\right]. \end{aligned} \tag{4.2}$$

where *a(t)* is the autocorrelation of the source signal *s(t)*, the ★ symbol represents cross correlation, and *h(t)* is the correlated measurement data. Assuming that *s(t)* and *n(t)* are uncorrelated, the correlated measurement *h(t)* can be regarded as the convolution of the autocorrelation *a(t)* with the acoustic Green's function *g(t)*. In other words, *a(t)* becomes our source signal and *h(t)* becomes our measurement data. This will be the signal model we will assume in this chapter to test our localization algorithm.

4.2 Receiver at depth 129 meters

Our first case uses the correlated data from the hydrophone located at a range of 1500 meters and a depth of 129 meters. Figure 4.3 shows the autocorrelation and the FFT of the original source signal which we treat as the source signal in our model. The signal energy is contained in a band from 25 Hz to 150 Hz. The correlated measurement data are shown in Figure 4.4 and comparison with the source signal shows the effect of the ocean environment on

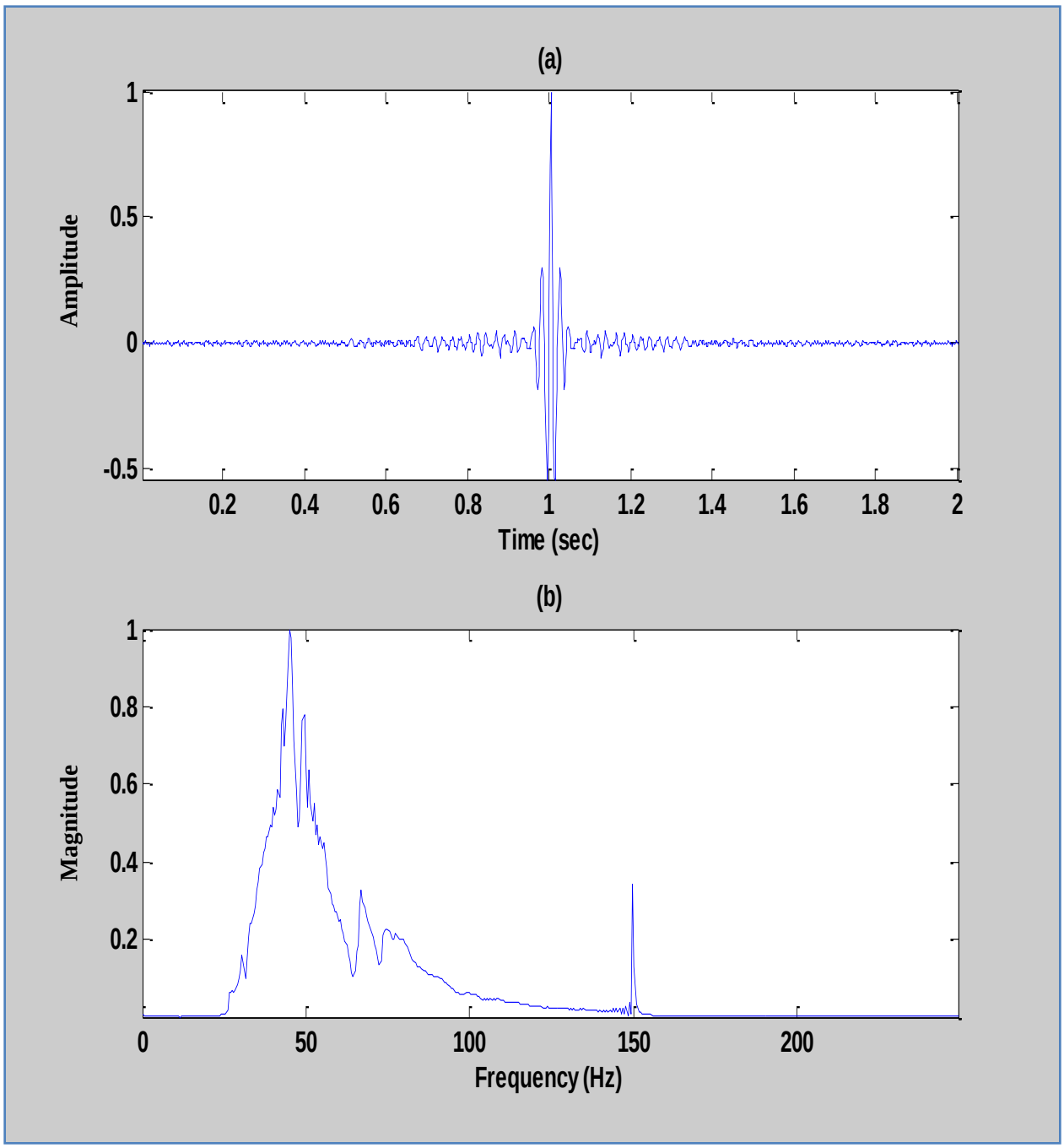

Figure 4.3. Autocorrelation of the source signal. (a) Correlated source signal in the time domain. (b) Frequency domain representation of the correlated source signal. The source is an LFM sweep from 25 Hz to 150 Hz and a 150 Hz tone.

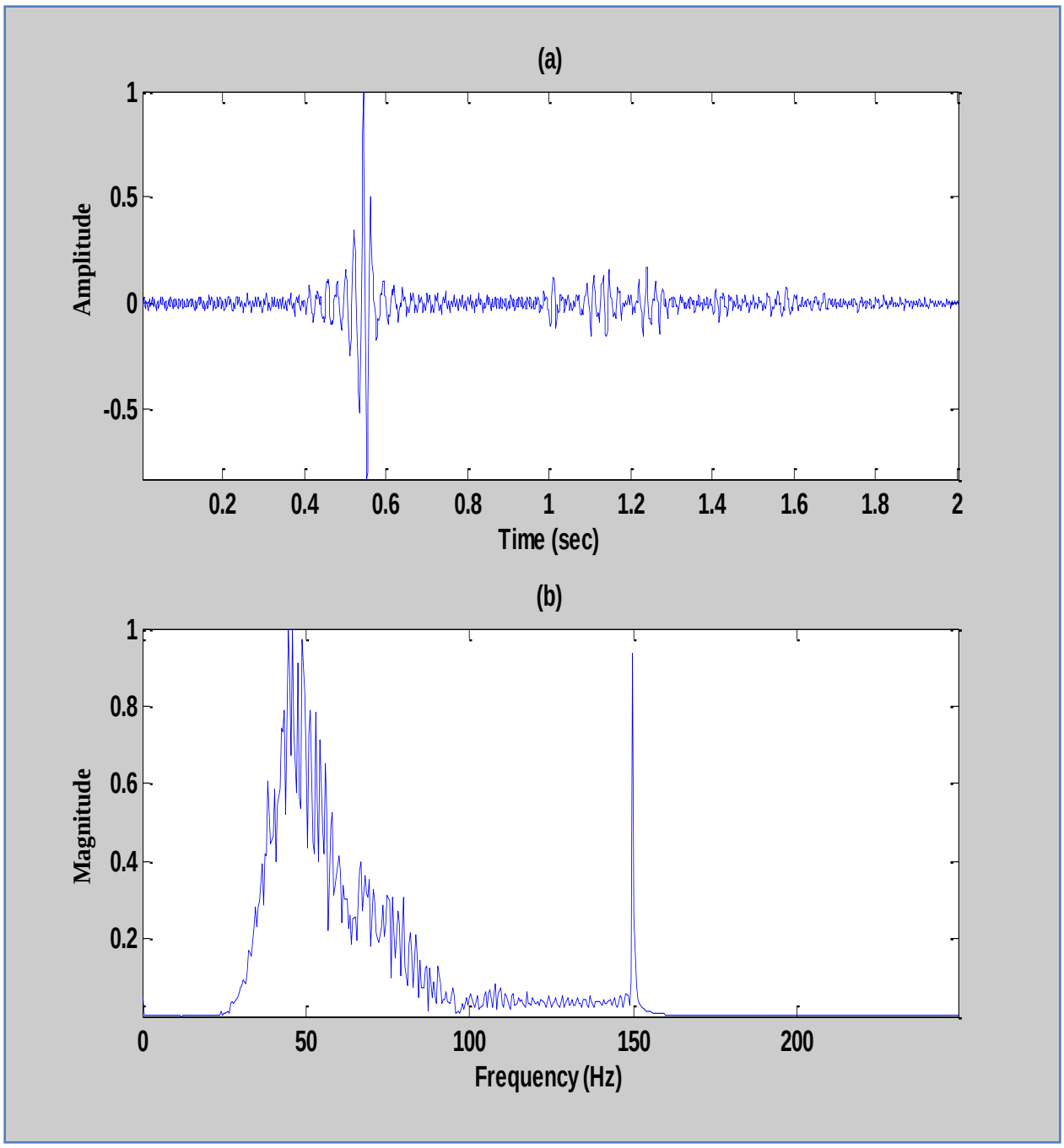

Figure 4.4. Correlated measurement data for the hydrophone located at a range of 1500 meters and a depth of 129 meters. (a) Time domain correlated measurement. (b) Correlated measurement in the frequency domain.

the source as it propagates to the receiver. The time domain plot shows two larger amplitude arrivals that are close together, but opposite in sign, between 0.5 and 0.6 seconds. The first arrival is the direct arrival from the source and the second is a result of a reflection from the surface of the water. Later arrivals show up after 1 second and are the result of interactions with both the bottom and the surface. The frequency domain plot shows the distortions introduced across all frequencies from the reflections of the energy. The absence of energy outside the pass band of the signal allows us to limit the frequency band over which we need to calculate the Green's functions. This is important in saving computational time. Figure 4.5 shows the Green's function calculated from SPARC for the correct source location. The time domain plot shows a strong resemblance to the correlated measurement data with two early arrivals and at least 4 later arrivals. The frequency domain plot shows the significant distortion across the pass band of the source signal and strong attenuation around 100 Hz. We cut the calculation off for frequencies above approximately 180 Hz because of the absence of source signal energy at these frequencies.

We begin by looking at the ambiguity plot for our localizer in Figure 4.6. The grid spacing we use to calculate the Green's function is 25 meters in range and 5 meters in depth. We only calculate down to a depth of 500 meters to conserve computational time. The source location estimate with the Chapin algorithm is 1525 meters in range and 95 meters in depth. Therefore we locate the source within 1 meter in the depth direction and within 25 meters in range. These are excellent results considering Field and Leclere (1993) state that the range is known within 25 meters of the nominal range of 1500 meters. One interesting feature of the plot is the band of higher amplitudes of the localizer function stretching from the upper left corner across the top to the right side at about a 100 meter depth. The direct and surface reflected arrivals follow this path and their spacing in both space and time is similar as the energy travels

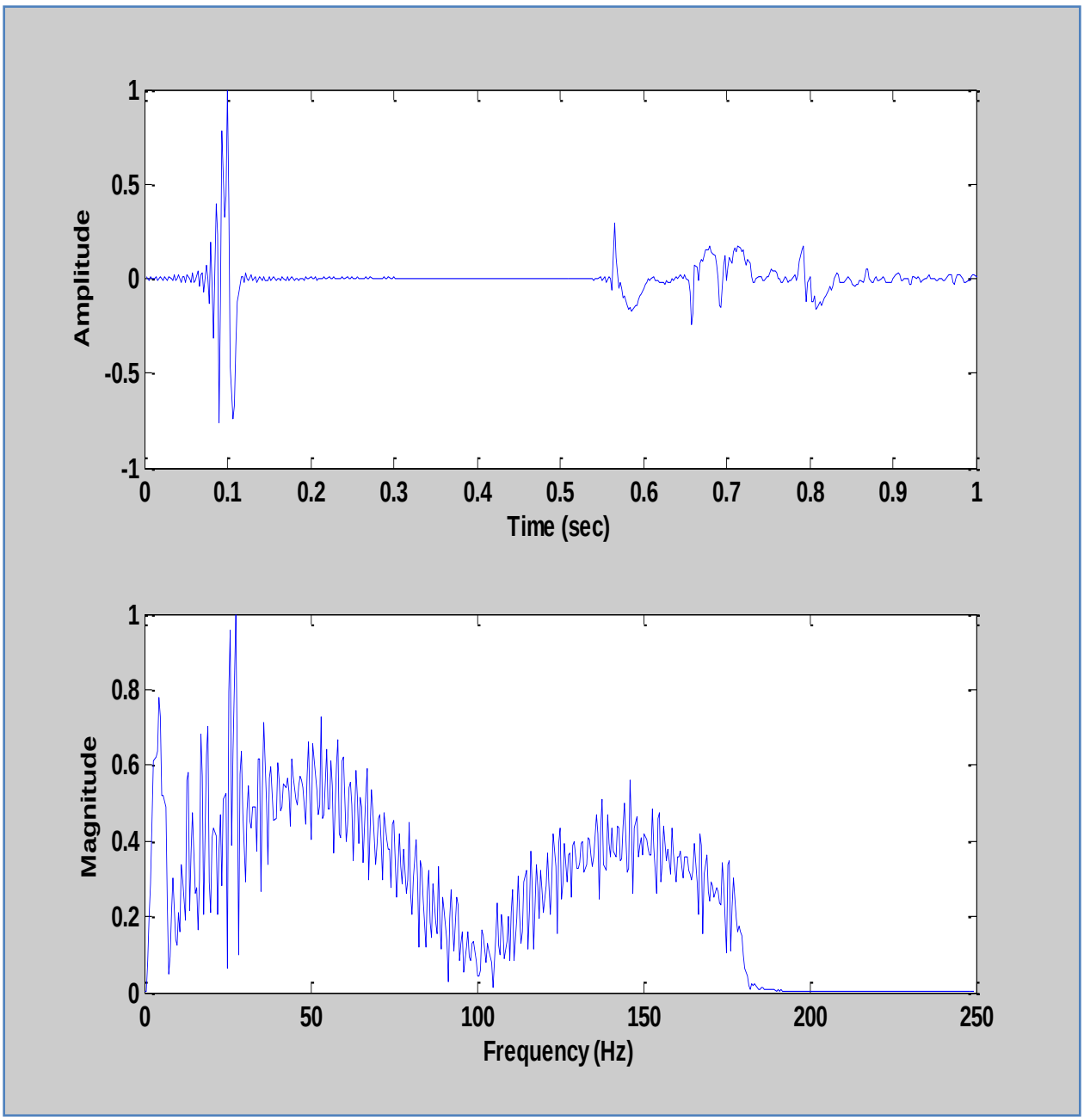

Figure 4.5. Green's function for 129 meter case calculated by SPARC. (a) Time domain plot. There are two early arrivals representing one direct arrival and one surface reflected arrival. At least 4 arrivals show up after nearly 0.5 seconds; those are reflections from the surface and the bottom. (b) Frequency domain plot showing distortion across the band and a null around 100 Hz. The calculation is cut off at approximately 180 Hz because there is no energy in the measured signal at these frequencies.

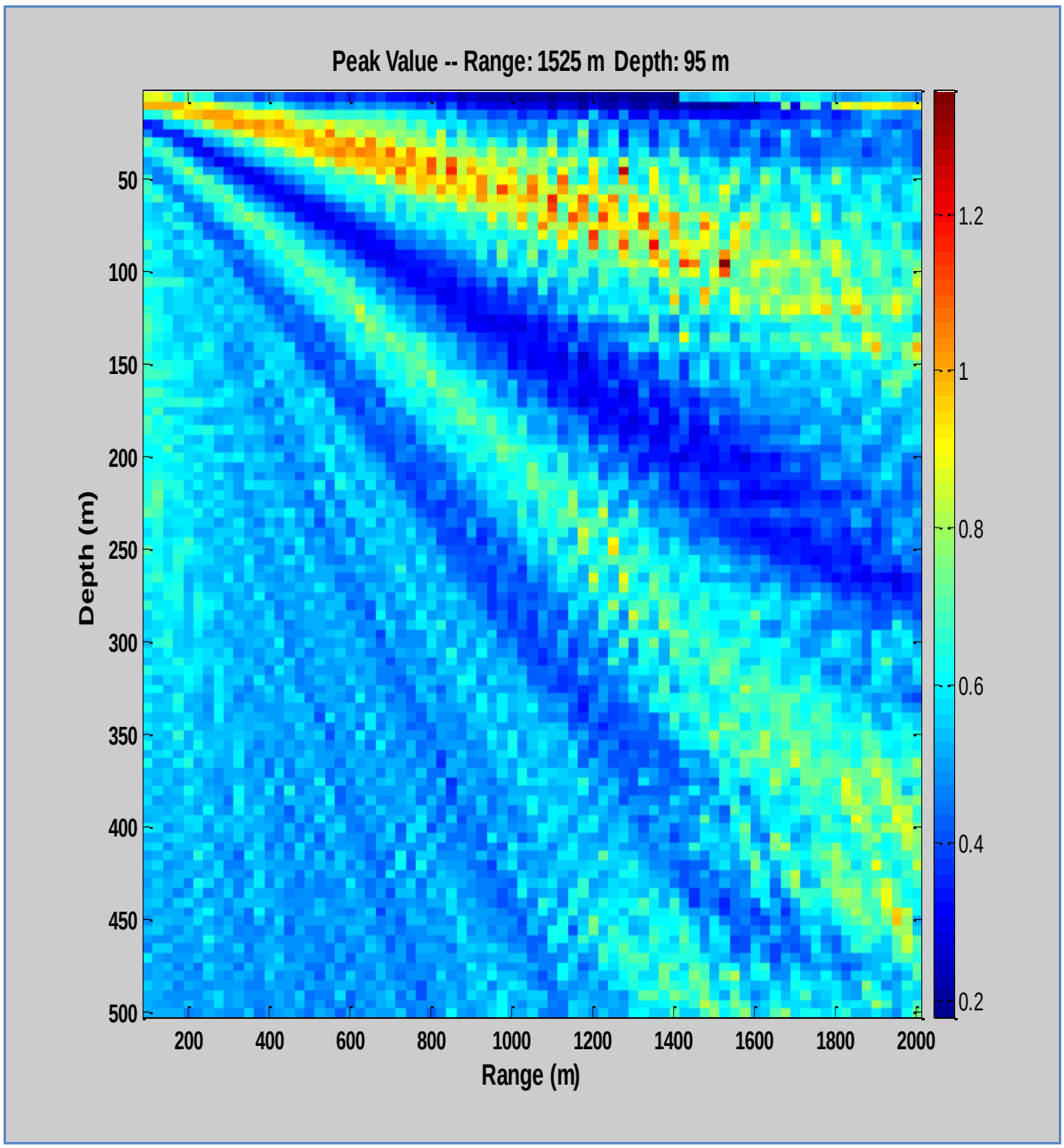

Figure 4.6. Ambiguity plot of our localizer for the hydrophone at range 1500 meters and depth 129 meters. The grid spacing is 25 meters in range and 5 meters in depth. The true source depth is 96 meters and we localize within 1 meter. The range is localized within 25 meters. The band of higher amplitudes across the top is caused by similarity of the Green's functions at these locations.

across the top of the waveguide. Therefore the early portions of the Green's functions in this region are very similar. Similarities in Green's functions for different locations introduce ambiguities in the localization. The arrival times of the energy that suffers multiple reflections are much more variable and these variations help to reduce the ambiguities. All localization algorithms rely on the uniqueness of the Green's functions at different locations to give unambiguous results.

For comparison we calculate the ambiguity plots for the other localizers and plot them in Figures 4.7 and 4.8. The first thing to notice is that the Jesus and Tiemann localizers perform well here. This is because the source signal is sufficiently broadband for the ray approximation to be reasonable. The Tiemann localizer works well here, when it did not in Chapter 3, because the correlated data shows the arrivals very distinctly. In the simulated cases of the previous chapter, the arrivals did not show up distinctly in the data and the Tiemann localizer performed poorly. This suggests that correlated data may be a better choice to use with the Tiemann localizer when the arrivals are not distinct, and when the correlated source signal is narrower in time than the original source signal. Another noteworthy feature of the ambiguity data is that the Porter, Lee, Clay/Frazer Chi2, Frazer Chi1, and Frazer Mu localizers perform poorly, after successes in the simulated data of Chapter 3. The ambiguity plots feature the large band of higher amplitudes near the surface that we discussed above with our localizer. The data indicate that the ambiguities in this region cause problems for these localizers suggesting they may not perform as well in environments like this one. The Porter localizer performs very poorly and this may be because it is based on the envelope of the signal which emphasizes broad features at the expense of detail. Using correlated data highlights both the large and small arrivals of the acoustic energy and these highlights are lost when using only the envelope of the data. The

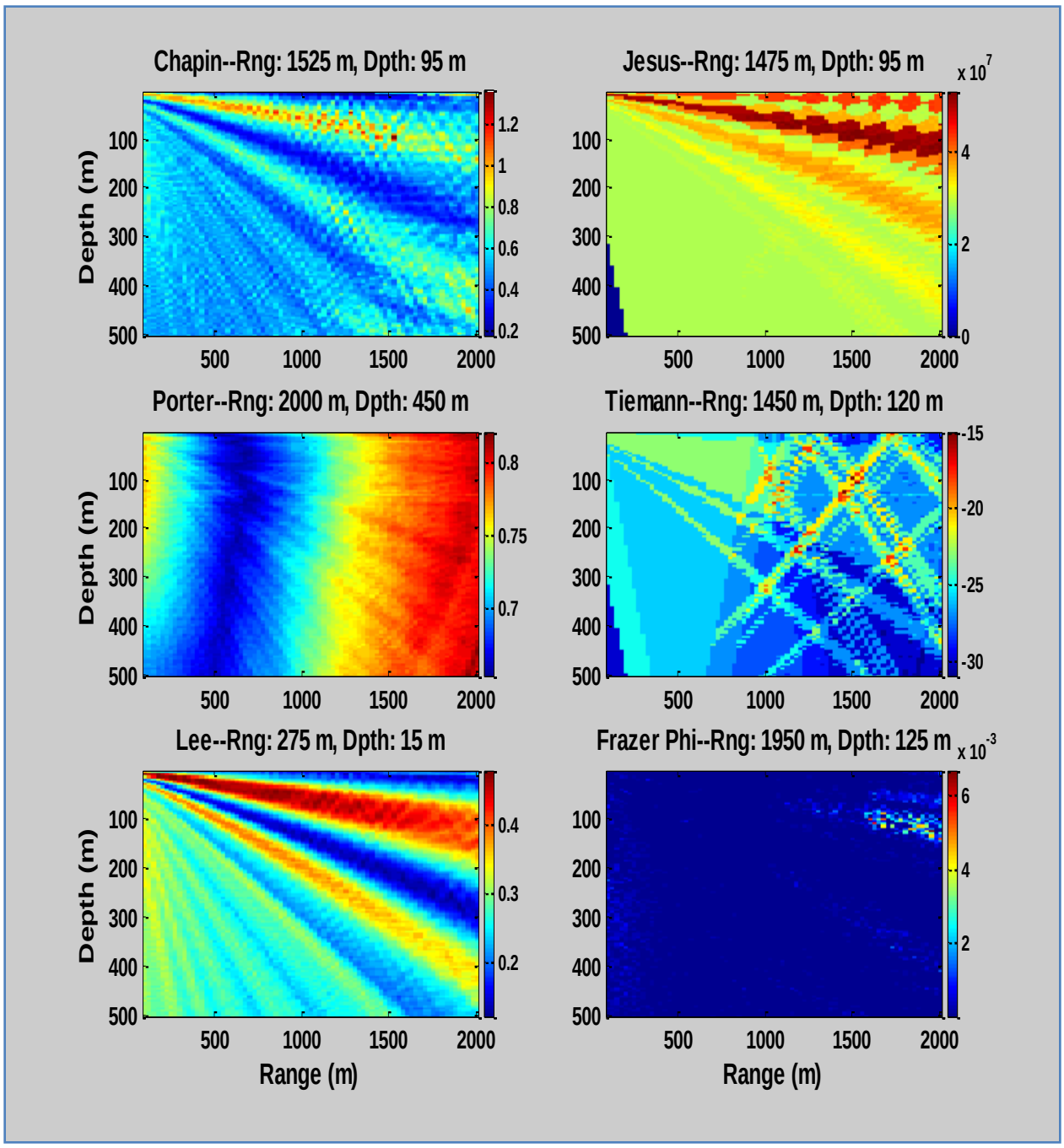

Figure 4.7. Localization results of several of the localizers for the receiver at 129 meters in depth and 1500 meters in range. Our localizer and the ray-based localizers of Jesus and Tiemann are successful in this case.

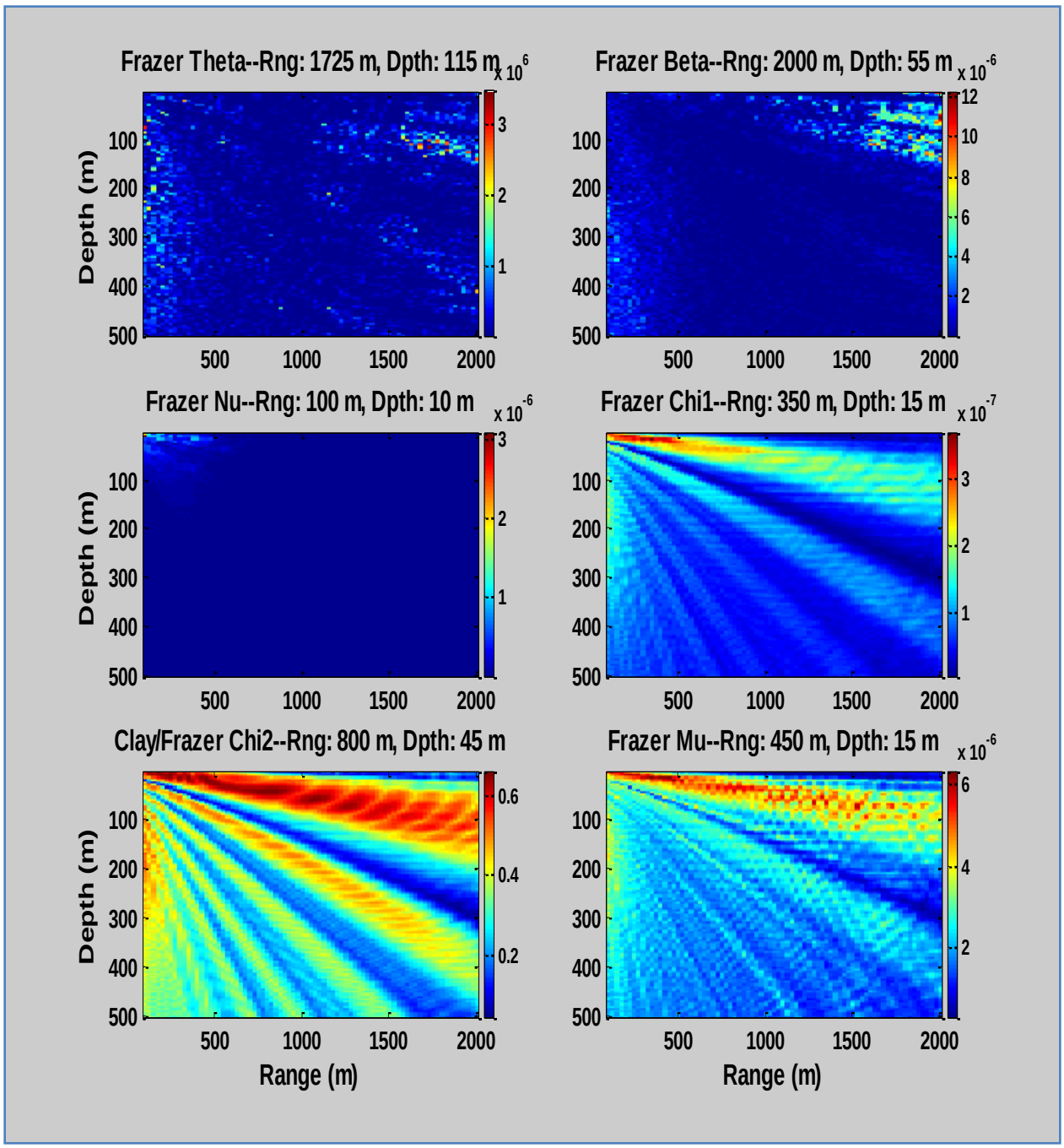

Figure 4.8. Localization results of several of the localizers for the receiver at 129 meters in depth and 1500 meters in range. None of these localizers is successful in this case.

remaining Frazer localizers continue to have difficulty and this is another reflection of their requirement of a very accurate representation of the Green's function.

The case we examine here shows another success for our localizer when others have difficulty. The ray-based localizers of Jesus and Tiemann also perform well here because of the broadband source signal. Many of the other localizers had difficulty in this case that did not show up in the simulations of Chapter 3. The primary difference is that we use experimental data here with its inherent uncertainties. Our localizer demonstrates the ability to locate the source signal with imperfect environmental information. Next we examine a second case with a different hydrophone.

4.3 Receiver at depth 250 meters

In this case we look at the hydrophone at a range of 1500 meters from the source and at a depth of 250 meters. The correlated measurement data are shown in Figure 4.9 and have similar features to the 129 meter case. There are two early arrivals followed by some later arrivals as in the previous case. The early arrivals are direct and surface reflected arrivals, and the later arrivals are the result of reflections from the surface and the bottom. The timing is a bit different since the hydrophone is lower in the ocean waveguide. The frequency domain shows some attenuation around 50 Hz and 100 Hz. The Green's function for the true source location calculated with the SPARC model is shown in Figure 4.10 and gives us some insight into the features of the measured signal. The later arrivals reach this hydrophone a bit sooner than the 129 meter case, approximately 0.1 seconds sooner. This is because the hydrophone is lower in the waveguide and bottom reflections arrive sooner. The frequency domain plot shows attenuation in the region of 50 Hz and 100 Hz, as the spectrum of the measured data show.

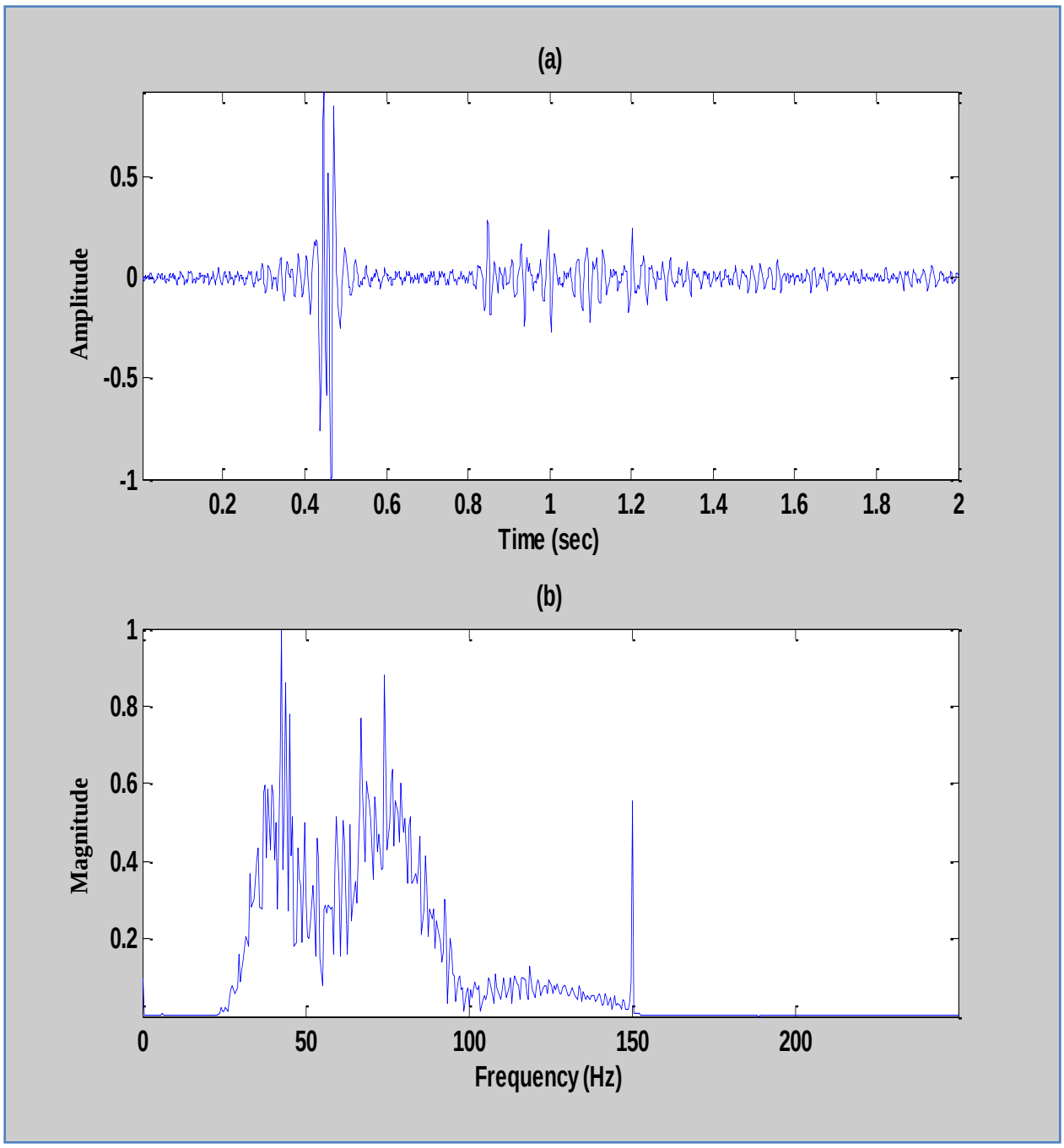

Figure 4.9. Correlated measurement data for the hydrophone located at a range of 1500 meters and a depth of 250 meters. (a) Time domain correlated measurement. (b) Correlated measurement in the frequency domain.

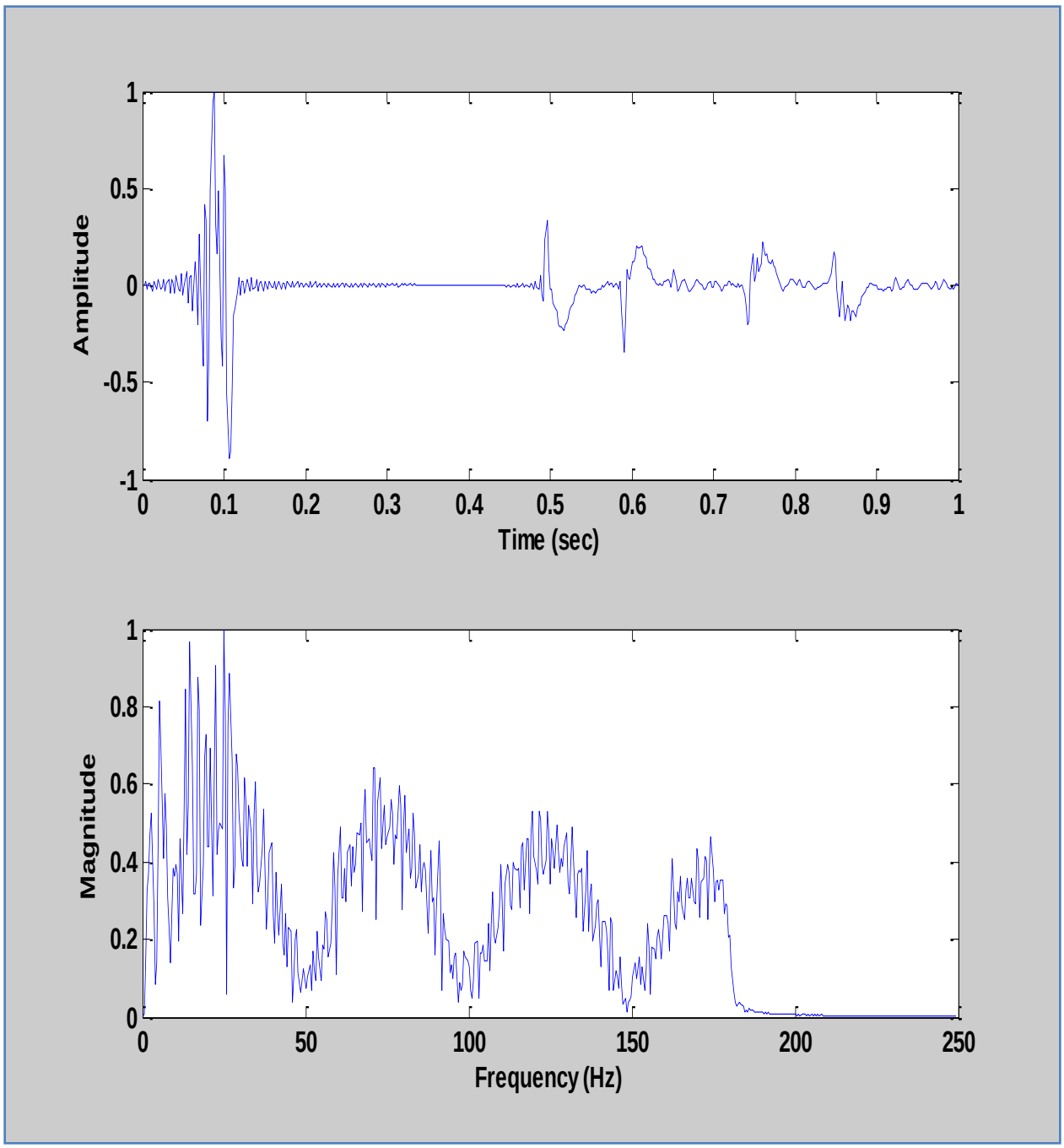

Figure 4.10. Green's function for 250 meter case calculated by SPARC. (a) Time domain plot. There are two early arrivals representing one direct arrival and one surface reflected arrival. At least 4 arrivals show up after nearly 0.4 seconds; those are reflections from the surface and the bottom. (b) Frequency domain plot showing distortion across the band and a null around 100 Hz. The calculation is cut off at approximately 180 Hz because there is no energy in the measured signal at these frequencies.

The ambiguity plot for our localizer is shown in Figure 4.11 and it shares features of the 129 meter case, particularly that band of higher amplitudes near the top of the plot. The physical reason for this is the same; the direct and surface reflected arrivals follow this path and their spacing in space and time is similar as the energy travels across the top of the waveguide. The result is that the early parts of the Green's functions for these locations are similar. The later arrivals help to differentiate the Green's functions and allow us to locate the source within 4 meters of its true location. We use a coarser depth spacing of 10 meters in this case to see how that might affect the localization. It does not appear to degrade the performance of our localizer, although the location estimate in depth is less precise with the coarser spacing.

Plots of the remaining localizers are shown in Figures 4.12 and 4.13. As in the 129 meter case, the Jesus localizer performs well, but the Tiemann localizer does not. It appears that the Tiemann localizer does have a peak near the true source location, but a different location has a higher peak and therefore gives an incorrect location estimate. This suggests that the Tiemann localizer may be sensitive to environments where there are similar Green's functions. Recall that the Tiemann localizer was successful in the 129 meter hydrophone case. The observations on the remaining localizers remain similar to the previous case. One noteworthy difference is the peak in the Frazer Phi localizer that occurs at a range of 1550 meters and a depth of 30 meters, approximately 83 meters from the true source location. This could be qualified a success in light of some of the higher amplitudes in the other ambiguity plots that appear closer to the surface.

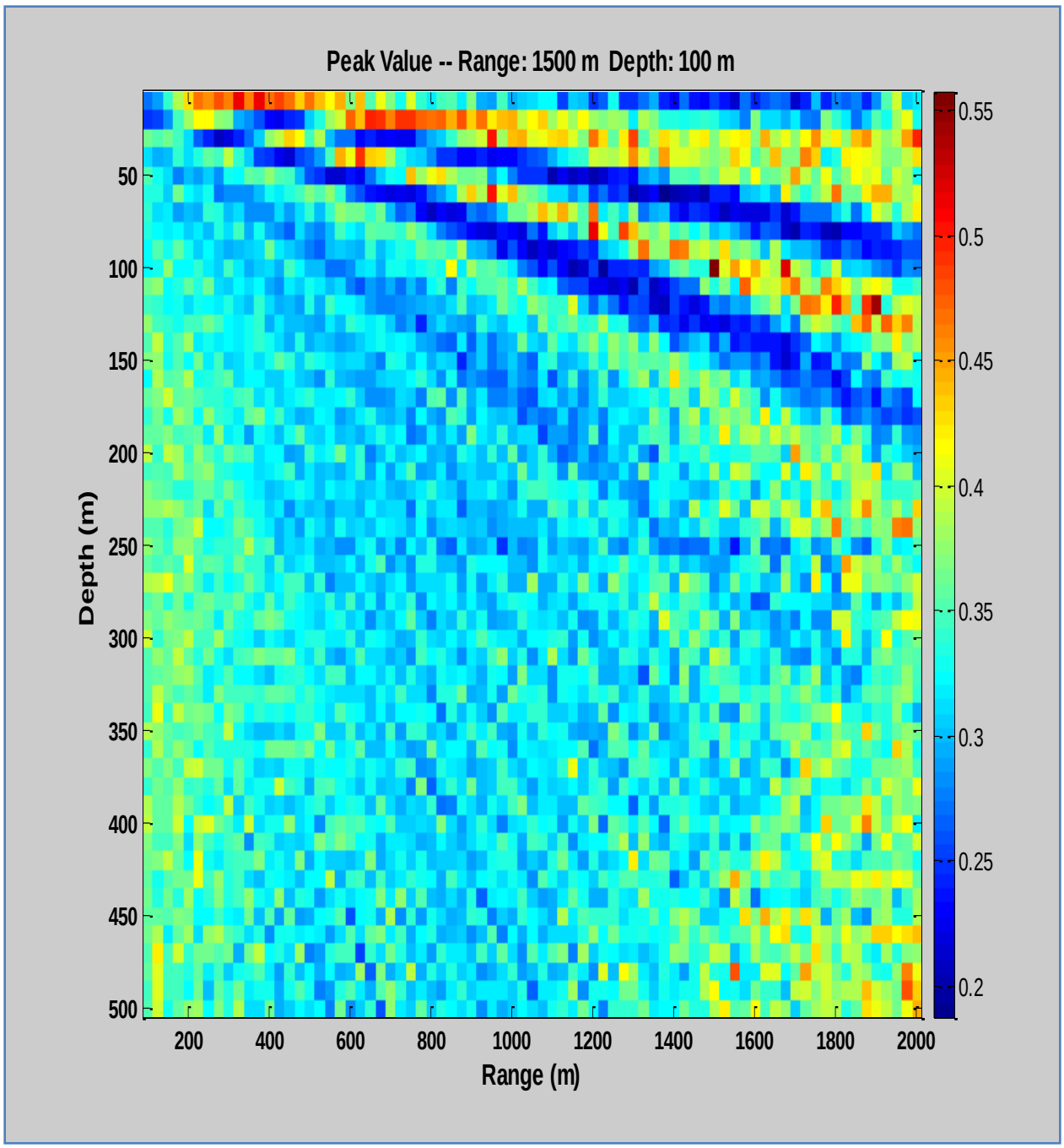

Figure 4.11. Ambiguity plot of our localizer for the hydrophone at range 1500 meters and depth 250 meters. The grid spacing was 25 meters in range and 10 meters in depth. The true source depth is 96 meters and we localize within 4 meters. The range is localized within 25 meters. The band of higher amplitudes across the top is caused by similarity of the Green's functions at these locations.

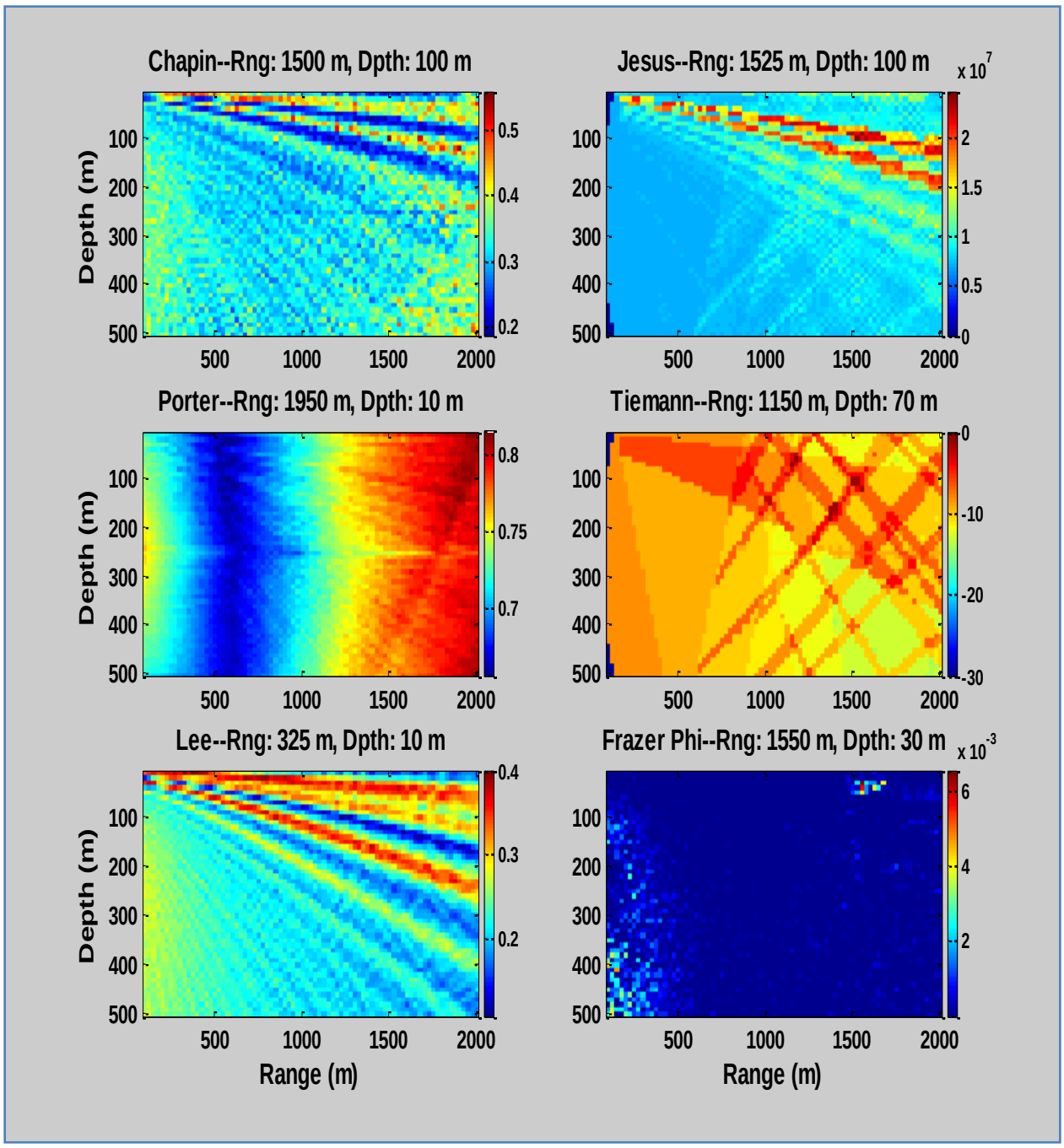

Figure 4.12. Localization results of several of the localizers for the receiver at 250 meters in depth and 1500 meters in range. Our localizer and the ray-based localizer of Jesus are successful in this case. The Frazer Phi localizer gives a peak within about 83 meters of the true source location.

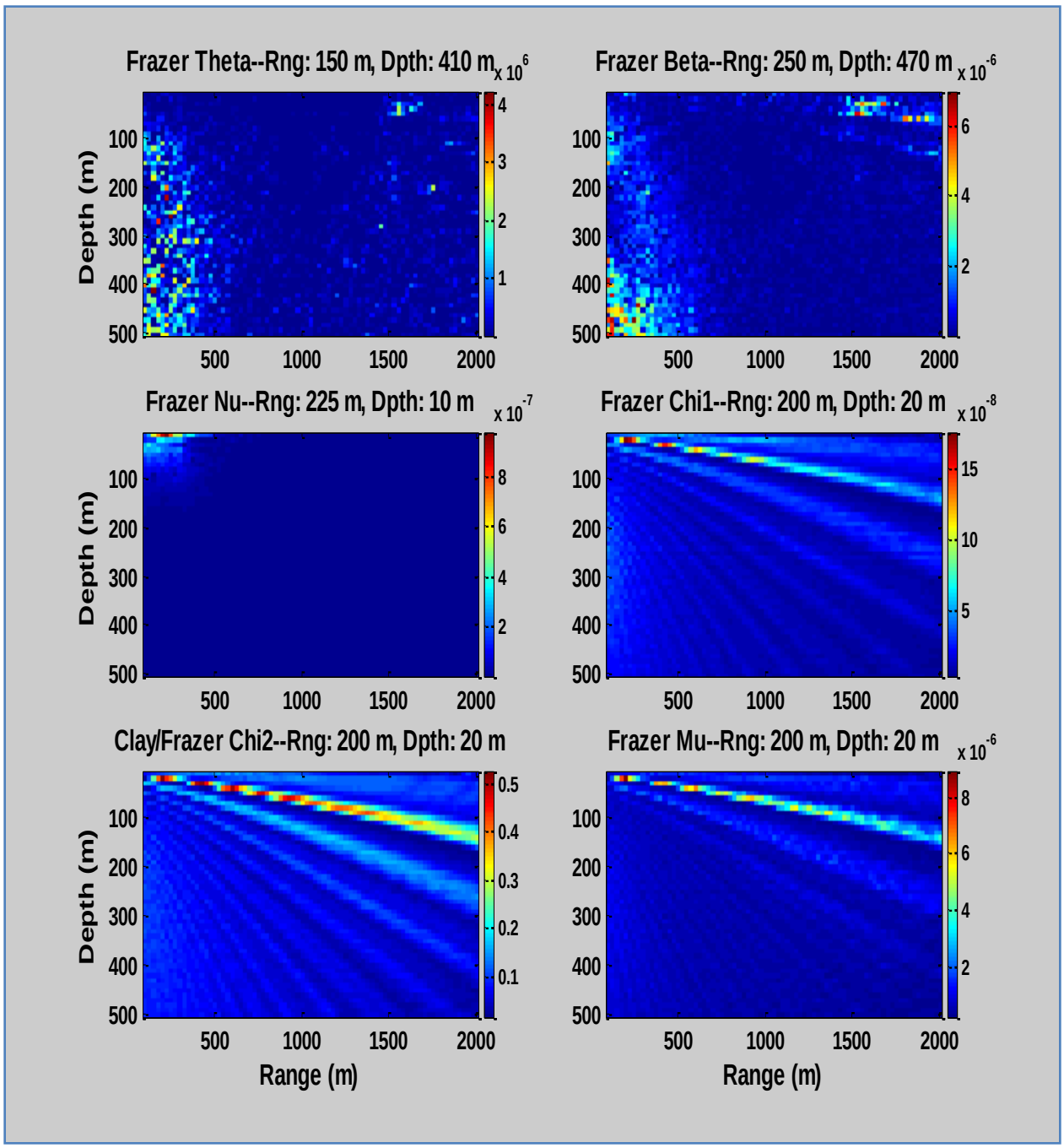

Figure 4.13. Localization results of several of the localizers for the receiver at 250 meters in depth and 1500 meters in range. None of these localizers is successful in this case.

4.4 Summary

We have shown two cases where our new localizer successfully estimates the location of an acoustic source using measured ocean acoustic data. The only information required is the measurement at one hydrophone and the ocean's environmental parameters to model the acoustic propagation. Our algorithm does not require any knowledge of the source signal in its calculations. In Chapter 3 we look at some simulated cases to understand how our localization algorithm is affected by the source signal bandwidth and noise. The results show that our localizer is successful at bandwidths as low as 10 Hz and at signal-to-noise ratios of 20 dB or higher. A number of the cases demonstrate our localizer is successful when many of the others from the literature are not, even when some include the source signal in their algorithms. While we do not claim that the new localizer we introduce will outperform the others in every scenario, the results show that it has promise to be a useful tool for single hydrophone localization.

Appendix

This appendix contains all of the ambiguity plots generated in the signal-to-noise ratio (SNR) analysis of section 3.3. They are not essential to the main presentation but are placed here for completeness and to preserve the continuity of the text. The ambiguity plots are calculated for signal-to-noise ratios of 60 dB, 40 dB, 20 dB, and 0 db. The calculations are done for the three source signal bandwidths discussed in Chapter 3, at each SNR. The ambiguity plots for all localizers discussed in this dissertation are included.

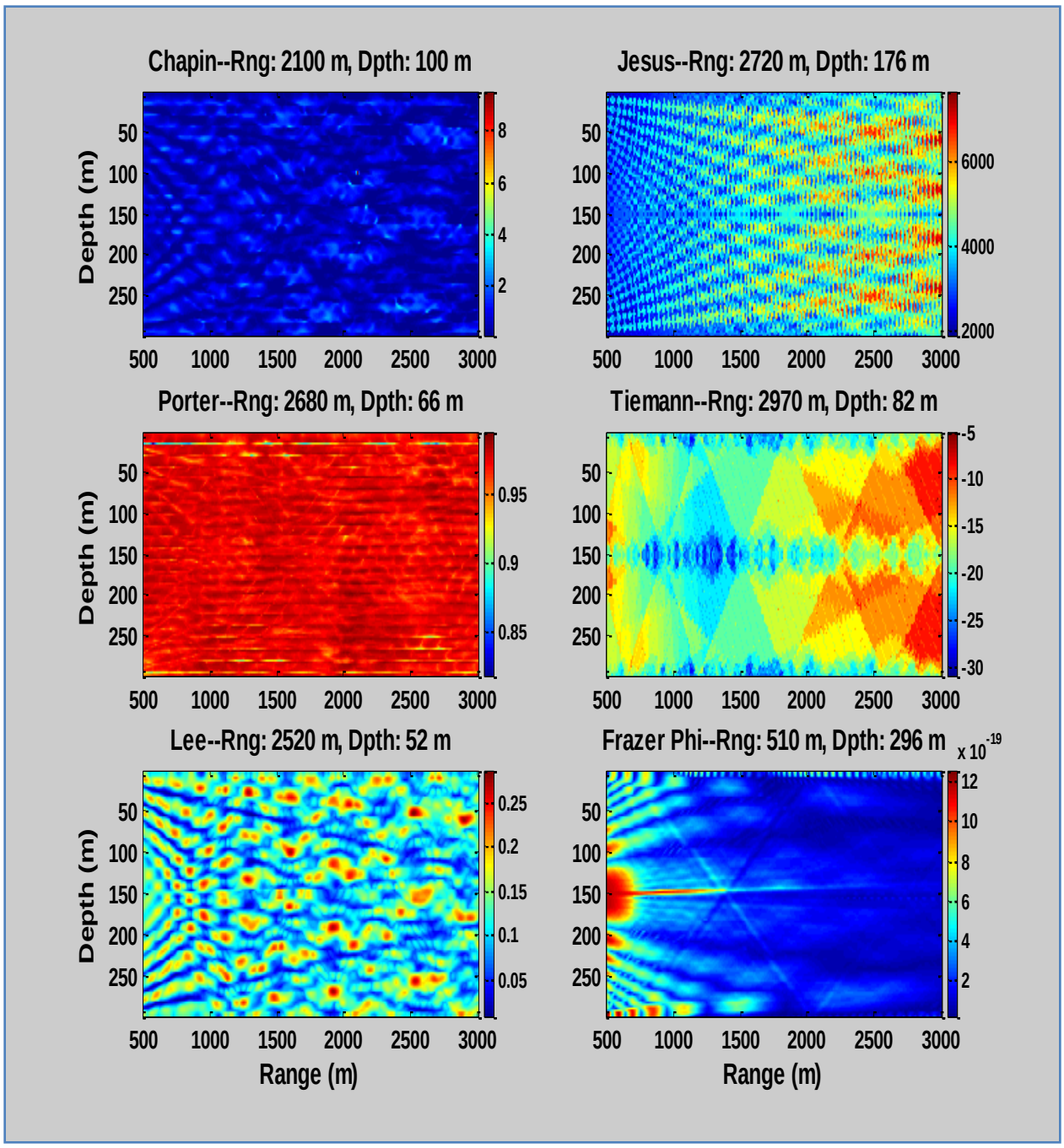

Figure A.1. Ambiguity plots for source signal bandwidth of 10 Hz and SNR=60 dB.

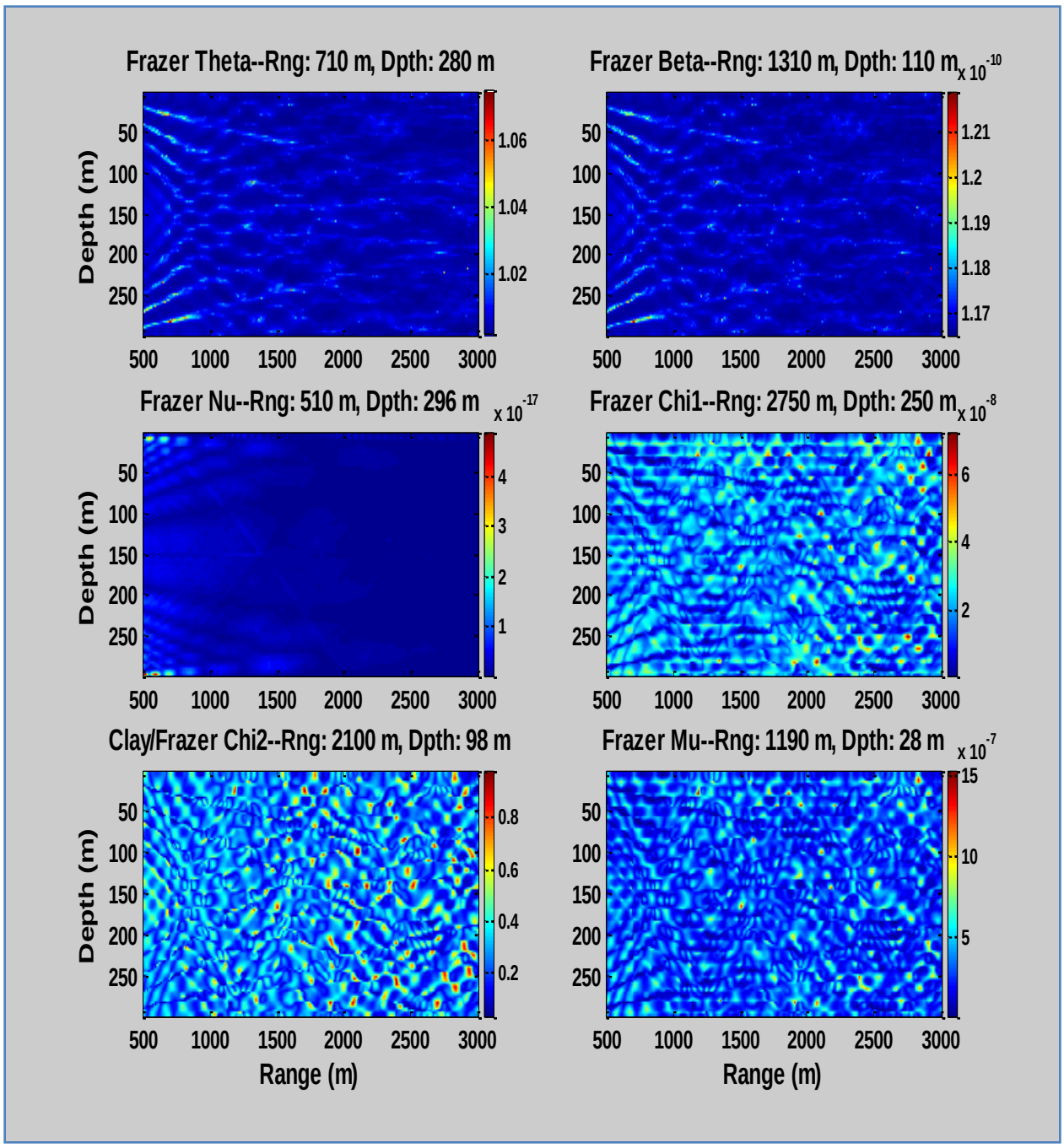

Figure A.2. Ambiguity plots for source signal bandwidth of 10 Hz and SNR=60 dB.

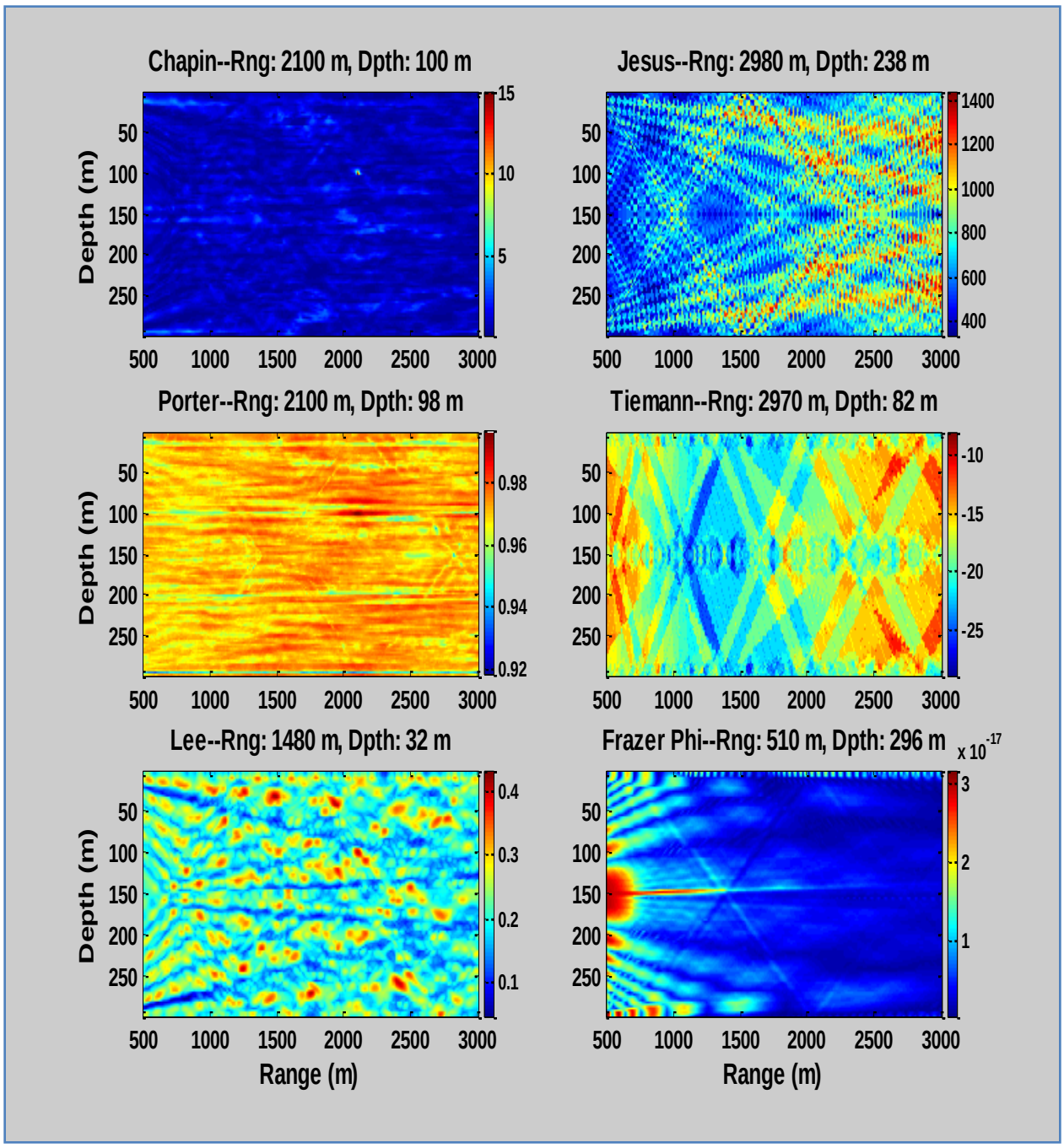

Figure A.3. Ambiguity plots for source signal bandwidth of 100 Hz and SNR=60 dB

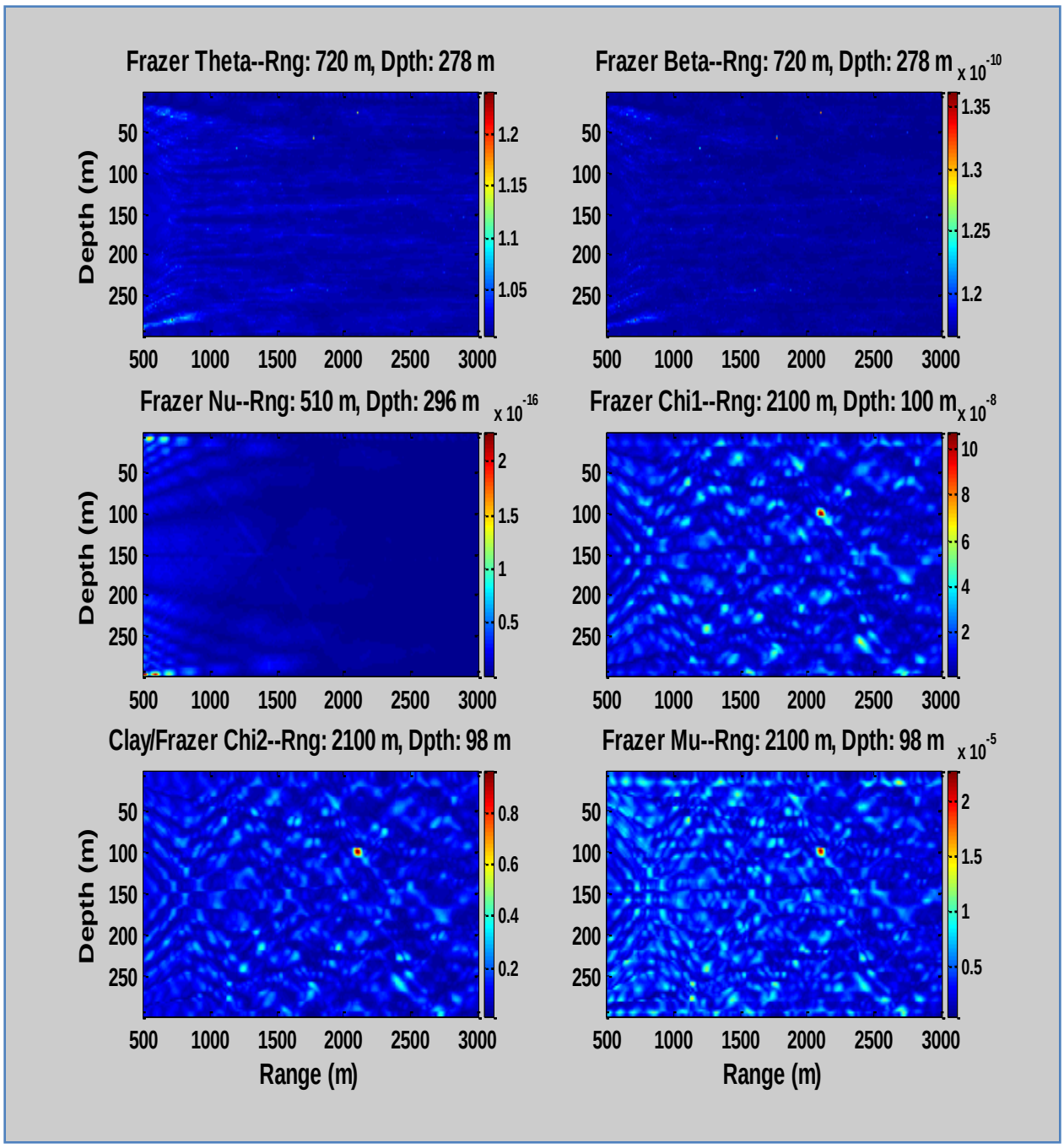

Figure A.4. Ambiguity plots for source signal bandwidth of 100 Hz and SNR=60 dB

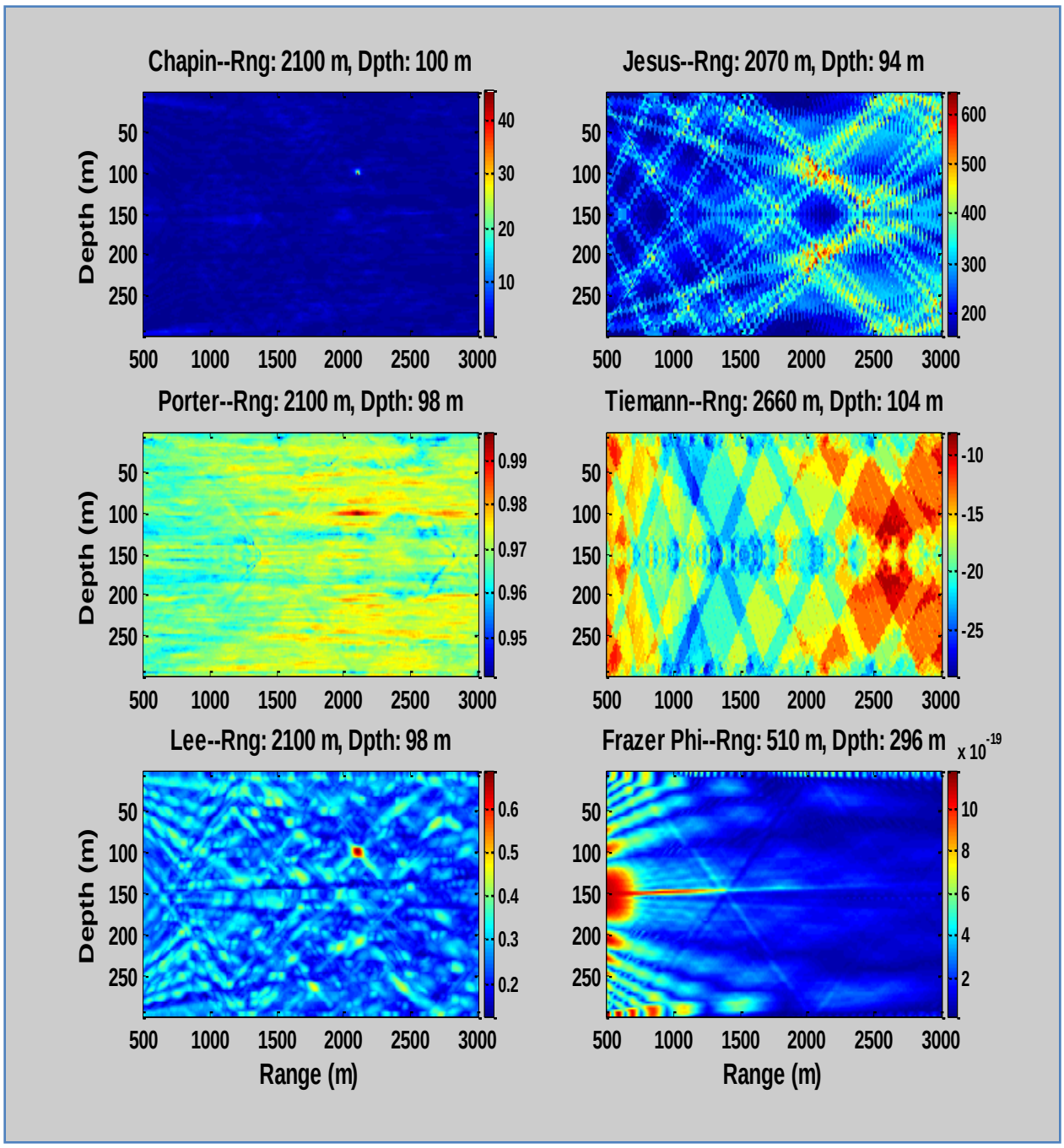

Figure A.5. Ambiguity plots for source signal bandwidth of 200 Hz and SNR=60 dB

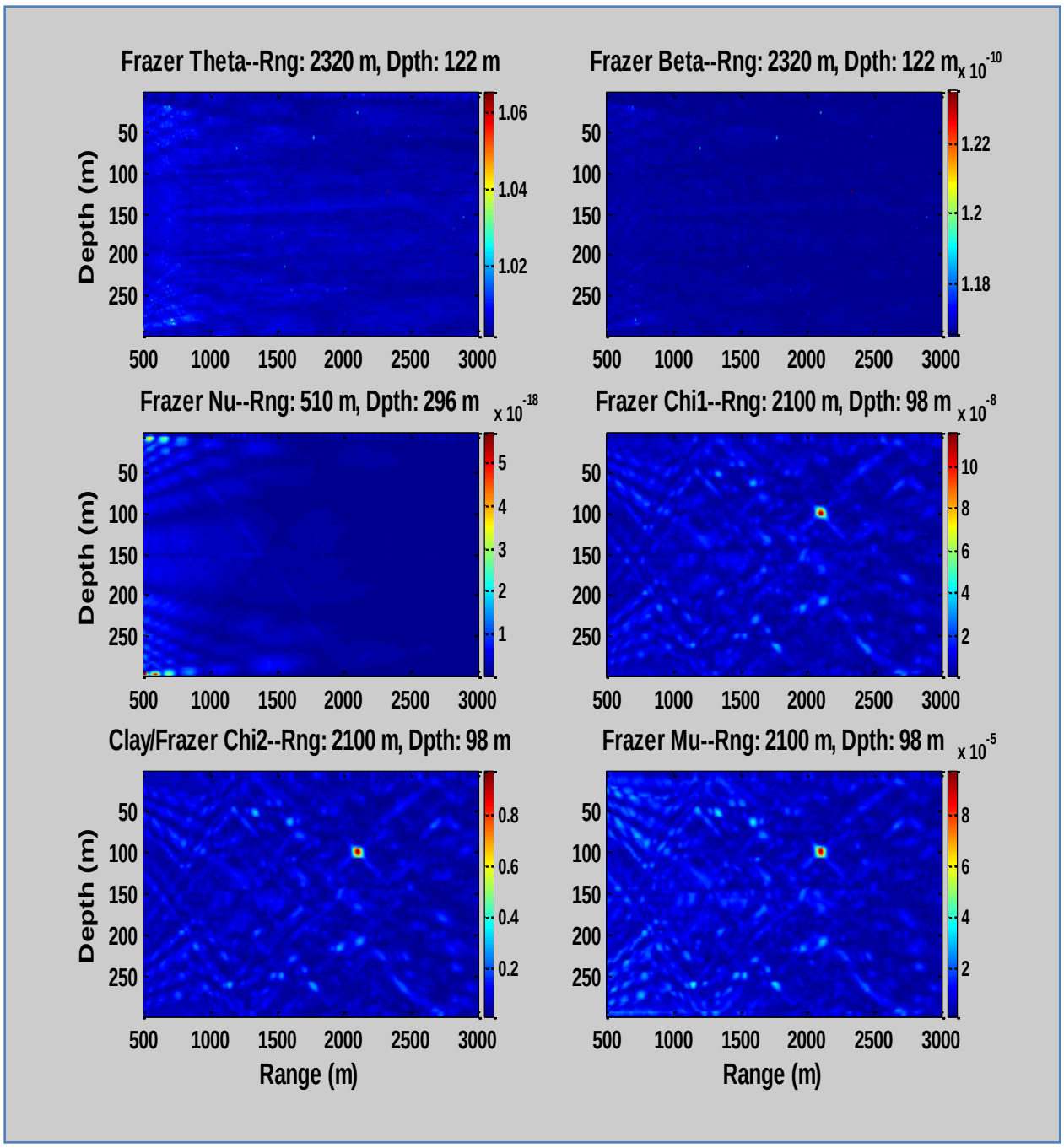

Figure A.6. Ambiguity plots for source signal bandwidth of 200 Hz and SNR=60 dB

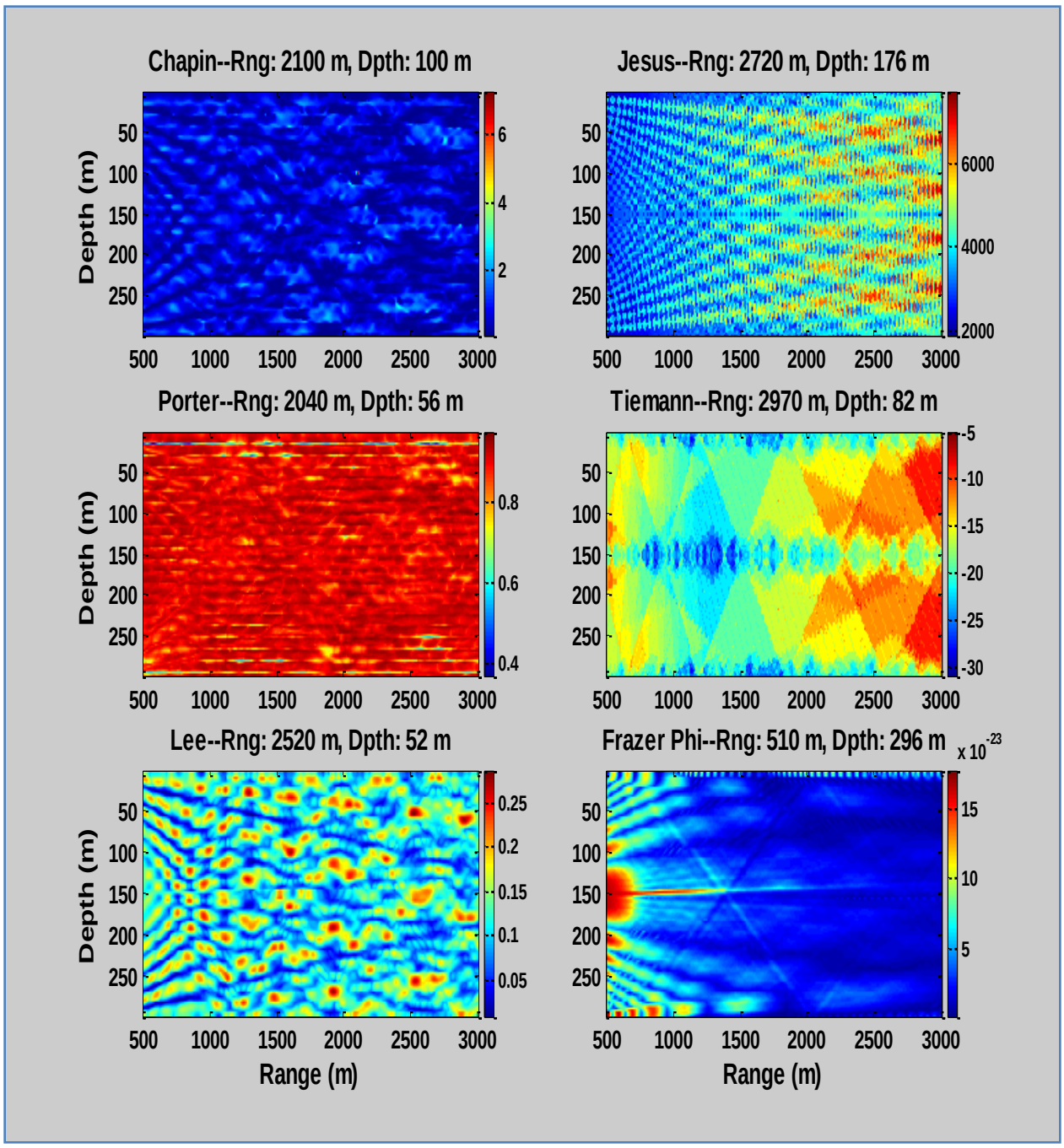

Figure A.7. Ambiguity plots for source signal bandwidth of 10 Hz and SNR=40 dB

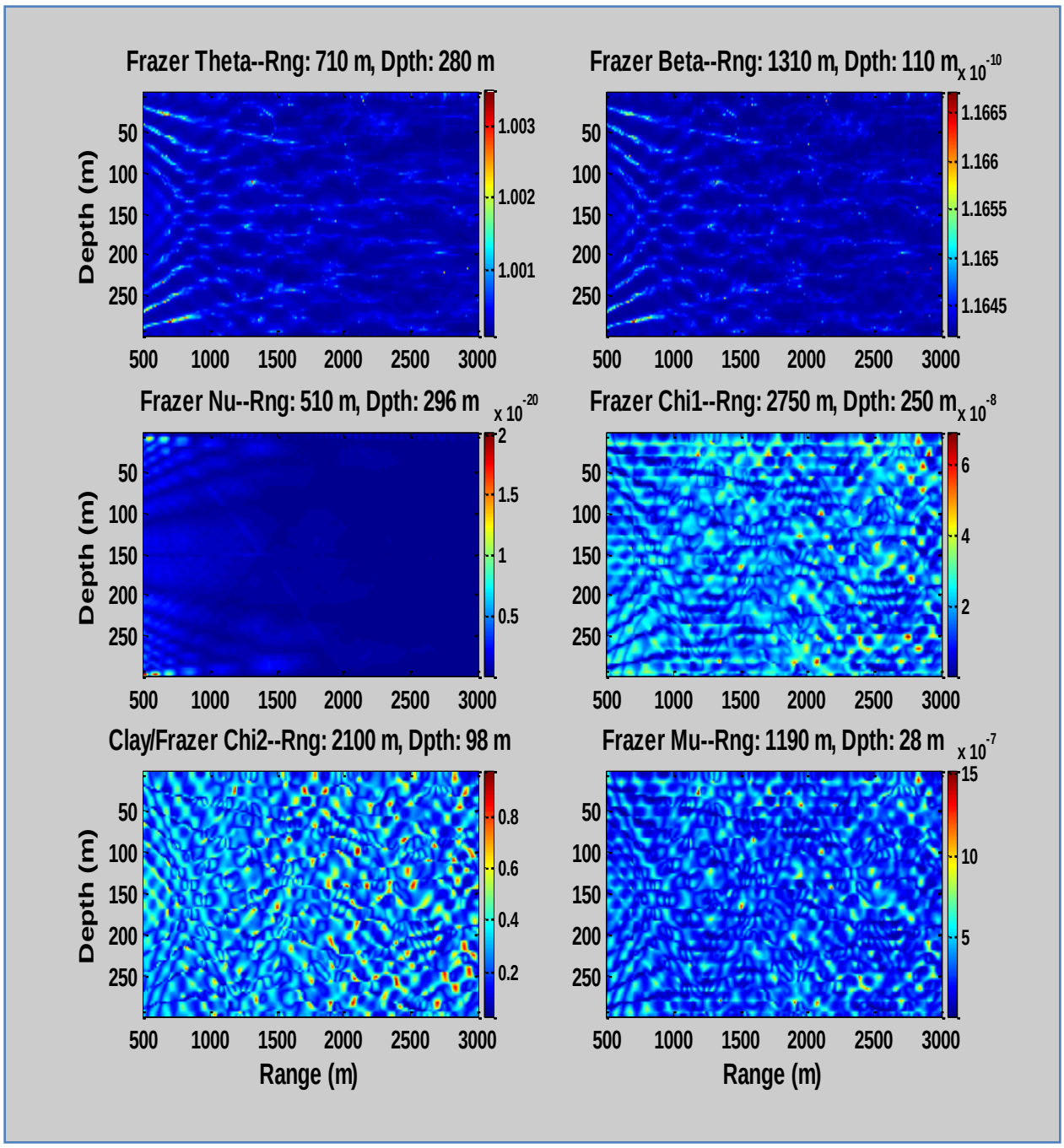

Figure A.8. Ambiguity plots for source signal bandwidth of 10 Hz and SNR=40 dB

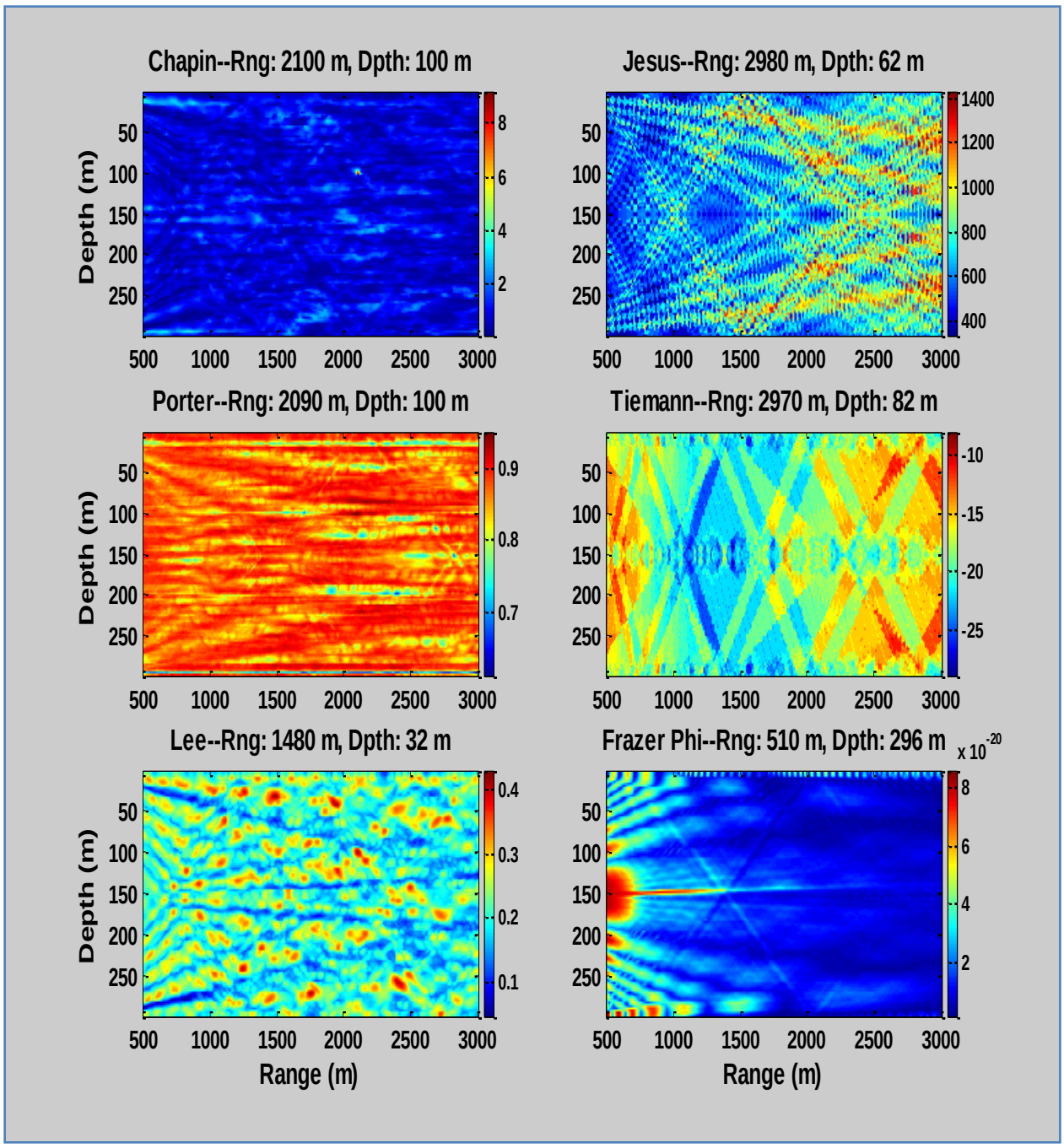

Figure A.9. Ambiguity plots for source signal bandwidth of 100 Hz and SNR=40 dB

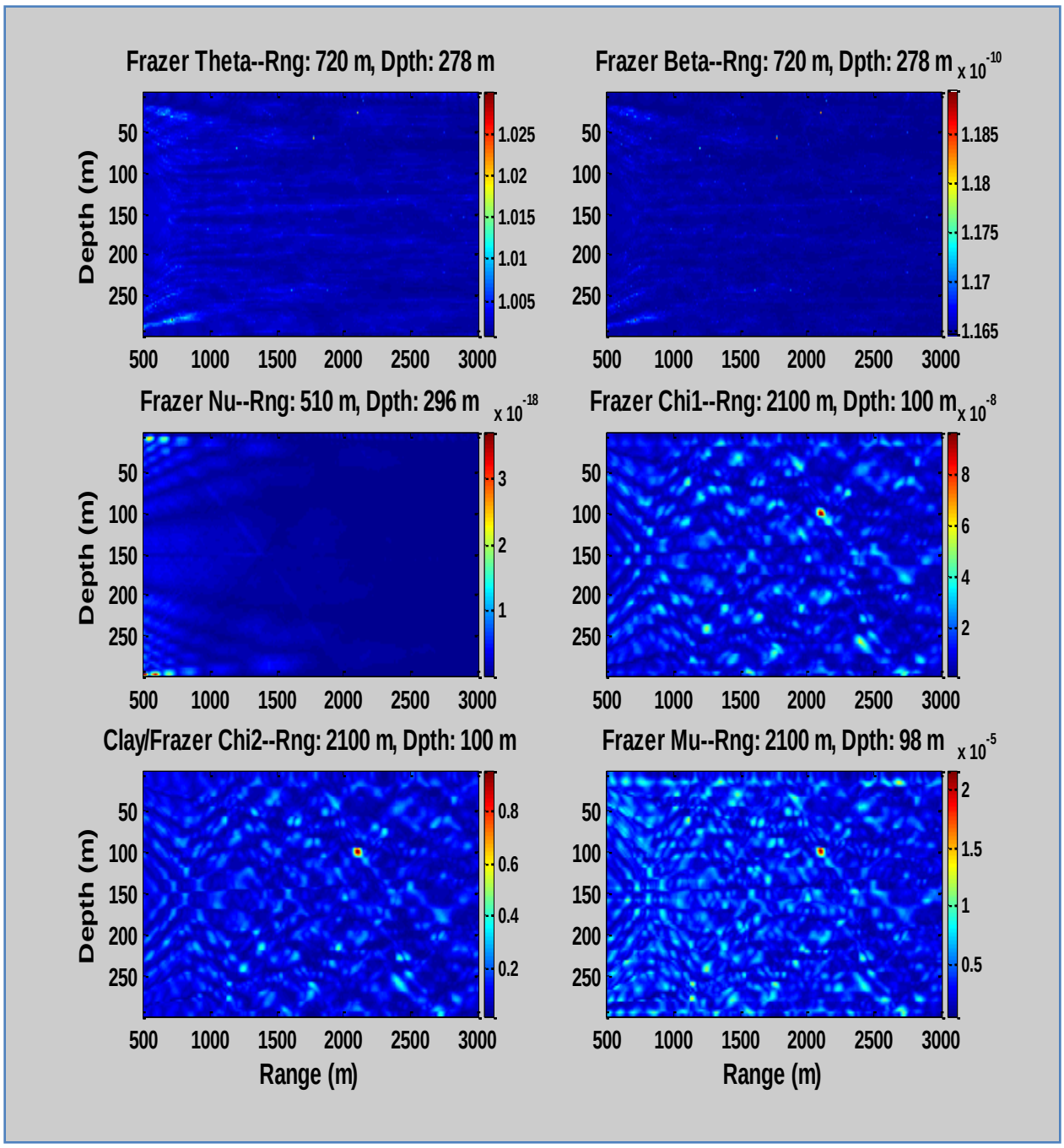

Figure A.10. Ambiguity plots for source signal bandwidth of 100 Hz and SNR=40 dB

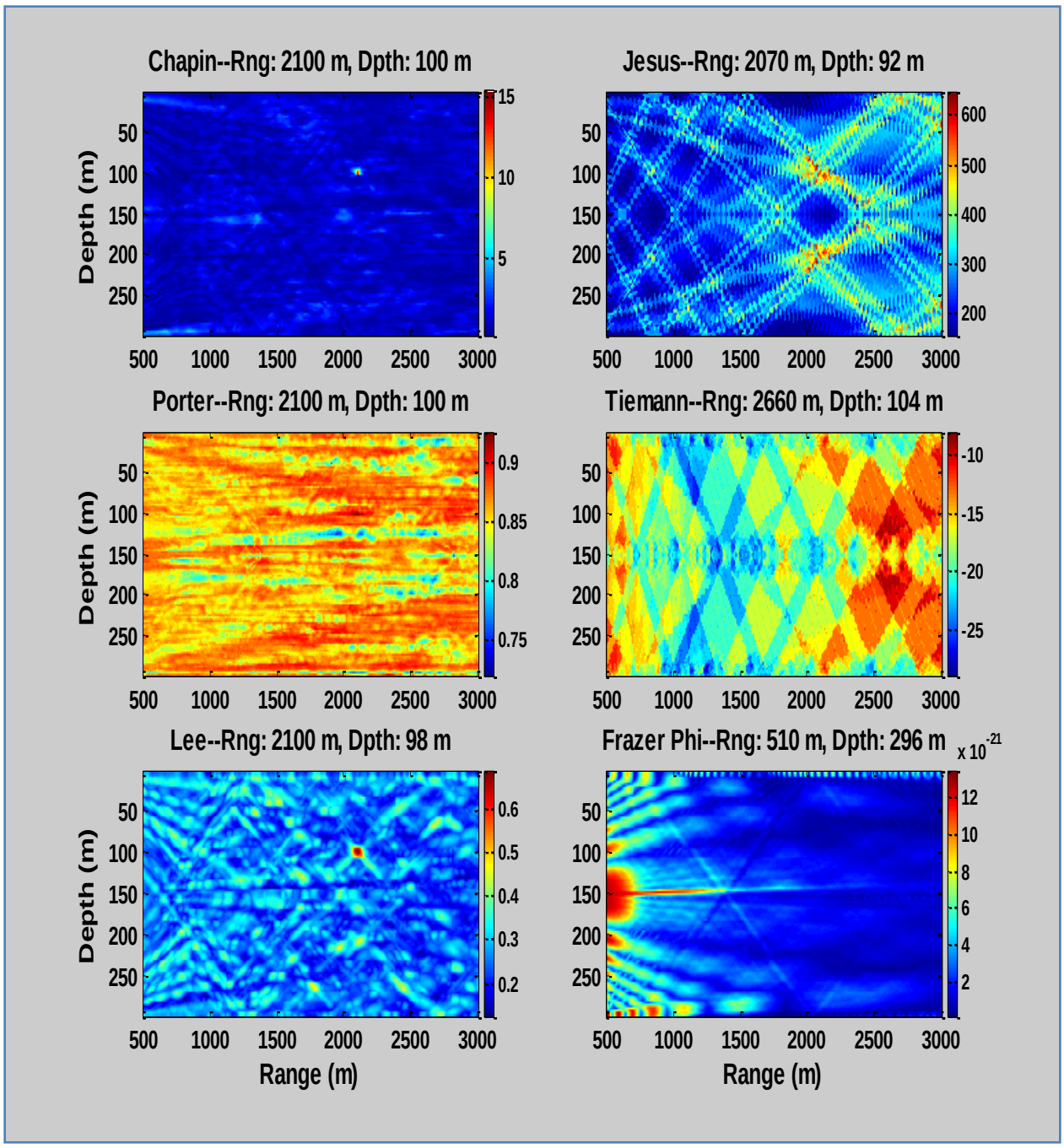

Figure A.11. Ambiguity plots for source signal bandwidth of 200 Hz and SNR=40 dB

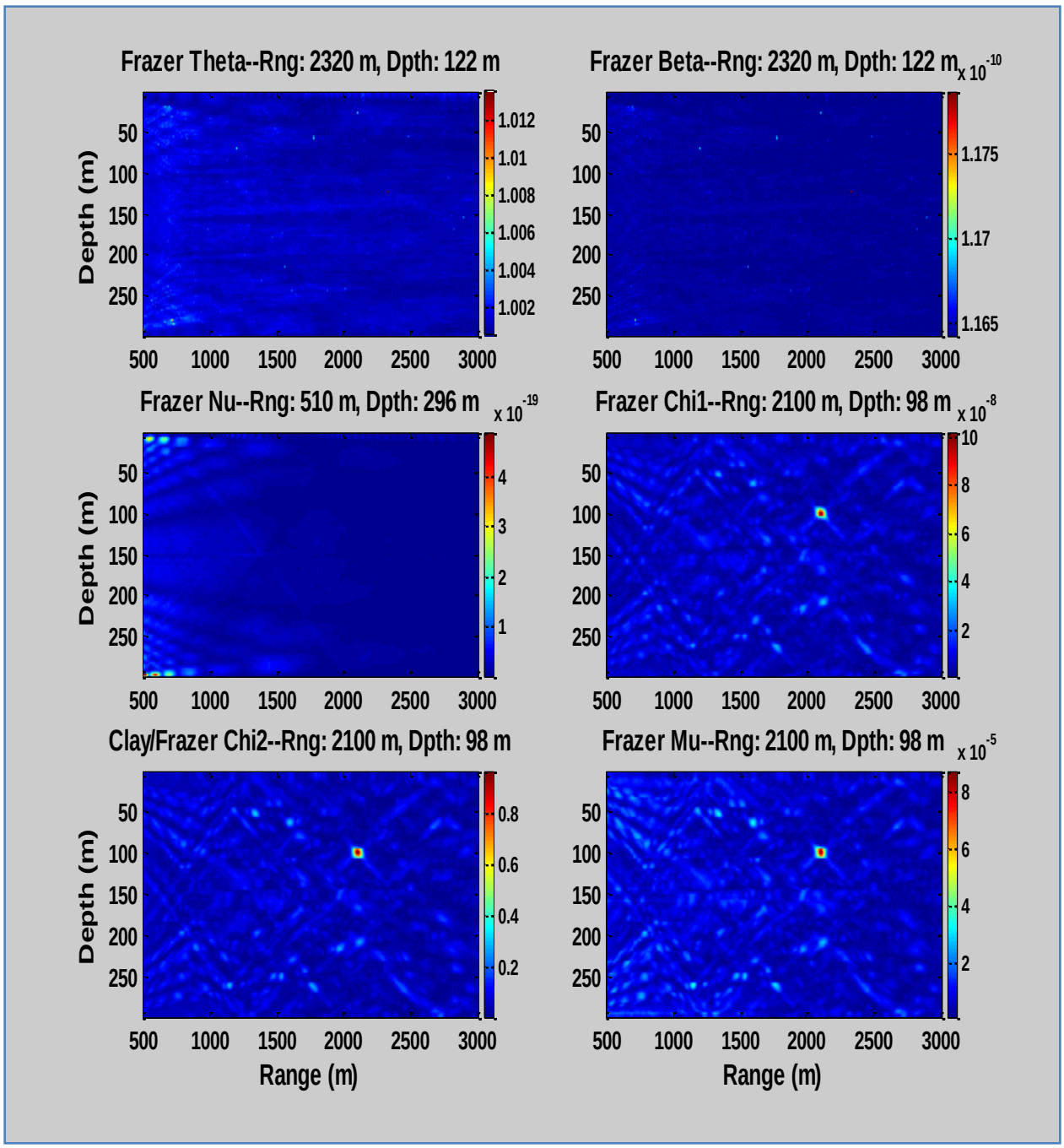

Figure A.12. Ambiguity plots for source signal bandwidth of 200 Hz and SNR=40 dB

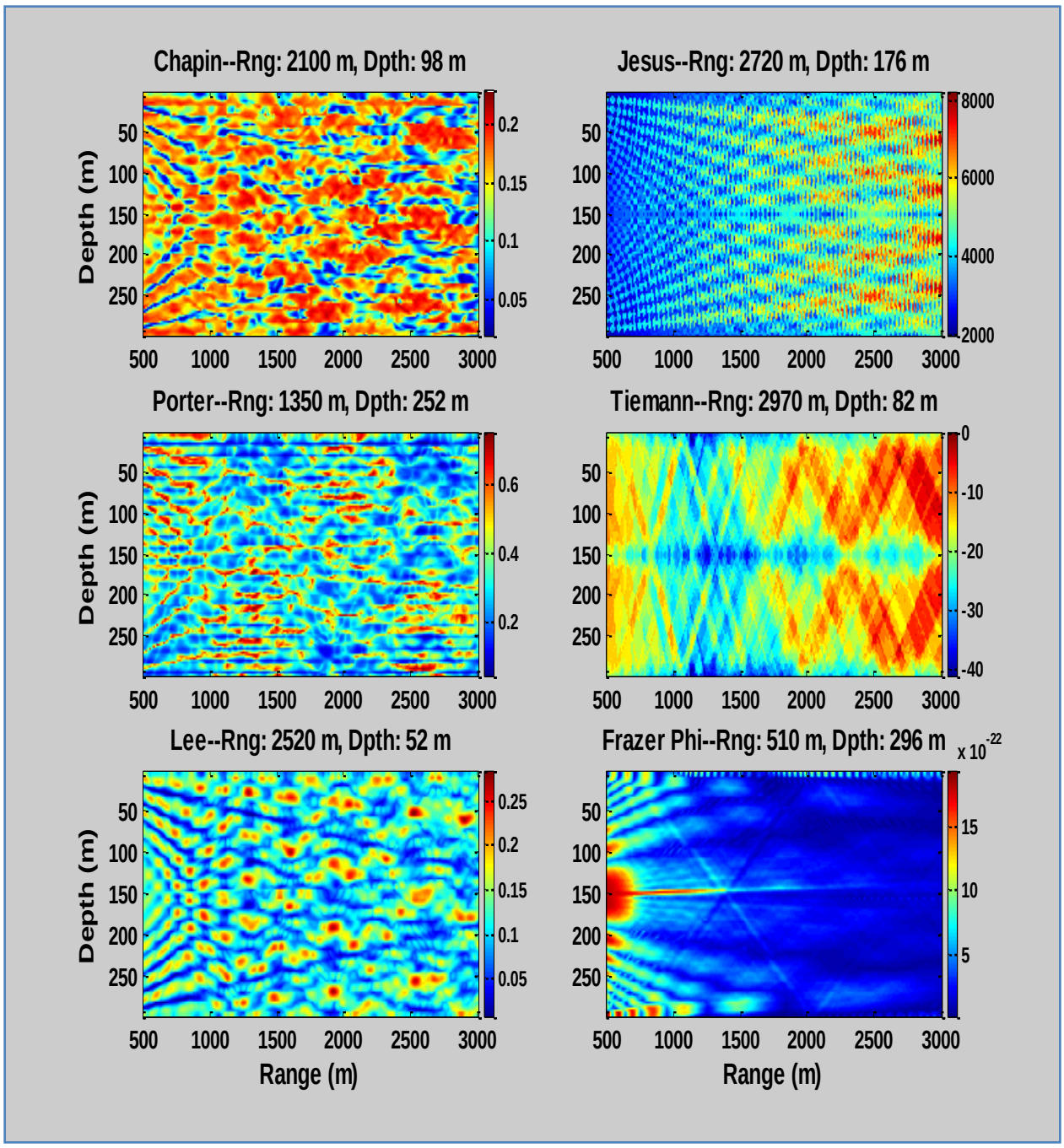

Figure A.13. Ambiguity plots for source signal bandwidth of 10 Hz and SNR=20 dB

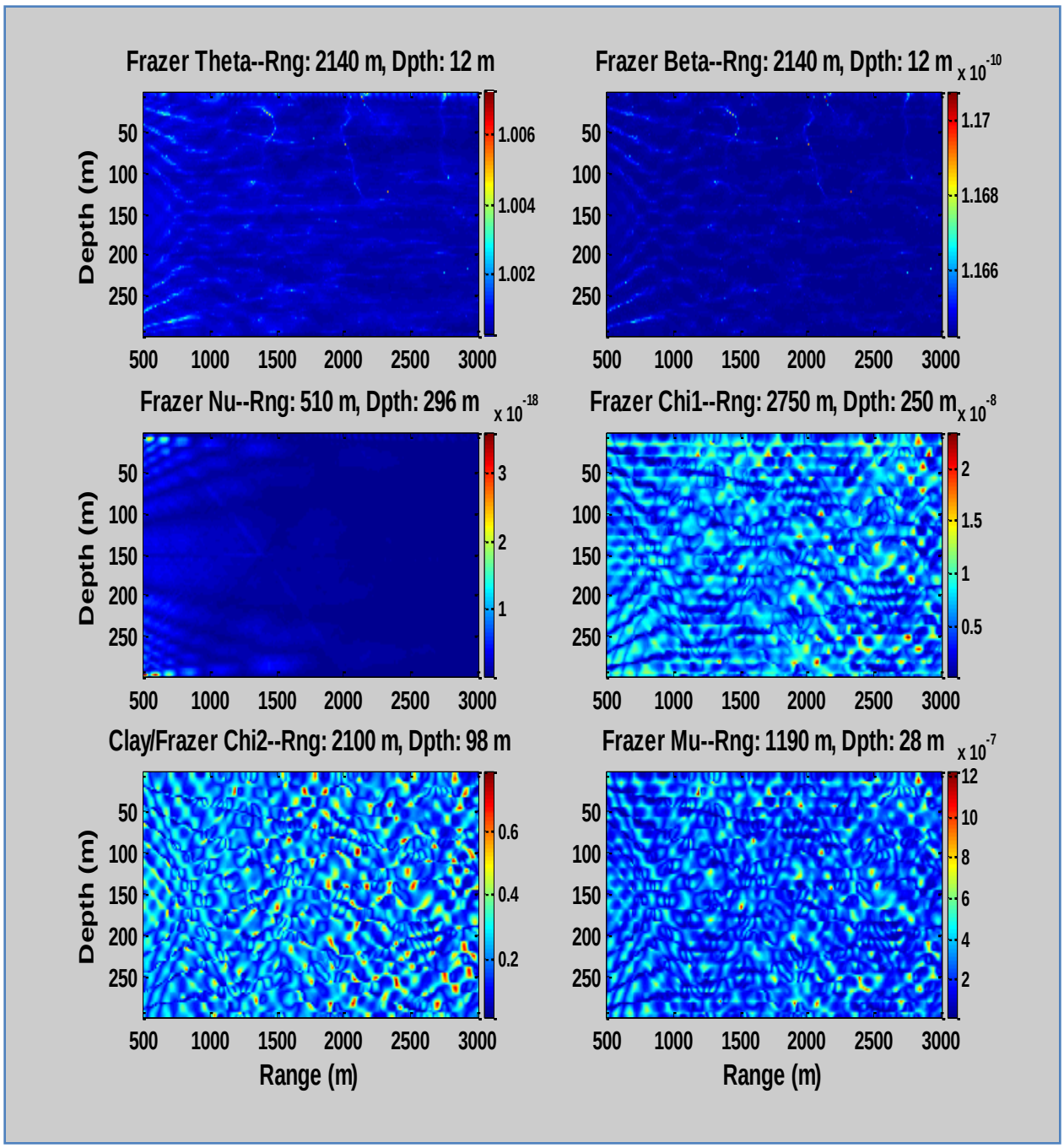

Figure A.14. Ambiguity plots for source signal bandwidth of 10 Hz and SNR=20 dB

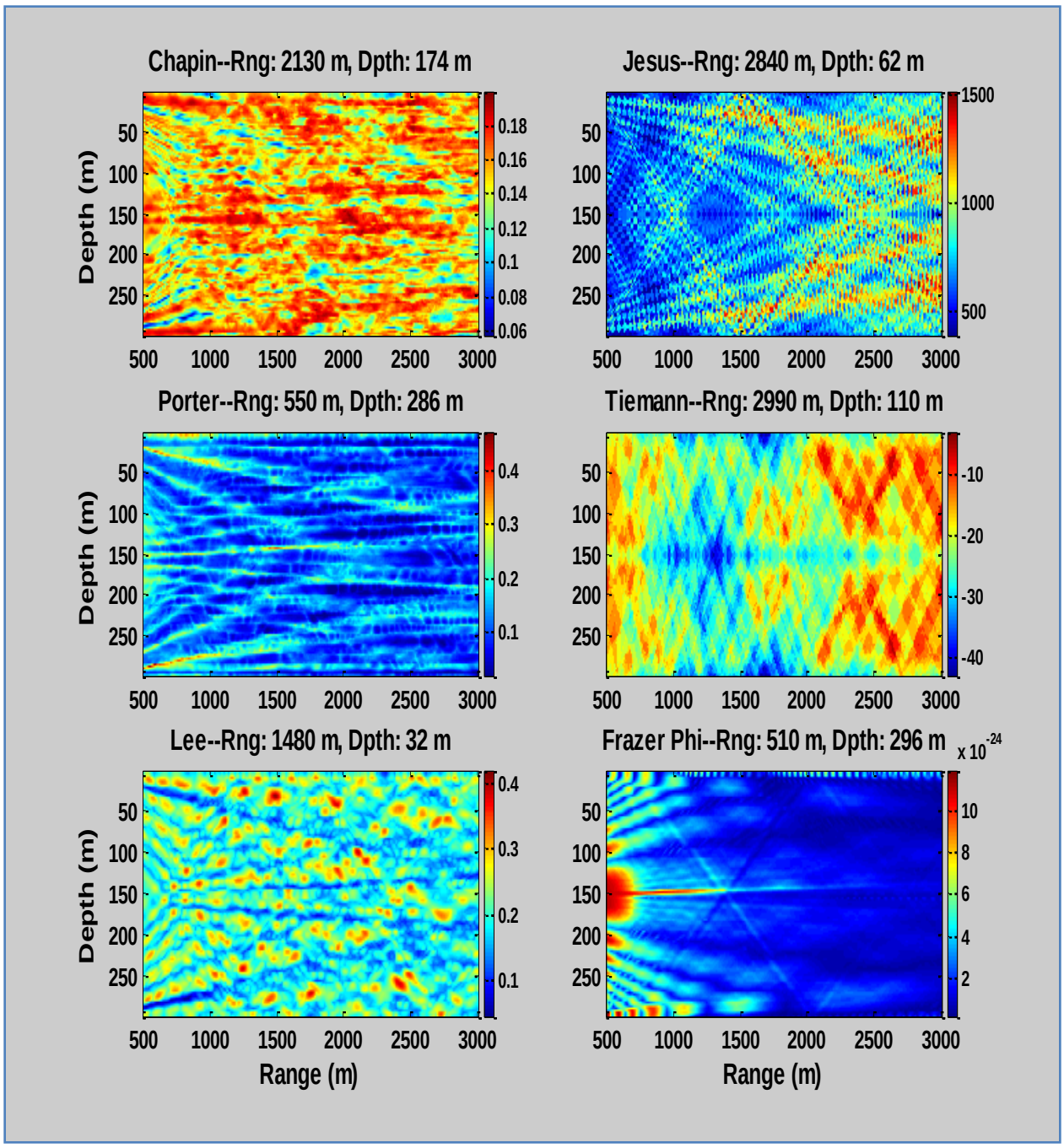

Figure A.15. Ambiguity plots for source signal bandwidth of 100 Hz and SNR=20 dB

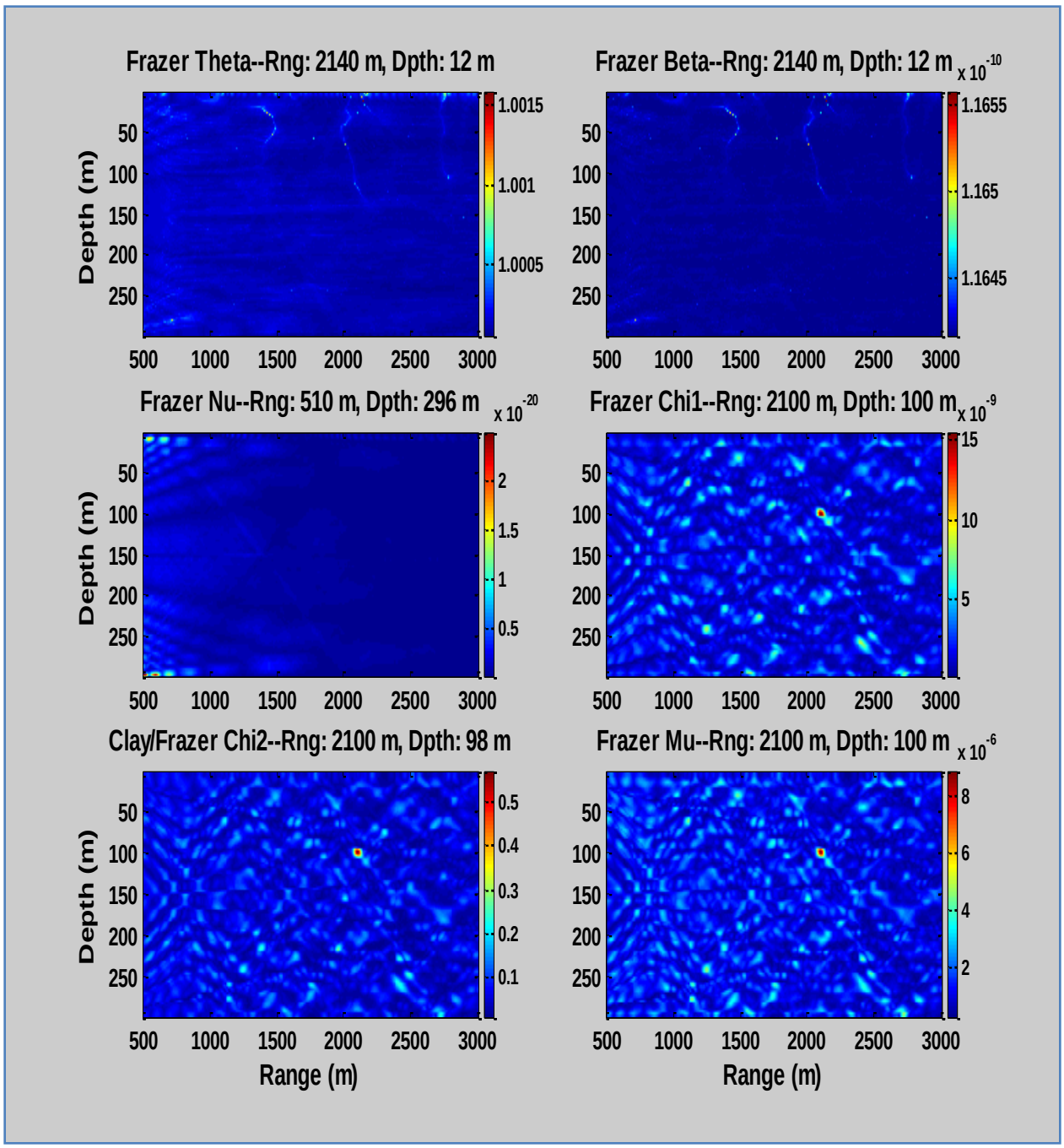

Figure A.16. Ambiguity plots for source signal bandwidth of 100 Hz and SNR=20 dB

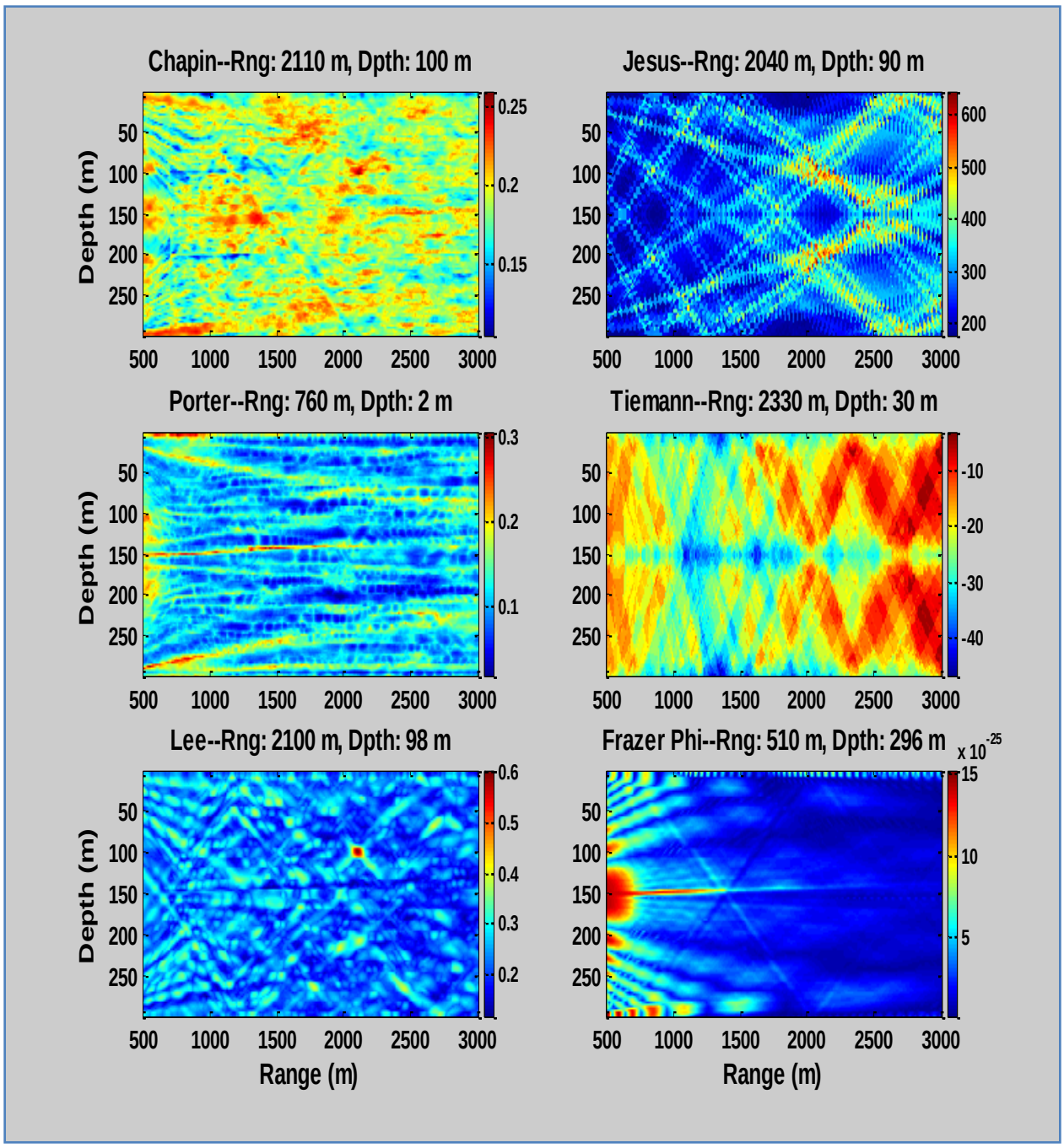

Figure A.17. Ambiguity plots for source signal bandwidth of 200 Hz and SNR=20 dB

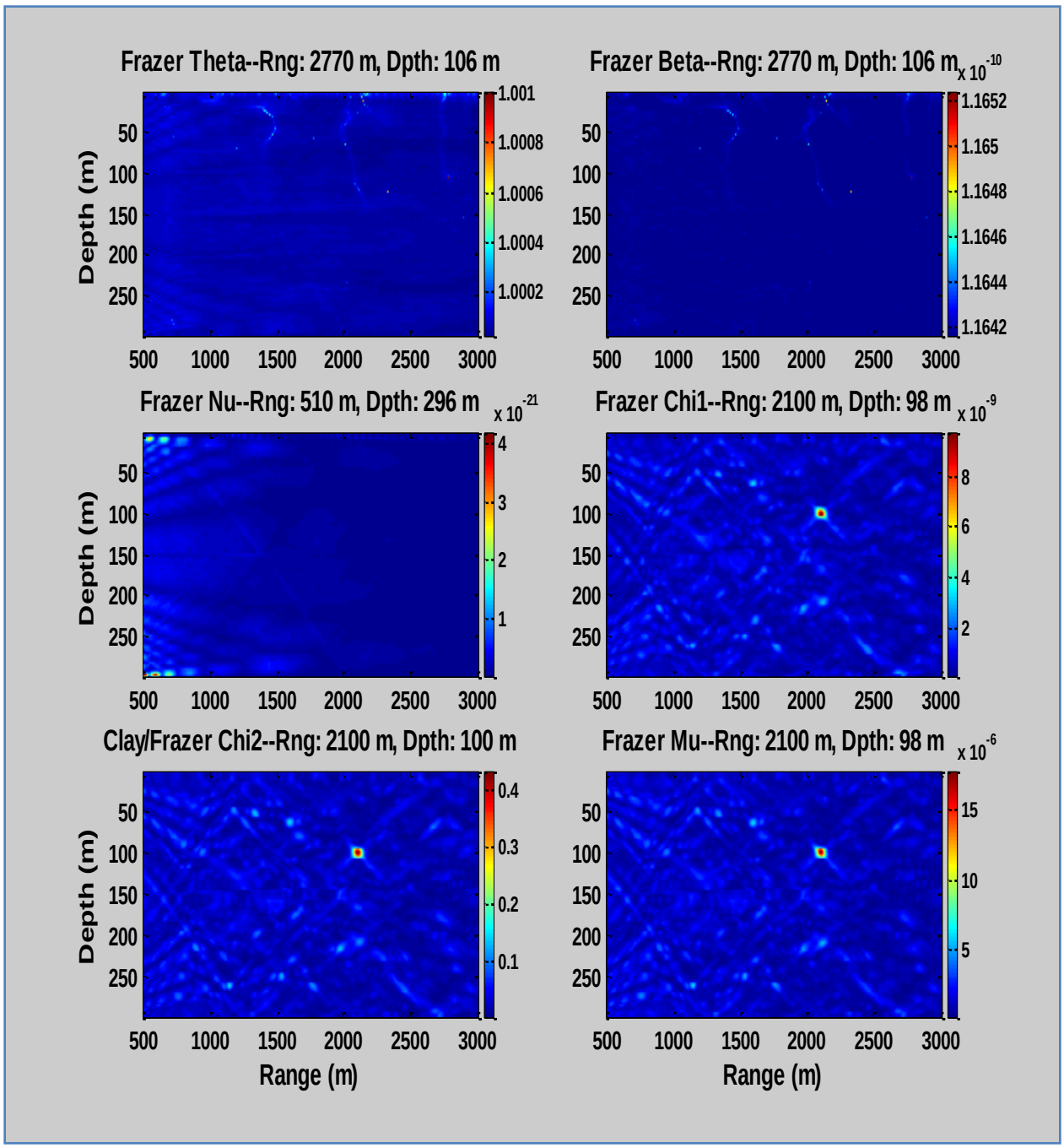

Figure A.18. Ambiguity plots for source signal bandwidth of 200 Hz and SNR=20 dB

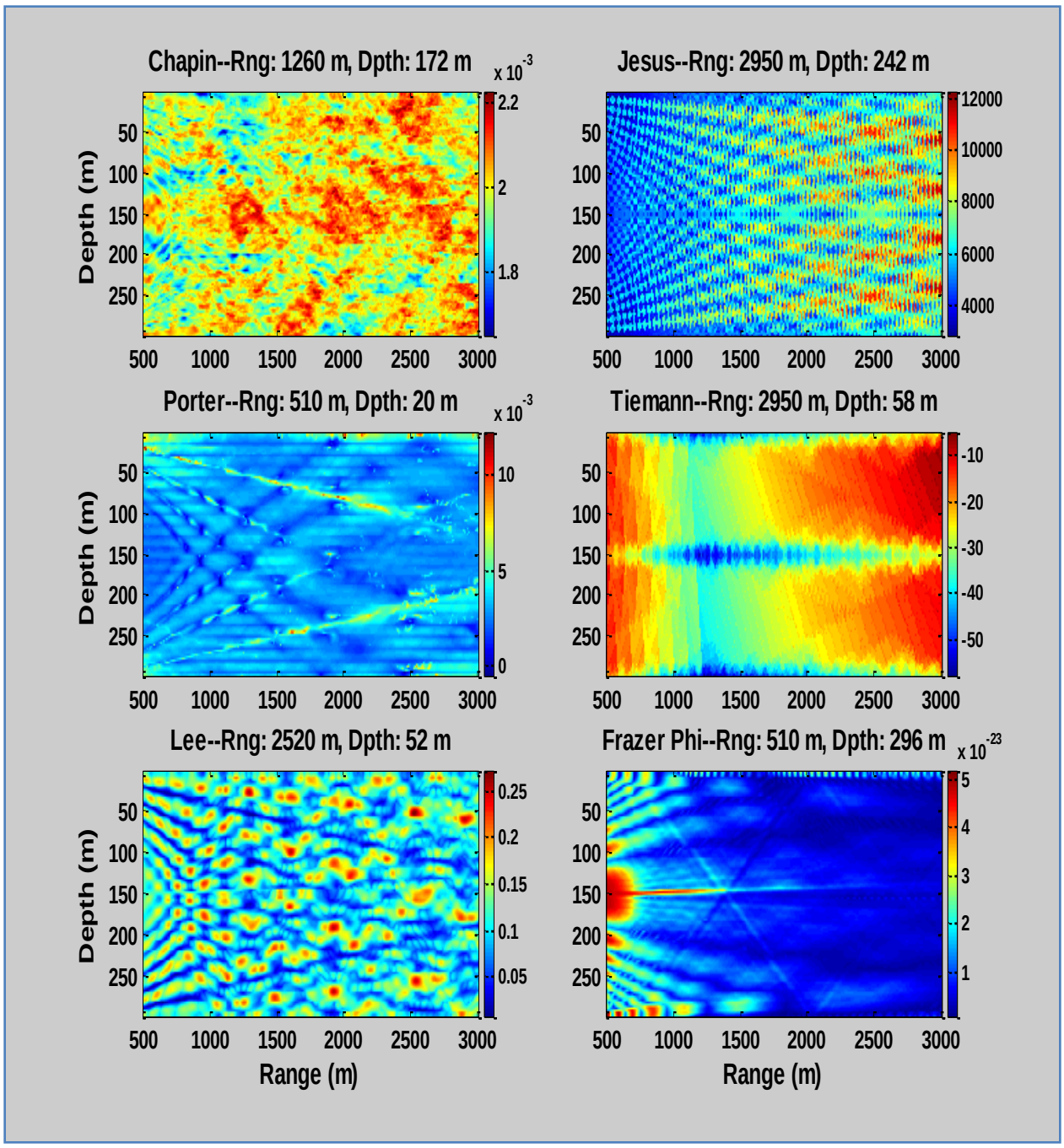

Figure A.19. Ambiguity plots for source signal bandwidth of 10 Hz and SNR=0 dB

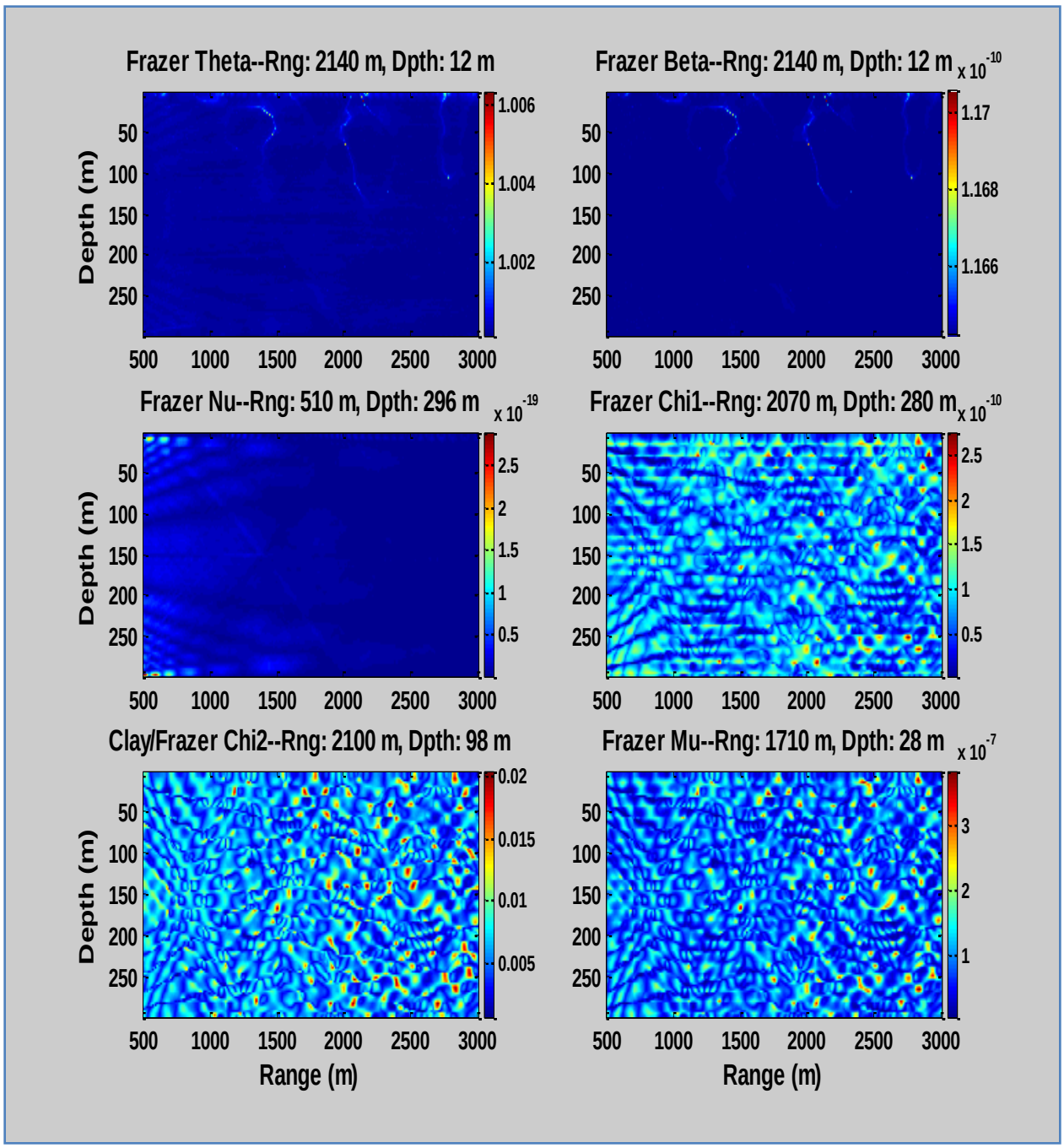

Figure A.20. Ambiguity plots for source signal bandwidth of 10 Hz and SNR=0 dB

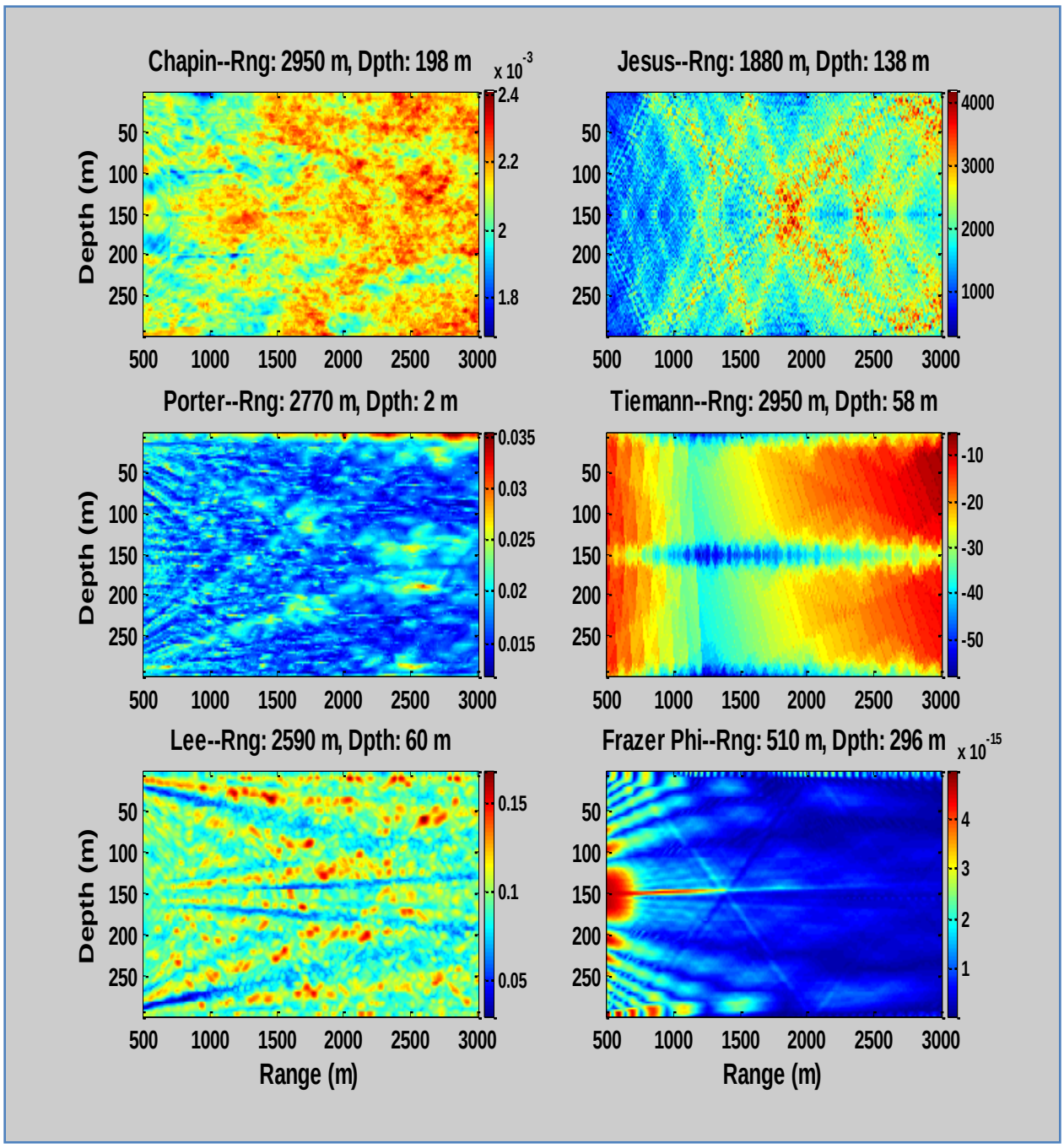

Figure A.21. Ambiguity plots for source signal bandwidth of 100 Hz and SNR=0 dB

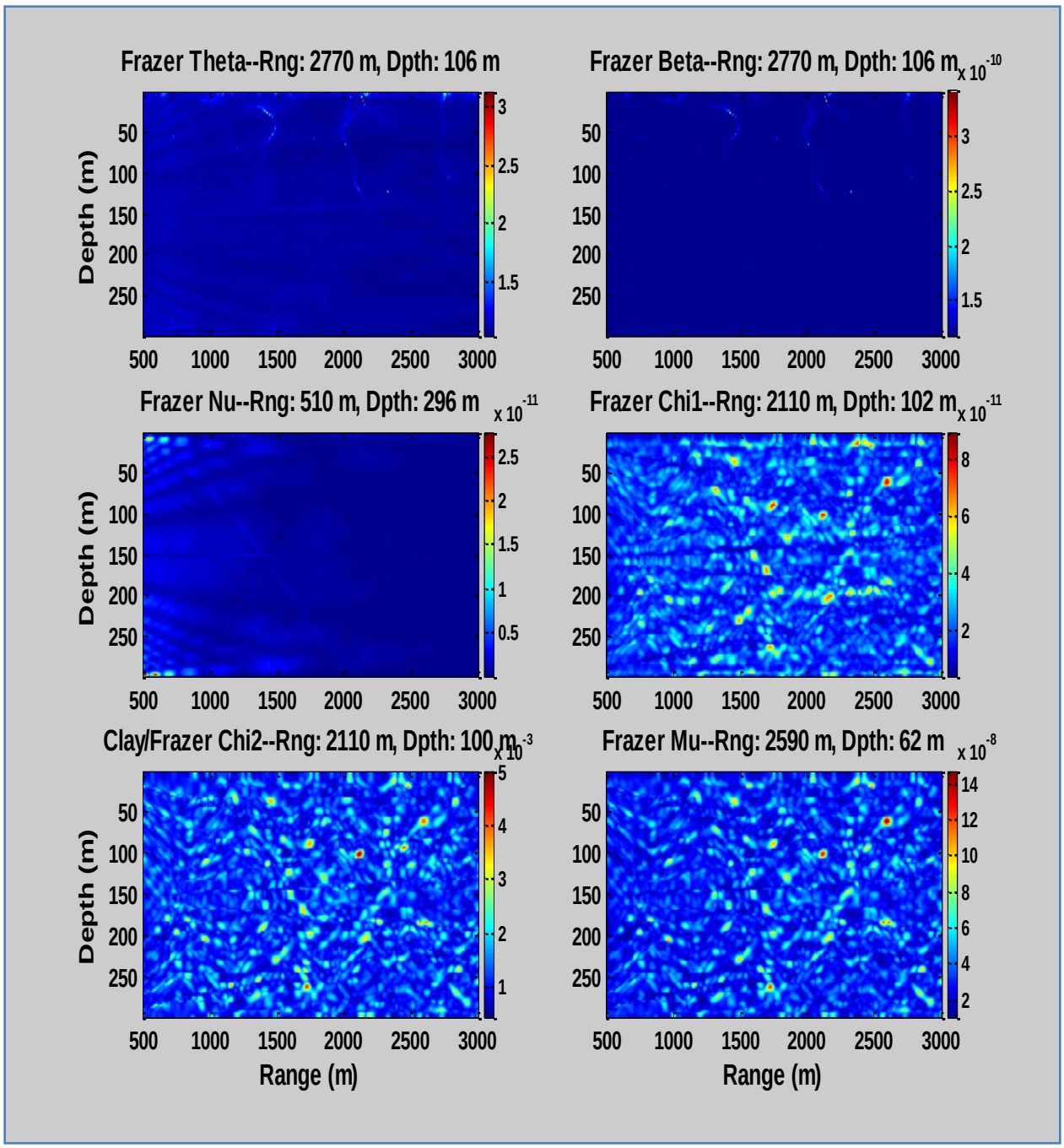

Figure A.22. Ambiguity plots for source signal bandwidth of 100 Hz and SNR=0 dB

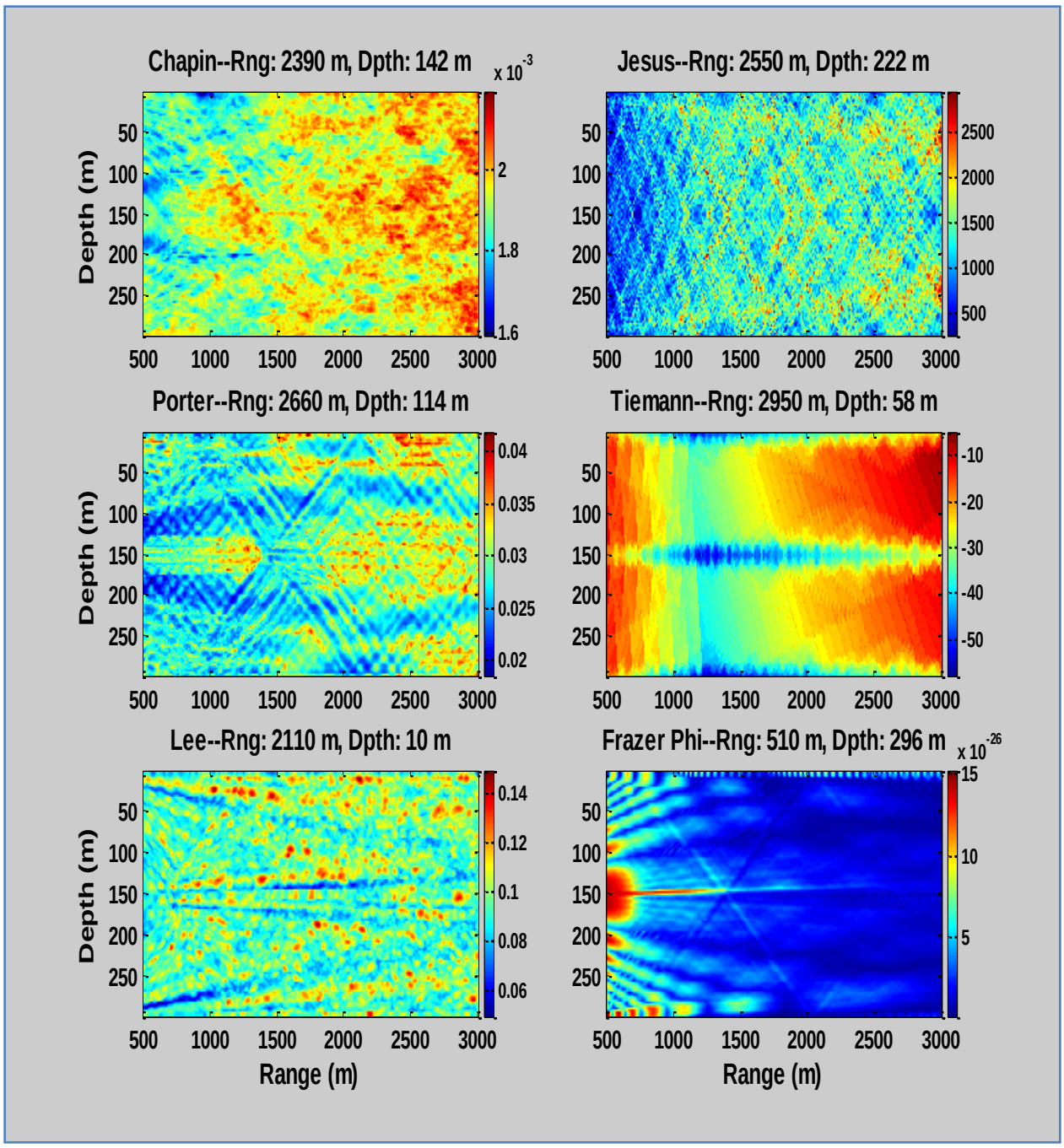

Figure A.23. Ambiguity plots for source signal bandwidth of 200 Hz and SNR=0 dB

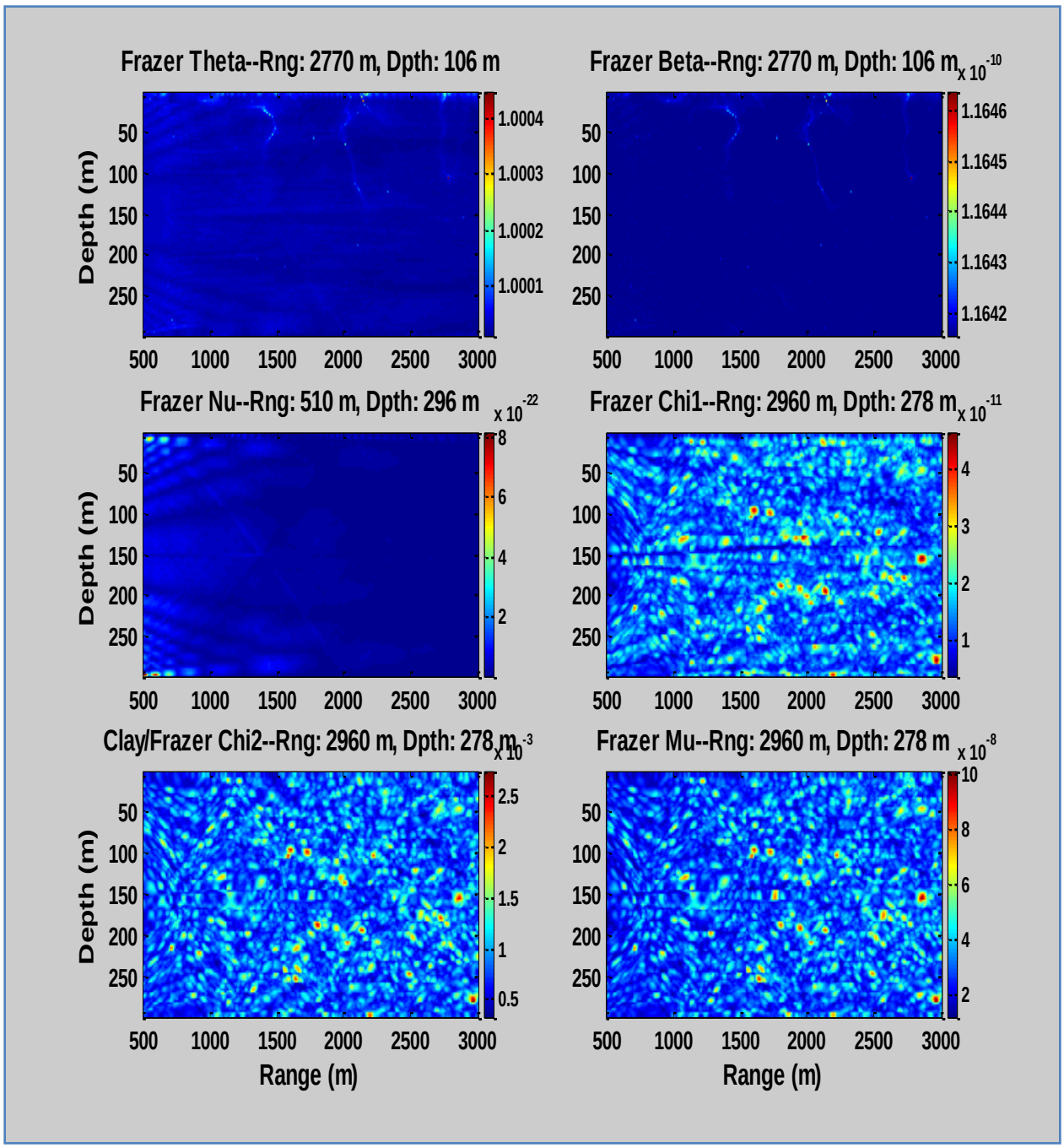

Figure A.24. Ambiguity plots for source signal bandwidth of 200 Hz and SNR=0 dB

References

Aubauer, R., M. Lammers, and W. Whitlow. 2000. One-hydrophone method of estimating distance and depth of phonating dolphins in shallow water. *Journal of the Acoustical Society of America* 107 (5): 2744-2749.

Baggeroer, A.B., W.A. Kuperman, and P.N. Mikhalevsky. 1993. An Overview of Matched Field Methods in Ocean Acoustics. *IEEE Journal of Oceanic Engineering* 18 (4): 401-424.

Bracewell, R.N. 2000. *The Fourier Transform and its Applications.* 3rd Edition. Boston: McGraw-Hill.

Brigham, E. 1988. *The Fast Fourier Transform and its Applications.* Englewood Cliffs: Prentice Hall.

Bucker, Homer P. 1976. Use of calculated sound fields and matched-field detection to locate sound sources in shallow water. *Journal of the Acoustical Society of America* 59 (2): 368-373.

Cato, D. 1998. Simple methods of estimating source levels and locations of marine animal sounds. *Journal of the Acoustical Society of America* 104 (3): 1667-1678.

Clay, C.S. 1987. Optimum time domain signal transmission and source location in a waveguide. *Journal of the Acoustical Society of America* 81 (3): 660-664.

Durbin, J. 1960. The fitting of time series models. *Rev. Int. Stat. Inst.* 28: 233-244.

Field, R.L., and J.H. Leclere. 1993. Measurements of bottom-limited ocean impulse responses and comparisons with the time-domain parabolic equation. *Journal of the Acoustical Society of America* 93 (5): 2599-2616.

Frazer, L.N., and P.I. Pecholcs. 1990. Single-hydrophone localization. *Journal of the Acoustical Society of America* 88 (2): 995-1002.

Harris, F.J. 1978. On the Use of Windows for Harmonic Analysis with the Discrete Fourier Transform. *Proceedings of the IEEE* 66 (1): 51-83.

Hassab, J.C. 1976. Passive tracking of a moving source by a single observer in shallow water. *Journal of Sound and Vibration* 44: 127-145.

Hinich, Melvin J. 1973. Maximum-likelihood signal processing for a vertical array. *Journal of the Acoustical Society of America* 54 (2): 499-503.

Jensen, F., W. Kuperman, M. Porter, and H. Schmidt 1994. *Computational Ocean Acoustics.* New York: AIP Press.

Jesus, S.M., M.B. Porter, Y. Stephan, E. Coelho, and X. Demoulin. 1998. Broadband source localization with a single hydrophone. *OCEANS '98.* Nice.

Jesus, S.M., M.B. Porter, Y. Stephan, E. Coelho, O.C. Rodriguez, and X. Demoulin. 2000. Single sensor source localization in a range-dependent environment. *MTS/IEEE Oceans 2000.* Providence.

Jesus, S.M., M.B. Porter, Y. Stephan, X. Demoulin, O.C. Rodriguez, and E. Coelho. 2000. Single Hydrophone Source Localization. *IEEE Journal of Oceanic Engineering* 25 (3): 337-346.

Kuperman, W.A., and G.L. D'Spain. 2001. Long range source localization from single hydrophone spectrograms. *Journal of the Acoustical Society of America* 109 (5): 1935-1943.

Lee, Y.P. 1998. Time-Domain Single Hydrophone Localization in a Real Shallow Water Environment. *OCEANS '98, 1074-1077.* Nice.

Levinson, N. 1947. The Wiener RMS (root-mean-square) error criterion in filter design and prediction. *Journal of Mathematical Physics* 25: 261-278.

Li, S., and C.S. Clay. 1987. Optimum time domain signal transmission and source location in a waveguide: Experiments in an ideal wedge waveguide. *Journal of the Acoustical Society of America* 82 (4): 1409-1417.

Lutkepohl, H. 1996. *Handbook of Matrices.* Chichester: John Wiley & Sons.

Pekeris, C.L. 1948. Theory of propagation of explosive sound in shallow water. *Geol. Soc. Am. Mem.* 27.

Porter, M. 2008. *Acoustics Toolbox*. http://oalib.hlsresearch.com/Modes/AcousticsToolbox.

Porter, M.B. 1990. The time-marched fast-field program (FFP) for modeling acoustic pulse propagation. *Journal of the Acoustical Society of America* 87 (5): 2013-2023.

Porter, M.B., and H.P. Bucker. 1987. Gaussian beam tracing for computing ocean acoustic fields. *Journal of the Acoustical Society of America* 82 (4): 1349-1359.

Porter, M.B., Y. Stephan, X. Demoulin, S. Jesus, and E. Coelho. 1998. Shallow-Water Tracking in the Sea of Nazare. *Undersea Technology '98, IEEE Oceanic Engineering Society.* Tokyo.

Strang, Gilbert 1993. *Introduction to Linear Algebra.* Wellesley, MA: Wellesley-Cambridge Press.

Tiemann, C., A. Thode, J. Straley, V. O'Connell, and K. Folkert. 2006. Three-dimensional localization of sperm whales using a single hydrophone. *Journal of the Acoustical Society of America* 120 (4): 2355-2365.

Tolstoy, A. 1993. *Matched Field Processing for Underwater Acoustics.* Singapore: World Scientific.

Tong, L., G. Xu, and T. Kailath. 1993. Fast blind equalization via antenna arrays. *Proc. ICASSP '93*, 272-275.

Unpingco, J., W.A. Kuperman, and W.S. Hodgkiss. 1999. Single sensor source tracking and environmental inversion. *Journal of the Acoustical Society of America* 106 (3): 1316-1329.

Vita

Sean Chapin received a B.S. in Physics from Western Michigan University and went to work as a Research Scientist at Ford Motor Company's Scientific Research Laboratory in Dearborn, Michigan. At Ford he tested experimental combustion engines on their dynamometers, including an engine modified to run on hydrogen gas. He then joined the Department of Physics at the University of New Orleans as a Teaching Assistant and later as a Research Assistant. He studied and researched topics in underwater acoustic signal processing. After completing his M.S. in Applied Physics, he entered the Ph.D. program in Engineering and Applied Science. Upon completion of his exams, Sean took a position as a Physicist at the Naval Surface Warfare Center in Dahlgren, Virginia. He has been involved in a variety of work with the Navy including image processing, radar signal processing, track processing, modeling and simulation, systems engineering, and systems analysis.